UNIVERSITY OF ALBERTA

DIAMONDS AND THEIR FORMATION: CHARACTERIZATION OF DIAMONDS FROM THE BUFFALO HEAD HILLS, ALBERTA

and

METASOMATISM RECORDED BY GARNET INCLUSIONS FROM THE DE BEERS POOL, SOUTH AFRICA

by

ANETTA BANAS

A thesis submitted to the faculty of Graduate Studies and Research in partial fulfillment of the requirements for the degree of MASTER OF SCIENCE

DEPARTMENT OF EARTH AND ATMOSPHERIC SCIENCES
EDMONTON, ALBERTA

SPRING 2006

Your file Votre référence
ISBN: 0-494-13787-8
Our file Notre référence
ISBN: 0-494-13787-8

ABSTRACT

This thesis encompasses the study of two principally different types of diamond source regions. The Buffalo Hills represent an unconventional diamond deposit located within the Proterozoic Buffalo Head Terrane. Diamonds from kimberlite pipes K11, K91 and K252 are predominantly of eclogitic paragenesis. Diamond formation occurred in multiple phases under both lithospheric - supported by the presence of Type IaA to IaAB diamonds and sublithospheric conditions - indicated by the presence of majorite and abundance of Type II and Type IaB diamonds. The De Beers Pool mines, located on the Archean Kaapvaal Craton, are the world's classical primary diamond deposit. Garnet inclusions in De Beers Pool diamonds represent the oldest, most depleted mantle samples available and constrain mantle compositions in the Archean. Combined with xenolith studies they indicate increasing fertility of the lithospheric mantle over time. Their re-enriched trace element signatures indicate an intimate association between metasomatism and diamond formation.

ACKNOWLEDGEMENTS

Although a thesis is a summary of a student's work it could not possibly be completed without the support and encouragement of all those who cross your path along the way.

This thesis would not have been nearly as enjoyable without the support and enthusiasm of my supervisor, Thomas Stachel. Thank you for convincing me to pursue this project and introducing me to the wonderful world of diamonds. I will always fondly remember my time with the DRG.

I am very grateful to Tom McCandless and Ashton Mining Canada for allowing me to work on their exploration samples (with no possibility of ever getting them back).

Fanus Viljoen and De Beers Consolidated Mines are thanked for providing the De Beers Pool garnet inclusions and supporting the research project.

A big thanks goes out to Jeffrey Harris who, with his lunch-time walks around Glasgow, taught me all I needed to know to get started in the diamond "business".

I would like thank Karlis Muehlenbachs for giving me unlimited access to his stable isotope lab and all his insightful contributions.

Sergei Matveev is thanked for all his help with the electron microprobe in analyzing research samples and perfectly set diamonds in engagements rings.

Nobu Shimizu is thanked for his hospitality at Woods Hole and instruction on the SIMS (and for the bread baking tips).

A degree would not be complete without copious good times and fond memories with fellow graduate students. In particular I thank Steven Creighton "Sweetie" for frequent discussions and planting ideas in my head that didn't always go over well with the *boss*. As well as for all his technical support, Adobe will be with me forever. Ralf Tappert is thanked for showing me the ropes with all things diamond related.

Mark Labbe and Donnie Resultay are thanked for their endless supply of ideas and quick fixes, and always finding time to do all those "other" things. Donnie thanks for lending me your camera which takes the most amazing photos.

TABLE OF CONTENTS

LIST OF TABLES

LIST OF FIGURES

LIST OF SYMBOLS AND ABBREVIATIONS

PDB	Pee-Dee belemnite
REE	Rare Earth Elements
REE_N	Rare Earth Elements normalized to C1 chondrite
REE_{J4}	Rare Earth Elements normalized to J4 primitive garnet
LREE	Light Rare Earth Elements
MREE	Middle Rare Earth Elements
HREE	Heavy Rare Earth Elements
HFSE	High Field Strength Elements
FTIR	Fourier Transform Infrared
SIMS	Secondary Ion Mass Spectrometry
EPMA	Electron Probe Microanalysis
Fo	forsterite
wt %	weight percent
ppm	parts per million
‰	per mil
cts	carats

In Tables:

thh	tetrahexahedroid
octa	octahedron
frag	fragment
irr	irregular
agg	aggregate
c	colorless
ly	light yellow
y	yellow
lb	light brown
b	brown
serp	serpentine
calc	calcite
grt	garnet
ol	olivine
cpx	clinopyroxene
maj	majorite
fper	ferropericlase
opx	orthopyroxene
chr	chromite

E	eclogitic
P	peridotitic
H	harburgitic
L	lherzolitic
Wh	wehrlitic

CHAPTER 1

INTRODUCTION

1.1 Introduction

Diamonds are treasured as the most precious gemstones for their spectacular brilliance and fire. In industrial processes their extreme properties (e.g. hardness, chemical durability, thermal conductivity) make them a valuable tool in many applications (i.e. cutting/grinding tools, heat sinks). Beyond these marketable attributes diamonds are ultimately pristine mantle specimens. Diamonds and their mineral inclusions provide a wealth of information on the conditions and characteristics of the Earth's mantle. Diamonds are usually found in kimberlite and lamproite intrusions and have a worldwide distribution closely associated with ancient continental crust. Traditionally exploration has been guided by Clifford's Rule which establishes an association between diamond occurrences and ancient cratons (Fig. 1.1; Clifford, 1966). However, continued exploration around the globe has led to the discovery of diamond deposits in regions where Proterozoic tectonothermal events have affected the Archean lithosphere (Argyle, Jaques et al., 1989; Guaniamo, Kaminsky et al., 2000) and in unconventional, non-Archean, settings (Buffalo Hills Kimberlite Province, (Carlson et al., 1999).

Emplacement ages for kimberlite pipes range from Proterozoic (e.g. Premier Mine in South Africa) to Tertiary (e.g. at Lac de Gras in the NWT), however the majority of kimberlites were emplaced during the Cretaceous (Gurney, 1989; Heaman et al., 2003). Isotopic studies on syngenetic inclusions in diamonds suggest that some diamonds have formation ages much older than their kimberlite hosts. Peridotitic diamonds generally have older ages (~3.3 Ga) whereas inclusions in eclogitic diamonds indicate younger ages with a broader range between ~2.4-0.9 Ga. This implies that diamonds are only passengers in a kimberlite magma sampled from the surrounding mantle during ascent.

Diamonds are composed of nearly pure carbon and thus provide a limited amount of information about their origin in the Earth's mantle. However, they contain inclusions of mantle minerals (silicates, oxides and sulfides) which provide valuable additional information on mantle conditions during diamond genesis. Diamond is chemically inert and therefore a perfect container for the preservation of inclusions during transport to the

Earth's surface. It protects the inclusions from re-equilibration due to changing pressure-temperature conditions and metasomatic alteration during transport. Thus, the inclusions remain pristine samples that provide information on the composition and evolution of the subcratonic lithospheric mantle.

1.2 Petrological and Geochemical Background

1.2.1 Physical characteristics

Diamond is composed almost purely of carbon, but may contain minor impurities of nitrogen and boron. The diamond structure is based on the arrangement of four carbon tetrahedra in a face-centered cubic array. This arrangement gives rise to the two primary forms of diamond: octahedra and cubes. Diamond shows perfect cleavage in four directions following {111}.

The PT conditions at the time of growth will determine the primary shape of adiamond crystal: at 'high' T conditions octahedral forms will be stable, at 'low' T conditions cubic forms will be stable. Combination forms, which contain both octahedral and cubic components, will grow under intermediate conditions. Octahedra are the most abundant primary shape found in most deposits, while cubes are rare and usually comprise <1% of a diamond population from a single deposit (Harris, 1992). Twinned crystals are commonly observed, the most common twin, the macle, is twinned on the {111} plane. Under super-saturated conditions crystal aggregates may be formed.

Secondary forms are formed through resorption of primary forms in the mantle or in kimberlite magma. Incomplete resorption of primary crystals results in partially resorbed forms with residual primary faces. Octahedra and cubes are resorbed to tetrahexahedroid forms (commonly referred to as dodecahedra). The amount of resorption a crystal undergoes depends on the crystal size and the depth at which the crystal was released into the magma.

Diamond crystal faces often show a variety of recognizable surface textures. Terracing of the octahedral faces is a common texture formed during diamond growth. Common surface textures due to etching are trigons, shield and serrate laminae. Trigons are trigonal shaped etch pits with negative relief which occur on octahedral faces (similar features are observed on cubic faces with a tetragonal shape). Shield and serrate laminae are expressed as thin elevated lines parallel to octahedral/cubic growth planes.

Secondary forms show a large variety of surface textures, which are documented in detail by Robinson (1979). Commonly observed features are hillocks, medial lines and lamination lines. Hillocks are positive, elongate, narrow ridges which run across the long axis of a tetrahexahedroidal face. Medial lines run across the short axis of a tetrahexahedroidal

face and are recognized by a change in relief. These features result from interaction with resorbing fluids. Lamination lines are very fine lines on a crystal face which are a surface expression of plastic deformation along {111} planes.

Diamond can exhibit a variety of colors caused by deformation or impurities. A Cape-yellow (golden) color is caused by nitrogen impurities in the N3 aggregation (3 nitrogen + vacancy). A canary-yellow (bright) color results from the presence of nitrogen in single substitution in the diamond lattice. Brown, pink and red colors, in turn, result from an increasing degree of plastic deformation. A blue color becomes evident when trace amounts (up to a few ppm) of boron are present in the lattice. Green color is usually a coat on the crystal surface formed during α-particle bombardment from the decay of Th to U in adjacent minerals.

1.2.2 Inclusion Petrology

Studies on mineral inclusions have enabled the classification of diamonds into two suites: peridotitic and eclogitic. The peridotitic inclusion suite is characterized by the presence of olivine, orthopyroxene, Cr-rich garnet and clinopyroxene and Mg-chromite. The peridotitic inclusion suite can be further subdivided into lherzolitic and harzburgitic parageneses, distinguished by the presence of Cr-diopside in lherzolitic mineralogies (Harris, 1992; Meyer, 1987). The eclogitic inclusion suite typically contains Cr-poor grossular-almandine-pyrope garnet, omphacitic clinopyroxene (Na-rich) as well as minor constituents such as rutile, kyanite, coesite and sanidine. Sulphide inclusions are commonly found associated with both suites and may be distinguished by their Ni contents, which is significantly lower for eclogitic sulphides. Peridotite is the most abundant rock type in the Earth's upper mantle; this is reflected by the majority of diamonds belonging to the peridotitic suite. However, certain mines (pipes) have a majority of eclogitic inclusions indicating either that the mantle was highly heterogeneous or that diamond formation in eclogite was favored.

Syngenetic mineral inclusions may be used to characterize the chemical and mineralogical properties of the source regions at the time of diamonds crystallization (Meyer, 1987). In particular garnet inclusions are an excellent tracer of prior processes that have affected the diamond source region. Detailed major and trace element analyses of garnet inclusions have shown that an analogous depletion - re-enrichment sequence has affected most diamond source regions around the world (Stachel et al., 2004 and references therein).

Additionally, applying well calibrated exchange equilibria to certain inclusion pairs provides estimates of the pressure-temperature conditions during diamond genesis. Non-touching inclusion pairs invariably retain this signature because the inclusions are isolated from each other and hence cannot re-equilibrate to changing ambient conditions.

Conversely, polymineralic inclusions (i.e. touching pairs of minerals) may re-equilibrate to changing pressure or temperature conditions and thus may record lithospheric cooling after diamond formation when compared with their counterpart non-touching inclusion pairs (Phillips et al., 2004). Within individual kimberlite pipes, the temperatures recorded by touching inclusion parageneses appear to be comparable to those derived from mantle xenoliths (Boyd and Nixon, 1978).

1.2.3 Geochemistry

Diamond itself can be analyzed to determine its carbon isotope and nitrogen compositions. Nitrogen is the only significant trace impurity found within the diamond lattice. Nitrogen content is used to separate diamonds into two groups: Type I - nitrogen present and Type II - nitrogen free (below the limit of detection, about 10 ppm, for infra-red (IR) spectroscopy). Nitrogen aggregation states further subdivide this classification into Type I*b* in which diamonds contain nitrogen in single substitution and Type I*a* in which diamonds contain aggregated nitrogen in the form of pairs (Type IaA), rings of four nitrogens surrounding a vacancy (Type IaB), or both (Type IaAB). The kinetics of nitrogen aggregation in diamond is well studied and may be used to determine either the approximate residence time or the residence temperature of individual diamonds in the Earth's mantle.

The worldwide distribution of carbon isotope values ($\delta^{13}C_{PDB}$) ranges from -34 to +3 ‰ (Kirkley et al., 1991). Each locality has its own distinct set of isotopic compositions and no single deposit has yet been observed that covers the full range in $\delta^{13}C$ values seen world-wide (Kirkley et al., 1991). Distinct ranges are evident for the peridotitic and eclogitic parageneses. Peridotitic diamonds, with very few exceptions, fall into a narrow normal distribution with a range in $\delta^{13}C$ from -10 to -1 ‰ and a sharp mode at -5 ‰. Eclogitic diamonds have the same mode in carbon isotopic composition (-5‰) but show a much broader range in $\delta^{13}C$ from -34 to +3 ‰ and a distribution that is noticeably skewed towards isotopically lighter (i.e. strongly negative) values.

Carbon isotopes provide important constraints on models of diamond genesis. The range in $\delta^{13}C$ for the peridotitic suite is consistent with "normal" mantle values suggesting that these diamonds formed from a primordial carbon source. The broad range in $\delta^{13}C$ exhibited by eclogitic diamonds encompasses the typical compositions of organic matter ($\delta^{13}C \sim$ -35 to -20 ‰) and marine carbonates ($\delta^{13}C \sim$ -2 to +2 ‰), (Kirkley et al., 1991). This has led to the suggestion that subducted oceanic crust containing organic matter and marine carbonates is involved in the formation of eclogitic diamonds. Additional support for this model is provided by oxygen isotope measurements from eclogite xenoliths (Garlick et al., 1971; Deines et al., 1991; Macgregor and Manton, 1986). The $\delta^{18}O$ distributions

show a wide range of values (~ 2 to 8 ‰), which are characteristic of oceanic crust that experienced alteration in thermal regimes ranging from normal sea water temperature at the top (leading to isotopic heavy values) to greenshist facies at depth (resulting in low $\delta^{18}O$ more similar to sea water itself; Muehlenbachs and Clayton, 1976). The wide spread seen in the sulphur isotopic composition of syngenetic sulphide inclusions in diamonds and, in particular, the presence of mass-independent fractionation trends also supports a crustal contribution (Farquhar et al., 2002). Formation temperatures, based on inclusion geothermobarometry, for both peridotitic and eclogitic diamonds, fall on similar modes of about 1150°C (Stachel et al., 2002 and 2003), which is inconsistent with crystallization of eclogitic diamonds in a cold subducting slab. Helmstaedt and Schulze, (1989) propose a model of craton formation whereby the imbrication of oceanic crust and lithosphere during shallow subduction is the source of cratonic eclogites and peridotites (Fig. 1.2). Peridotitic and eclogitic diamond formation in the imbricted slices would occur under similar PT conditions but in chemically distinct reservoirs during repeated metasomatic events.

1.3 Thesis

1.3.1 Buffalo Head Hills, Alberta, Canada

The first part of this project focuses on the characterization of diamonds and their inclusions from the newly discovered Buffalo Hills Kimberlite Field in north-central Alberta. The kimberlite field is located within the Buffalo Head Terrane which is of Lower Proterozoic metamorphic age (2.3-2.0 Ga; Theriault and Ross, 1991) and hence an unconventional setting for diamond exploration. Diamondiferous kimberlites, such as K252 with a diamond grade of 55 cts/100 tonnes, have rejuvenated interest in the region and facilitated further study into this atypical setting. Diamonds from three kimberlite pipes, K11, K91 and K252, were examined and classified according to morphology, carbon isotope composition, nitrogen content and aggregation state, and inclusion chemistry. The results provide further constraints and new insights into the formation of diamonds and the composition of the subcontinental lithospheric mantle beneath the Buffalo Head Terrane.

1.3.2 De Beers Pool, South Africa

The second part of the project focuses on REE (rare earth element) and trace element analyses of ultra-depleted garnet inclusions from diamonds from the De Beers Pool kimberlites, South Africa. The De Beers Pool garnet inclusions have major element compositions which indicate that the deep lithosphere at the time of diamond formation was even more depleted than what is suggested by the xenoliths in the Jurassic-Early Cretaceous

Group 2 kimberlites. Peridotitic garnet inclusions from diamonds from the De Beers Pool have been dated at 3.3 Ga (Richardson et al., 1984). The De Beers Pool inclusions, thus, represent a unique opportunity to study pristine samples of Archean lithospheric mantle. Consequently, this study concentrated on the trace element composition of the De Beers Pool garnet inclusions to elucidate the original signature of the Archean lithosphere and the role of metasomatic processes during diamond formation.

References

Boyd, F.R. and Nixon, P.H., 1978. Ultramafic nodules from the Kimberley pipes, South Africa. Geochimica et Cosmochimica Acta, 42(9): 1367-1371.

Carlson, S., Hillier, W., Hood, C., Pryde, R. and Skelton, D., 1999. The Buffalo Hills kimberlites: A newly discovered diamondiferous kimberlite province in North-central Alberta, Canada. In: J.J. Gurney, J.L. Gurney, M.D. Pascoe and S.H. Richardson (Editors), The J.B. Dawson Volume, Proceedings of the VIIth International Kimberlite Conference. Red Roof Design, Capetown, SA, pp. 109-116.

Clifford, T.N., 1966. Tectono-metallogenetic units and metallogenetic provinces of Africa. Earth and Planetary Science Letters, 1: 421-434.

Deines, P., Harris, J.W., Robinson, D.N., Gurney, J.J. and Shee, S.R., 1991. Carbon and Oxygen isotope variations in diamond and graphite eclogites from Orapa, Botswana, and the Nitrogen-content of their diamonds. Geochimica et Cosmochimica Acta, 55(2): 515-524.

Farquhar, J. et al., 2002. Mass-independent sulfur of inclusions in diamond and sulfur recycling on early earth. Science, 298(5602): 2369-2372.

Frey, F.A. and Green, D.H., 1974. The mineralogy, geochemistry and origin of lherzolite inclusions in Victorian basanites. Geochimica et Cosmochimica Acta, 38: 1023-1059.

Garlick, G.D., MacGregor, I.D. and Vogel, D.E., 1971. Oxygen isotope ratios in eclogites from kimberlites. Science, 172(3987): 1025-1027.

Gurney, J.J., 1989. Diamonds. In: J. Ross and et al. (Editors), Kimberlites and related rocks. GSA Spec Publ 14. Blackwell, Carlton, pp. 935-965.

Harris, J.W., 1992. Diamond geology. In: J.E. Field (Editor), The properties of natural and synthetic diamond. Academic Press, London, pp. 345-393.

Heaman, L.M., Kjarsgaard, B.A. and Creaser, R.A., 2003. The timing of kimberlite magmatism in North America: implications for global kimberlite genesis and diamond exploration. Lithos, 71(2-4): 153-184.

Helmstaedt, H.H. and Schulze, D.J., 1989. Southern African kimberlites and their mantle sample: implications for Archean tectonics and lithosphere evolution. In: J. Ross and et al. (Editors), Kimberlites and related rocks. GSA Spec Publ 14. Blackwell, Carlton, pp. 358-368.

Janse, A.J.A., 1994. Is Clifford's rule still valid? Affirmative examples from around the world. In: Leonardos, O.H. and Meyer, H.O.A. (Editors), Diamonds: characterization, genesis and exploration. CPRM Spec Publ, Brasilia, pp. 215-235.

Jaques, A.L. et al. (Editors), 1989. Composition of crystalline inclusions and C-isotopic composition of Argyle and Ellendale diamonds. Kimberlites and related rocks. GSA Spec Publ 14, 2. Blackwell, Carlton, 966-989 pp.

Kaminsky, F.V., Zakharchenko, O.D., Griffin, W.L., Channer, D.M.D. and Khachatryan-Blinova, G.K., 2000. Diamond from the Guaniamo area, Venezuela. Canadian Mineralogist, 38: 1347-1370.

Kirkley, M.B., Gurney, J.J., Otter, M.L., Hill, S.J. and Daniels, L.R., 1991. The application of C isotope measurements to the identification of the sources of C in diamonds: a review. Applied Geochemistry, 6: 477-494.

MacGregor, I.D. and Manton, W.I., 1986. Roberts-Victor eclogites - Ancient oceanic-crust. Journal of Geophysical Research-Solid Earth and Planets, 91(B14): 14063-14079.

Meyer, H.O.A., 1987. Inclusions in diamond. In: P.H. Nixon (Editor), Mantle xenoliths. John Wiley & Sons Ltd., Chichester, pp. 501-522.

Muehlenbachs, K. and Clayton, R.N., 1976. Oxygen isotope composition of the oceanic crust and its bearing on seawater. Journal of Geophysical Research, 81(4365-4369).

Phillips, D., Harris, J.W. and Viljoen, K.S., 2004. Mineral chemistry and thermobarometry of inclusions from De Beers Pool diamonds, Kimberley, South Africa. Lithos, 77: 155-179.

Richardson, S.H., Gurney, J.J., Erlank, A.J. and Harris, J.W., 1984. Origin of diamonds in old enriched mantle. Nature, 310(5974): 198-202.

Robinson, D., 1979. Surface Textures and Other Features of Diamonds. PhD Thesis, University of Cape Town, 220 pp.

Stachel, T., Harris, J.W., Aulbach, S. and Deines, P., 2002. Kankan diamonds (Guinea) III: delta C-13 and nitrogen characteristics of deep diamonds. Contributions to Mineralogy and Petrology, 142(4): 465-475.

Stachel, T., Harris, J.W., Tappert, R. and Brey, G.P., 2003. Peridotitic diamonds from the Slave and the Kaapvaal cratons - similarities and differences based on a preliminary data set. Lithos, 71(2-4): 489-503.

Stachel, T. et al., 2004. The trace element composition of silicate inclusions in diamonds: a review. Lithos, 77: 1-19.

Theriault, R. and Ross, G., 1991. Nd isotopic evidence for crustal recycling in the ca. 2.0 Ga subsurface of Western Canada. Canadian Journal of Earth Sciences, 28(8): 1140-1147.

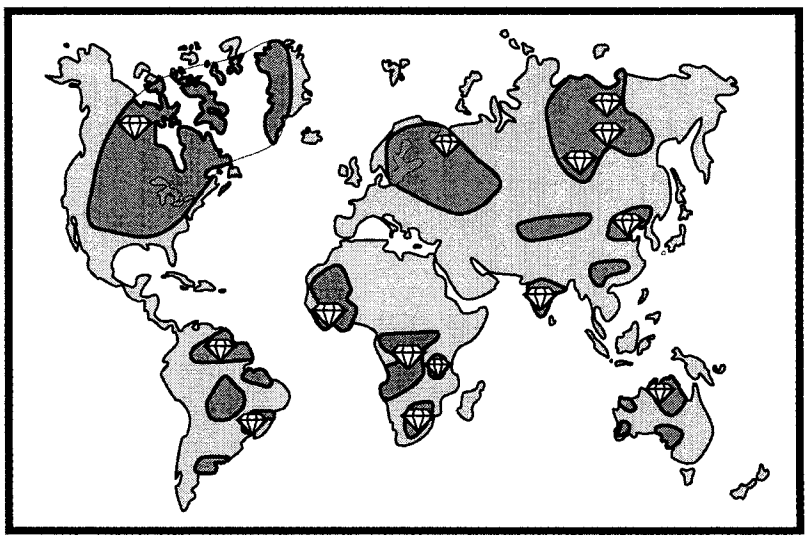

Fig 1.1 World map outlining cratonic areas (dark pink) and associated diamond deposits (diamonds) (after Janse, 1994).

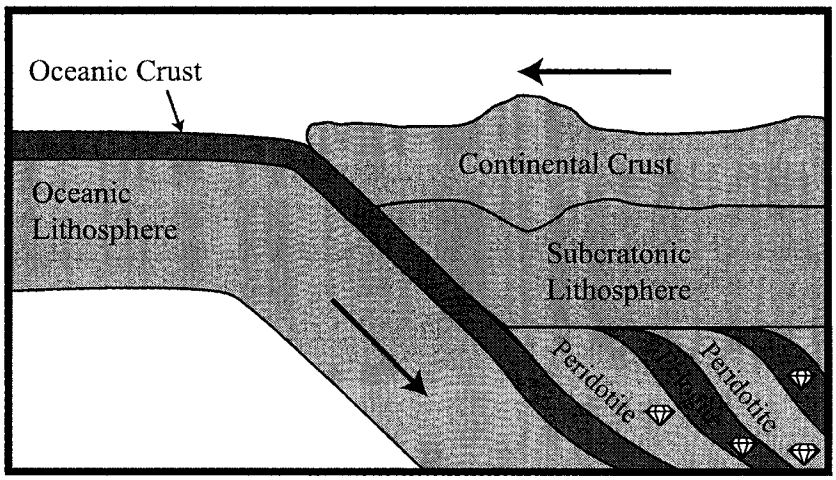

Fig 1.2 Formation of cratonic lithosphere by the imbrication of oceanic crust and lithosphere during shallow subduction (after Helmstaedt and Schulze, 1989). The formation of eclogitic and peridotitic diamonds would occur under similar PT conditions in chemically distinct reservoirs during metasomatism.

CHAPTER 2

CHARACTERIZATION OF DIAMONDS FROM THE BUFFALO HEAD HILLS, ALBERTA

The content of this chapter has been submitted for publication to *Lithos* as:

Diamonds from the Buffalo Head Hills, Alberta:
Formation in a non-conventional setting;

Banas, A., Stachel, T., Muehlenbachs, K., McCandless, T.E.

2.1 Introduction

Traditionally diamond exploration has focused on cratons stabilized in the Archean with no or only minor subsequent tectonothermal overprint. However, in 1997 re-examination of geophysical data originally obtained during hydrocarbon exploration lead to the discovery of diamondiferous kimberlites in an unconventional (non-Archean) setting: the Proterozoic Buffalo Head Terrane in Northern Alberta. Discovered and explored by the Ashton/ Encana/Pure Gold joint venture this cluster of diatremes is now known as the Buffalo Hills Kimberlite Field.

The subcontinental lithospheric mantle beneath the Buffalo Head Terrane has been characterized by Aulbach et al. (2004) and Hood and McCandless (2004) using xenocryst and xenolith compositions. Typical Archean lithospheric mantle is characterized by the presence of distinctly subcalcic garnets derived from strongly depleted harzburgitic sources (e.g. Griffin et al., 1999). The lithospheric mantle beneath the Buffalo Head Terrane, however, is dominated by lherzolite with only minor components of wehrlite, relatively Ca-rich harzburgite, websterite, pyroxenite and eclogite, (Aulbach et al., 2004) and hence lacks a typical Archean signature. Peridotitic xenocryst data presented by Hood and McCandless (2004) also indicate a strong predominance of lherzolitic garnets, with only a small proportion of harzburgitic garnets present. The very high Cr_2O_3 content (12-18 wt%) and relatively high CaO (5-7 wt%) compositions of most of the harzburgitic garnets and the absence of ultradepleted garnet compositions (<1.8 wt% CaO) are again inconsistent with a typical Archean signature (e.g. Grütter et al., 1999). This lack of characteristic Archean

features indicates that either an Archean mantle root is absent beneath the Buffalo Head Terrane or that it has been obliterated during later tectonothermal and metasomatic events (Aulbach et al., 2004).

Subsequent discoveries of diamondiferous kimberlites, such as K252 with a diamond grade of 55 cts/100 tonnes, have rejuvenated interest in the region and facilitated further study into this atypical setting. Diamonds from three additional kimberlite pipes, K11, K91 and K252, were examined and classified according to morphology, carbon isotope composition, nitrogen content and aggregation state, and inclusion chemistry. The results provide further constraints and new insights into the formation of diamonds and the composition of the subcontinental lithospheric mantle beneath the Buffalo Head Terrane.

2.2 Geological Setting

The Buffalo Hills kimberlite field consists of 38 kimberlite pipes, 26 of which are diamondiferous (Hood and McCandless, 2004). The field is located in north-central Alberta and lies within the confines of the Buffalo Head Terrane (Fig. 2.1). The Buffalo Head Terrane is of Lower Proterozoic metamorphic age (2.0 - 2.3 Ga) with presumed Archean precursors (Theriault and Ross, 1991; Villeneuve et al., 1993). It is bounded to the north by the Great Slave Lake shear zone, and bordered by the Taltson, Wabamun and Chinchaga domains to the east, south and west, respectively. The basement rocks are overlain by up to 1600 m of Devonian and Cretaceous sedimentary deposits (Mossop and Shetsen, 1994). The area is variably covered by Quaternary till, glaciofluvial and glaciolacustrine deposits which in places exceed 100 m in thickness (Carlson et al., 1999a; Creighton and Eccles, 2002). The Buffalo Hills kimberlite diatremes intrude into the sedimentary bedrock, and are seismically imaged to reach below the Phanerozoic – Proterozoic boundary (Carlson et al., 1999a), drilling being restricted to the uppermost 200 m. Most bodies are steep-sided, carrot shaped pipes that contain crater facies lithologies (Carlson et al., 1999a). The pipes range in size from less than 1 to 47 Ha with U-Pb perovskite emplacement ages between 88 - 85 Ma (Carlson et al., 1999b; Eccles et al., 2003).

2.3 Samples and techniques

2.3.1 Samples

All diamonds (~700) recovered from pipes K11, K91 and K252 were examined and classified according to morphology and color. A set of 107 diamonds, 0.4 – 3.3 mm in size, was selected for FTIR (Fourier Transform Infrared) analyses. A subset of twenty-two diamonds, 0.6 - 1.2 mm in size, was further analyzed for their carbon isotope composition.

A second set of 54 diamonds was chosen for complete analyses including nitrogen, carbon and inclusion analyses, these samples were restricted to sizes less than 1.2 mm.

2.3.2 Analytical Techniques

Analytical work included the characterization of diamond morphology, surface features and color, infrared spectroscopy, carbon isotopic analyses and identification and analysis of mineral inclusions.

Nitrogen concentrations and aggregation states were determined using a Thermo-Nicolet Fourier Transform Infrared (FTIR) Spectrometer coupled with a Continuum microscope equipped with a KBr beam splitter. The system was purged with a dry nitrogen-oxygen mix to maintain a stable environment. Analyses were carried out on fragments from crushed diamonds (samples A100-141, A200-208, A300-303) and on whole diamonds (samples B100-174, B200-211, B300-318). Spectra (600 – 4000 cm^{-1}) were collected for 200 sec with a spectral resolution of 4 cm^{-1} and an aperture ranging between 50 and 100 μm (determined by sample size). A Type II diamond standard was measured and, after baseline correction, converted to absorption coefficient through normalization of the absorbance at 1995 cm^{-1} (wavenumber) to 11.94 cm^{-1} (absorption coefficient). Sample spectra were first baselined and then the normalized Type II spectrum was subtracted, thereby removing the two phonon (pure diamond) absorption and converting the spectrum to absorption coefficient simultaneously. Spectral deconvolution was used to determine nitrogen contents and aggregation states, based on software provided by David Fischer (Research Laboratories of the Diamond Trading Company, Maidenhead, UK). Concentrations (atomic ppm) were calculated from absorption coefficient values at 1282 cm^{-1} using the factors derived by Boyd et al. (1994) for the A-center and Boyd et al. (1995) for the B-center. Detection limits and errors are strongly dependant on sample quality but typically range from 5 - 15 ppm and about 5-10% of the concentration respectively.

Carbon isotope ratios were measured with a Finnigan Mat 252 Mass Spectrometer, with a precision of ±0.1‰. Diamond fragments (0.5 - 0.15 mg) were combusted (980°C) for 10 hours in evacuated silica glass tubes with 1.0 - 2.0 g of CuO to ensure oxidation. Carbon isotope ratios are reported relative to the VPDB standard.

Mineral inclusions were extracted from the diamonds using a steel crusher. Syngenetic mineral inclusions were identified prior to breakage by the absence of fractures connected to the diamond surface around the inclusion and their geometric shapes. Epigenetic inclusions were identified by the presence of fractures reaching the diamond surface and their altered appearance once released from the diamond. The recovered inclusions were placed in brass pips, set in Araldite epoxy and polished. Major element concentrations were

measured using a JEOL 8900 Electron Microprobe with an accelerating voltage of 15 KeV and a beam current of 20 nA. Peak count times were 15-20 s, background time was ½ peak time. Three spots were measured on each sample and averaged. Resulting detection limits are ~0.03 wt%.

A reference database (Stachel et al., 2000; Stachel and Harris, 1997) is used to compare the mineral inclusion chemistry, the carbon isotopic ratios, and the nitrogen contents and aggregation states of the host diamonds.

2.4 Diamond characteristics

2.4.1 Color

The diamonds show a range of colors from colorless to yellow and brown and overall are mainly clear and transparent (Table 2.1; Appendix B). Colorless diamonds are most abundant, comprising ~60% of the population of each pipe. Brown colors range from light to dark, and are often associated with evidence of plastic deformation (c.f. Harris, 1992). There are no significant differences between the color distributions for each pipe.

2.4.2 Morphology

Diamond shapes include octahedral, tetrahexahedroidal, cuboid as well as twinned and aggregated forms (Table 2.1; Appendix B). Diamond fragments are categorized according to their residual primary features. Irregular shaped stones show no recognizable features and are grouped separately.

The majority of crystals, ~45%, show resorbed octahedral morphologies (tetrahexahedroidal). There are no major differences in morphological distribution between different size classes or pipes (Fig. 2.2). Twins are most common in K252 but are present in smaller quantities in K11 and K91. Cubes are found only in K252 but even there form only a very minor component.

Octahedra

Sharp edged octahedra with smooth faces dominate the octahedral population (Fig. 2.3a). About 0.5% of diamonds show pronounced development of triangular plates (a growth feature) and can be classified as stacked octahedra. Other octahedral surface textures, evident on a minority of the population, are dominated by resorption and etch features: ~10 % of octahedra show minor shield laminae and serrate laminae (Fig. 2.3b). Negative trigons are abundant on approximately 30% of the crystal faces and hexagons were noted

on 2% of crystal faces. A small proportion show signs of minor resorption along the crystal edges tending toward tetrahexahedroidal shapes; crystals with less than 10% resorbed features were classified as octahedra.

Tetrahexahedroida

Tetrahexahedroidal crystals form through the resorption of octahedra (Robinson et al., 1989; Fig. 2.3d). Varying stages of resorption from partial to complete are observed; incomplete resorption with residual octahedral faces is quite common. Tetrahexahedroidal faces are invariably covered with hillock patterns. Three types of hillock patterns were distinguished: 1) fine, narrow, elongate hillocks (Fig. 2.3e), 2) flat, broad hillocks, 3) pyramidal, high relief hillocks. The majority of crystal faces have rough, dull textures usually associated with an abundance of the fine hillock pattern. This often makes the interior of the diamonds difficult to examine. A minority of tetrahexahedroida have smooth, shiny faces associated with the latter two types of hillock patterns (Fig. 2.3d).

Twins

Twinned crystals are represented by contact (macles) and interpenetrant twins with octahedral and tetrahexahedroidal morphologies (Fig. 2.3c). Twins are readily recognized by the presence of twin planes, often expressed by a herringbone pattern. In many tetrahexahedroidal samples it is difficult to identify the twin plane due to extensive resorption but a flattened crystal shape may indicate the presence of twinning. Surface features of twinned crystals are the same as those observed on single crystals.

Aggregates

A small proportion of aggregated crystals with octahedral and tetrahexahedroidal morphology are present. The aggregates observed are formed from 3 up to 6 crystals. The surface features are the same as those observed on single crystals.

Irregular

Irregular crystals have no defining characteristics that allow them to be classified into the above groups. They are commonly fragments with breakage surfaces (both fresh and resorbed) on all sides and no remnant recognizable faces.

2.4.3 Deformation

Deformation, recognized by the presence of lamination lines, was observed in 17% of the diamonds. Lamination lines occur as single or multiple sets of fine lines, parallel to

{111}. Lamination lines along all four octahedral planes have previously been observed on single stones (Harris, 1987), however, usually only one or less commonly up to two sets were observed in this population (Fig. 2.3f). An additional indicator of deformation can be color; Orlov (1973) relates brown coloration to plastic deformation. If lamination lines and color are taken into account ~35% of diamonds indicate some form of plastic deformation. Identification of plastically deformed crystals becomes important when considering the effects of nitrogen aggregation as discussed below.

2.5 Mineral inclusions in diamond

Mineral inclusions of the eclogitic and peridotitic suite, ranging in size from 15-60 μm, were recovered from a restricted sample set. Fourteen of the twenty-seven inclusions were determined to be epigenetic. Table 2.1 lists the inclusion abundance and distribution among the pipes, electron microprobe analyses are reported in Table 2.2.

2.5.1 Syngenetic Inclusions

2.5.1.1 Garnet

Five garnet inclusions were recovered from four diamonds. Garnet inclusion parageneses can be identified by their CaO and Cr_2O_3 content (Gurney et al., 1984; Sobolev et al., 1973). Three garnet inclusions plot within the eclogitic field with Cr_2O_3 contents less than 2 wt% and CaO contents that fall within the normal range for eclogitic garnet inclusions worldwide (Fig. 2.4). Davies et al. (2004) reported nine eclogitic garnets from pipe K14 with compositions that are consistent with our findings but that extend the compositional range to higher CaO contents.

A pyropic garnet inclusion with 6.2 wt% Cr_2O_3 plots within the Ca-saturated field and consequently is assigned to the lherzolitic paragenesis (Fig. 2.4). Davies et al. (2004) recovered two more lherzolitic garnet inclusions with slightly higher Cr_2O_3 contents. Our lherzolitic garnet has a moderate majorite component recognized by an excess of Si (6.41 Si cations per formula unit based on 24 oxygens; Fig. 2.5). Based on the experimental data of Irifune, (1987) a depth of ~400 km is implied for the formation of this garnet. From K14 Davies et al. (2004) report majoritic garnets of the eclogitic suite with associated depths of formation ranging from ~300 – 370 km.

A second peridotitic garnet inclusion, recovered from K252, shows an affinity with the wehrlitic paragenesis. It has a CaO content of 7.2 wt % and Cr_2O_3 5.8 wt % and thus plots above the lherzolite field in Fig 2.4. This paragenesis is rare as an inclusion in diamond,

with only three previous occurrences having been reported: Ellendale, (Jaques et al., 1989); Yakutia, (Sobolev, 1984); Udachnaya, (Sobolev et al., 2004). However, it has been observed from numerous kimberlite occurrences, particularly in Canada (Kopylova et al., 2000), including xenocrysts from the Buffalo Head Hills (Aulbach et al., 2004; Hood and McCandless, 2004).

2.5.1.2 Olivine

Four olivine inclusions were recovered from three diamonds: one from K252 and three from K11. The olivines have Fo contents between 90.7-91.8 mol%. Two olivines have CaO contents that are too low (below 0.04 wt%) to have crystallized in equilibrium with clinopyroxene indicating a harzburgitic affinity (Fig. 2.6). Davies et al. (2004) also recovered two olivines with CaO contents below 0.04 wt% although with higher Fo contents. Two olivines have CaO contents which are unusually high (0.11 and 0.14 wt%) indicating that they crystallized in a Ca-rich wehrlitic environment where Ca in olivine is not buffered by the presence of orthopyroxene (Köhler and Brey, 1990). Davies et al. (2004) report two olivine inclusions with similarly high CaO contents as well as several olivines with intermediate CaO contents representing lherzolitic and harzburgitic parageneses.

2.5.1.3 Clinopyroxene

Three clinopyroxene inclusions were recovered from two diamonds from K252. These inclusions have low Cr_2O_3 contents (≤ 0.03 wt%), Mg # (100*Mg/[Mg+Fe]) of 67-72 and variable Ca # (100*Ca/[Ca+Mg+Fe]) of 39-47 (Fig. 2.7), characteristics that place them within the eclogitic paragenesis. Two inclusions have Na_2O and Al_2O_3 contents indicative of an omphacitic character. The third (A131) inclusion has low Na_2O and Al_2O_3 and can be classified as an augite. Davies et al. (2004) report clinopyroxene inclusion compositions that span the eclogitic (shown in Fig. 2.7), websteritic and peridotitic parageneses.

2.5.1.4 Rutile

One rutile inclusion was recovered from diamond A201 from pipe K11. Analyses reveal the presence of trace amounts of FeO and Al_2O_3. Rutile is associated with the eclogitic paragenesis (Meyer, 1987).

2.5.2 Epigenetic Inclusions

Epigenetic inclusions are found as fracture infillings and altered primary phases. Epigenetic inclusions were recovered from all three pipes and include serpentine, calcite, dolomite and biotite and are not further considered.

2.6 Carbon Isotopic Composition

A subset of 77 samples, spanning the whole range of nitrogen contents and aggregation states, was selected for carbon isotope analyses. These samples show a range in carbon isotopic composition from -22.8‰ to -2.5‰, with a bimodal distribution and modes around -5‰ and -17‰ (Fig. 2.8). No correlation between carbon isotopic composition and morphology or color was observed. The lower $\delta^{13}C$ population (~-17‰) is dominated by diamonds of eclogitic paragenesis as indicated by the presence of eclogitic inclusions. Two of the samples with peridotitic inclusions also plot within this lower range, one of which contains the wehrlitic garnet and this diamond has the lightest measured composition at -22.8‰. The higher peak around -5‰ is populated by diamonds of both peridotitic and eclogitic paragenesis.

Davies et al. (2004) report isotopic data for 39 samples from pipes K10 and K14. $\delta^{13}C$ ranges from -20.6‰ to -2.7‰ and again has a bimodal distribution (modes at -5‰ and -15‰) in agreement with this study.

Worldwide, diamonds have a broad range in carbon isotope composition from -30 ‰ to +3 ‰ with a normal distribution (mode ~ -5‰). Peridotitic diamonds are mainly restricted to values between -10 and -2 ‰ whereas eclogitic diamonds have isotopic compositions that span the whole range (Cartigny et al., 1998a and b; Kirkley et al., 1991).

2.7 Impurities

Nitrogen is the most abundant substitutional impurity in diamond. It enters the diamond lattice in single substitution during diamond growth, with variable amounts being incorporated. Worldwide concentrations ranging from below detection to ~5500 ppm have been reported (Sellschop et al., 1979). Most diamonds have nitrogen concentrations <500 ppm but many deposits exhibit broad ranges from 0 to >2500 ppm (Bibby, 1982). Buffalo Hills diamonds have nitrogen contents ranging from below detection to 3300 ppm. Variations within single diamond crystals are as high as a few hundred ppm; however, systematic variations with growth could not be assessed as nitrogen was measured on cleavage fragments after breakage. Hydrogen impurities, indicated by a narrow absorption band at 3107 cm^{-1}, were noted in 77% of the samples.

Diamonds without detectable nitrogen (i.e. ≤10 ppm) are classified as Type II. In this population ~20% of the diamonds are classified as Type II (Table 2.1). The Type II diamonds span the whole range of sizes and have a broad range of carbon isotope compositions (-16.6 to -2.5‰). Davies et al. (2004) also noted a high proportion (~ 45%) of Type II diamonds

within their data set. Worldwide, Type II diamonds comprise only about 2% of the diamond population, however a small number of deposits show a higher abundance (e.g. Akwatia in Ghana, 37%, Stachel and Harris, 1997).

Diamonds with measurable nitrogen concentrations are classified as Type I and can be further subdivided based on the aggregation state of nitrogen (Evans et al., 1981). Diamonds with nitrogen in single substitution are classified as Type Ib and are rare in nature. Diamonds with aggregated nitrogen are classified as Type Ia. Nitrogen aggregation proceeds to form pairs, classified as Type IaA and rings of four surrounding a vacancy, classified as Type IaB (Davies, 1976; Evans et al., 1981). Type IaAB diamonds, containing nitrogen in both aggregation states, are common and often also have an absorbance peak at 1370 cm^{-1} associated with platelets (Evans et al., 1981; Sobolev et al., 1968). Eighty percent of the samples in our study are Type Ia with varying stages of aggregation present at all nitrogen concentrations (Fig. 2.9). Aggregation in Type Ia diamonds is measured as the relative proportion of nitrogen present in the B-center (%B). Type IaA (%B < 10%) comprise 10% of the population, with nitrogen concentrations between 40 and 2400 ppm. Approximately 32% of the diamonds are Type IaAB (defined as %B = 10 - 90%) and have nitrogen concentrations ranging from 8 ppm to 2500 ppm. About 60% of the type IaAB diamonds also show an absorbance at 1370 cm^{-1} (i.e. have a platelet component). The lack of a platelet component in 30% of the samples and the low platelet component of 75% of the remaining Type IaAB samples indicates that catastrophic platelet degradation (Woods, 1986), possibly related to transient heating events (Evans et al., 1995), occurred (Fig. 2.10). Type IaB (%B > 90%) diamonds are the most abundant comprising 37% of the samples and show nitrogen concentrations from 6 ppm to 3300 ppm. The occurrence of diamonds with fully aggregated nitrogen (Type IaB) and very low nitrogen concentrations is highly unusual and distinct to this area.

There are major differences between the three pipes with respect to nitrogen content and distribution of aggregation. K252 (117 diamonds) dominates the above distribution and hence the values reported above reflect mainly this pipe. K11 (21 diamonds) shows a much higher proportion of Type II diamonds, ~50%, and no Type IaB diamonds. K91 (23 diamonds) has only one Type II diamond and is dominated by Type IaB diamonds. The discrepancy maybe due to small sample sizes for the three pipes precluding statistically valid comparisons. K14 (29 diamonds, Davies et al. 2004) shows a distribution similar to that K252.

2.8 Discussion

Studies of mantle derived xenoliths (e.g. Boyd, 1989; Griffin et al., 2003; Schulze, 1989) and inclusions in diamonds (e.g. Gurney, 1989; Harris, 1992; Meyer, 1987; Stachel et al., 2004) have shown that in diamond source regions the subcratonic lithospheric mantle is dominated by peridotite, with only a minor eclogite component. Several lines of evidence indicate that diamonds from the Buffalo Hills kimberlites are distinct from the peridotite dominated production of many of the classical diamond deposits.

2.8.1 Implications from carbon isotope composition

The Buffalo Hills diamonds show a high proportion of low $\delta^{13}C$ compositions associated with inclusions of eclogitic paragenesis. If this association is extended to the diamonds without inclusions for which only carbon isotope data are available it implies that the composition of the diamond-bearing mantle beneath the Buffalo Head Terrane is dominated by eclogite with only a minor peridotitic component. This places the Buffalo Hills within a small group of deposits worldwide that are characterized by a predominance of eclogitic diamonds including the Argyle lamproite (Jaques et al., 1989); the Orapa (Deines et al., 1993; Gurney et al., 1984), Premier (Gurney et al., 1985), and Jwaneng kimberlite pipes (Deines et al., 1997), and the Guaniamo deposits (Kaminsky et al., 2000). On the Kalahari craton a high proportion of eclogitic diamonds is characteristic of areas that were affected by Proterozoic tectonothermal events (Shirey et al., 2002). However, these areas retained an Archean subcontinental lithospheric mantle, while an Archean signature is not preserved in the Buffalo Head Terrane (Aulbach et al., 2004).

The source of isotopically light carbon for diamonds is still debated. The broad range in $\delta^{13}C$ exhibited by eclogitic diamonds encompasses the typical isotopic compositions of organic matter, $\delta^{13}C \sim -35$ to -20 ‰, and marine carbonates, $\delta^{13}C \sim -2$ to +2 ‰, (Kirkley et al., 1991). This has led to the suggestion that subducted oceanic crust containing organic matter and marine carbonates is involved in the formation of eclogitic diamonds. Subducting basaltic oceanic crust recrystallizes to eclogite during prograde metamorphism, the accompanying carbonaceous material would be converted to eclogitic diamond (Kirkley et al., 1991; McCandless and Gurney, 1997). Alternatively, the broad range of $\delta^{13}C$ values in eclogites could be created through fractionation processes. An unbuffered, free CO_2-fluid phase can exist in eclogite (Luth, 1993), escape of CO_2 (e.g. from an ascending carbonatite) would leave an isotopically depleted residue encompassing the observed isotopic range (Cartigny et al., 1998a). In peridotite, CO_2 is buffered by the presence of olivine and orthopyroxene (Brey et al., 1983; Wyllie and Huang, 1976) and hence fractionation of carbon isotopes involving an oxidized fluid phase cannot occur.

2.8.2 Sublithospheric diamonds

The incorporation of nitrogen into the diamond lattice is not fully understood. It has been suggested that the uptake of nitrogen is a function of the growth rate of the diamond (Boyd et al., 1994; Cartigny et al., 2001). In this case slower growth would cause less nitrogen to be incorporated into the diamond lattice. Additionally, based on observations that diamonds of similar $\delta^{13}C$ composition and paragenetic association have varied nitrogen contents, Deines et al. (1989) suggested that local variations in nitrogen content exist in the mantle and influence nitrogen concentrations in diamond. Furthermore an association of nitrogen-free diamonds with a deep origin has been reported from various occurrences (Davies et al., 1999; Hutchison et al., 1999; Kaminsky et al., 2001; Stachel et al., 2002). A large proportion of Type II diamonds is a distinguishing characteristic of the Buffalo Head Terrane and may suggest that a portion of the diamonds grew under stable conditions at high temperatures (great depth).

The remaining nitrogen-bearing diamonds have variable nitrogen concentrations and aggregation states suggesting they are derived from multiple populations. The kinetics of nitrogen aggregation has been quantified experimentally and is understood to be dependent on concentration, temperature and storage time (Evans and Harris, 1989). Plastic deformation may increase the rate of nitrogen aggregation, hence the dataset was tested for a possible correlation between nitrogen concentration, aggregation and evidence of deformation (lamination lines, color) in the diamonds. However, no correlation between nitrogen concentration/aggregation state and deformation is evident in the Buffalo Hills samples. This is important when considering the implications of Type IaB diamonds especially those with low nitrogen concentrations. Although some of these diamonds show signs of deformation, most appear undeformed and consequently the high aggregation must be caused by a different mechanism: high time averaged mantle residence temperature. Time averaged temperatures do not distinguish between storage at constant temperature and for example, formation in a very hot environment, in which the nitrogen aggregates quickly, and subsequent storage for longer periods in a cool lithosphere. Considering Type IaB diamonds with the lowest nitrogen concentrations, under normal lithospheric conditions, at temperatures below 1250°C, the time required to fully aggregate such low nitrogen concentrations exceeds the age of the earth. If these diamonds had formed and been stored in the lithosphere then a very high geothermal gradient below the Buffalo Head Terrane would be required. This is contrary to the "normal" geothermal gradient of ~38-39 mW/m^2 reported by Aulbach et al. (2004) from their xenocryst analyses. Alternatively, the diamonds could have formed and been stored under sublithospheric conditions which

would produce the observed aggregation states and nitrogen contents within reasonable residence times (e.g. 1 Ga; Fig. 2.9).

Additional evidence for sublithospheric diamond formation beneath the Buffalo Head Terrane is derived from the presence of majoritic garnet inclusions with formation depths of ~300-400 km. All the majoritic inclusions are associated with Type II diamonds. This strengthens the assumption that part of the Type II diamond population could be derived from a sublithospheric source. Furthermore Davies et al. (2004) report in a Type II diamond the recovery of a ferropericlase inclusion suggestive of diamond sources in the lower mantle.

2.8.3 Lithospheric diamonds

The Type IaAB diamonds are associated with both the eclogitic and peridotitic suites. The diamonds have variable aggregation states and nitrogen contents consistent with lower temperatures (Fig. 2.9) and thus shallower depths typical of "normal" lithospheric conditions.

The Type IaA diamonds indicate either that diamond storage occurred at even lower temperatures (shallower depths) or that there was a younger phase of diamond formation.

2.8.4 Diamond growth beneath the Buffalo Head Terrane

Multiple phases of diamond formation are supported by the data collected in this study. Formation under sublithospheric conditions is supported by the presence of a majorite inclusion in diamond and the high abundance of Type II and Type IaB diamonds. Davies et al. (2004) also noted the presence of majorite inclusions and proposed crystallization in an ascending plume. The three majorites recovered from two diamonds by Davies et al. (2004) from K14 have Mg-numbers of 54-56, constant CaO of 11 wt%, TiO_2 of 1.3 -1.6 wt % and Na_2O of 1.5-1.6 wt%. Such compositions are inconsistent with precipitation from very deep seated, plume-derived melts and suggest formation in a source of "basaltic" bulk composition. The lherzolitic majorite recovered from K11 has 6.3 wt % Cr_2O_3, again a signature inconsistent with a high pressure plume origin but indicative of a source that experienced previous melt depletion at low pressure (Stachel et al., 1998 and references therein).We interpret these majorite inclusions to indicate formation at ~300-400 km depth in the eclogitic and peridotitic portion of a subducting oceanic slab. At the 660 km discontinuity subducting slabs may become buoyant forming, over time, large accumulations (megaliths) of relatively cool but deformed former oceanic lithosphere (Ringwood, 1991). A portion of the Type II and Type IaB diamonds may have formed under transition zone and lower mantle conditions in such a megalith. The single ferropericlase

inclusion recovered by Davies et al. (2004) may reflect the lower mantle portion of this megalith.

The remaining diamonds formed under "normal" conditions in the lithospheric mantle. The large range of carbon isotopic compositions for lithospheric eclogitic and wehrlitic diamonds may result from isotopic fractionation within a percolating C-H-O fluid/melt or may point to variable organic input. Infiltrating fluids of carbonatitic affinity could be the source of the Ca-enrichment needed to form the wehrlitic suite.

Transport of transition zone and lower mantle diamonds to the base of the lithosphere through mantle plumes, as envisaged by Davies et al. (2004), is certainly viable. Alternatively, disaggregation and melting of megaliths and the surrounding pyrolite may generate melt batches that ascend more rapidly towards the lithosphere and that may directly relate to kimberlite volcanism. A temporal link between exhumation of ultradeep diamonds and kimberlite activity is indicated by the unexsolved nature of majorite inclusions in the Buffalo Hills diamonds. Within its primary stability field diamond is not a rigid pressure vessel but deforms plastically through slip along octahedral planes (De Vries, 1975). If sub-lithospheric diamonds had resided within the lithospheric mantle for extended periods of time, majorite garnet should have converted to touching inclusion pairs of "normal" garnet and pyroxene. The observation that pyroxene exsolutions are absent suggests rapid exhumation from the transition zone and asthenosphere in a kimberlite magma (Ringwood et al., 1992) leading to Cretaceous volcanism in the Buffalo Hills.

2.9 Conclusion

The Buffalo Hills kimberlites intrude the Proterozoic Buffalo Head Terrane, a setting uncharacteristic for economically viable diamond occurrences. The recovered xenocryst and xenolith suites show a scarcity of typical mantle indicator minerals suggesting an atypical mantle composition (Aulbach et al., 2004; Hood and McCandless, 2004). A lack of typical inclusion minerals such as subcalcic harzburgitic garnet is also observed for the diamonds. A high relative abundance of eclogitic inclusions and low $\delta^{13}C$ diamonds and the presence of a wehrlitic inclusion paragenesis point to mantle sources which are distinctly different from that of diamond occurrences worldwide. Additionally, the observation of a high abundance of Type II and Type IaB diamonds combined with the presence of majorite inclusions indicate that a portion of the diamonds are of sublithospheric origin, probably derived from an oceanic slab and resulting megalith. Combined these characteristics define a deposit which is distinctive in character from typical diamond deposits and emphasize that unconventional tectonic settings may host economically viable diamond deposits albeit with unique characteristics.

References

Aulbach, S., Griffin, W.L., O'Reilly, S.Y. and McCandless, T.E., 2004. Genesis and evolution of the lithospheric mantle beneath the Buffalo Head Terrane, Alberta (Canada). Lithos, 77(1-4): 413-451.

Bibby, D., 1982. Impurities in natural diamond. Chemistry and Physics of Carbon, 18: 1-91.

Boyd, F.R., 1989. Compositional distinction between oceanic and cratonic lithosphere. Earth and Planetary Science Letters, 96(1-2): 15-26.

Boyd, S.R., Kiflawi, I. and Woods, G.S., 1994. The relationship between infrared absorption and the A defect concentration in diamond. Philosophical Magazine B, 69(6): 1149-1153.

Boyd, S.R., Kiflawi, I. and Woods, G.S., 1995. Infrared absorption by the B nitrogen aggregate in diamond. Philosophical Magazine B, 72(3): 351-361.

Brey, G.P. et al., 1983. Pyroxene-carbonate reactions in the upper mantle. Earth and Planetary Science Letters, 62: 63-74.

Carlson, S.M., Hillier, W.D., Hood, C.T., Pryde, R.P. and Skelton, D.N., 1999a. The Buffalo Hills kimberlites: A newly discovered diamondiferous kimberlite province in North-central Alberta, Canada. In: J.J. Gurney, J.L. Gurney, M.D. Pascoe and S.H. Richardson (Editors), The J.B. Dawson Volume, Proceedings of the VIIth International Kimberlite Conference. Red Roof Design, Capetown, SA, pp. 109-116.

Carlson, J.A., Kirkley, M.B., Thomas, E.M. and Hillier, W.D, 1999b. Recent Canadian kimberlite discoveries. In: J.J. Gurney, J.L. Gurney, M.D. Pascoe and S.H. Richardson (Editors), The J.B. Dawson Volume, Proceedings of the VIIth International Kimberlite Conference. Red Roof Design, Capetown, pp. 81-89.

Cartigny, P., Harris, J.W. and Javoy, M., 1998a. Eclogitic diamond formation at Jwaneng: No room for a recycled component. Science, 280(5368): 1421-1424.

Cartigny, P., Harris, J.W., Phillips, D., Girard, M. and Javoy, M., 1998b. Subduction-related diamonds? The evidence for a mantle-derived origin from coupled delta C-13-delta N-15 determinations. Chemical Geology, 147(1-2): 147-159.

Cartigny, P., Harris, J.W. and Javoy, M., 2001. Diamond genesis, mantle fractionations and mantle nitrogen content: a study of delta C-13-N concentrations in diamonds. Earth and Planetary Science Letters, 185(1-2): 85-98.

Creighton, S. and Eccles, R., 2002. Compilation of Alberta ultramafic rock occurrences: Location, ground geophysics, drill hole logs and diamond content, Geo-Note 2002-23: Electronic PDF format. Alberta Energy and Utilities Board, Alberta Geological Survey, Edmonton.

Davies, G., 1976. The A nitrogen aggregate in diamond - its symmetry and possible structure. J. Phys. C: Solid State Phys., 9: L537-L542.

Davies, R.M. et al., 1999. Diamonds from the deep: pipe DO-27, Slave Craton, Canada. In: J.J. Gurney, J.L. Gurney, M.D. Pascoe and S.H. Richardson (Editors), The J.B. Dawson Volume, Proceedings of the VIIth International Kimberlite Conference. Red Roof Design, Cape Town, pp. 148-155.

Davies, R.M., Griffin, W.L., O'Reilly, S.Y. and McCandless, T.E., 2004. Inclusions in diamonds from the K14 and K10 kimberlites, Buffalo Hills, Alberta, Canada: diamond growth in a plume? Lithos, 77(1-4): 99-111.

De Vries, R.C., 1975. Plastic deformation and "work-hardening" of diamond. Mater. Res. Bull., 10: 1193-1200.

Deines, P., Harris, J.W., Spear, P.M. and Gurney, J.J., 1989. Nitrogen and ^{13}C content of Finsch and Premier diamonds and their implications. Geochimica et Cosmochimica Acta, 53(6): 1367-1378.

Deines, P., Harris, J.W. and Gurney, J.J., 1993. Depth-related carbon isotope and nitrogen concentration variability in the mantle below the Orapa kimberlite, Botswana, Africa. Geochimica et Cosmochimica Acta, 57: 2781-2796.

Deines, P., Harris, J.W. and Gurney, J.J., 1997. Carbon isotope ratios, nitrogen content and aggregation state, and inclusion chemistry of diamonds from Jwaneng, Botswana. Geochimica et Cosmochimica Acta, 61(18): 3993-4005.

Eccles, D., Pana, D., Paulen, R., Olson, R. and Magee, D., 2003. Discovery and geological setting of the northern Alberta kimberlite province. In: B. Kjarsgaard (Editor), 8th International Kimberlite Conference, Slave Province and Northern Alberta Field Trip Guidebook, pp. 1-10.

Evans, T., Qi, Z. and Maguire, J., 1981. The stages of nitrogen aggregation in diamond. Journal of Physics. C: Solid State Physics, 14(12): L379-L384.

Evans, T. and Harris, J.W., 1989. Nitrogen aggregation, inclusion equilibration temperatures and the age of diamonds. In: J. Ross et al. (Editors), Kimberlites and related rocks. GSA Spec Publ 14. Blackwell, Carlton, pp. 1001-1006.

Evans, T., Kiflawi, I., Luyten, W., Vantendeloo, G. and Woods, G.S., 1995. Conversion of Platelets into Dislocation Loops and Voidite Formation in Type Iab Diamonds. Proceedings of the Royal Society of London Series A-Mathematical and Physical Sciences, 449(1936): 295-313.

Griffin, W.L., O'Reilly, S.Y. and Ryan, C.G., 1999. The composition and origin of subcontinental lithospheric mantle. In: Y. Fei, C.M. Bertka and B.O. Mysen (Editors), Mantle Petrology: Field Observations and High Pressure Experimentation: A tribute to Francis R. (Joe) Boyd. Special Publication. The Geochemical Society, Houston, pp. 13-45.

Griffin, W.L. et al., 2003. The origin and evolution of Archean lithospheric mantle. Precambrian Research, 127(2003): 19-41.

Grütter, H.S., Apter, D.B. and Kong, J., 1999. Crust-mantle coupling: evidence from mantle-derived xenocrystic garnets. In: J.J. Gurney, J.L. Gurney, M.D. Pascoe and S.H. Richardson (Editors), The J.B. Dawson Volume, Proceedings of the VIIth International Kimberlite Conference. Red Roof Design, Cape Town, pp. 307-313.

Gurney, J.J., 1989. Diamonds. In: J. Ross et al. (Editors), Kimberlites and related rocks. GSA Spec Publ 14. Blackwell, Carlton, pp. 935-965.

Gurney, J.J., Harris, J.W. and Rickard, R.S., 1984. Silicate and oxide inclusions in diamonds from the Orapa Mine, Botswana. In: J. Kornprobst (Editor), Kimberlites II: the mantle and crust-mantle relationships. Elsevier, Amsterdam, pp. 3-9.

Gurney, J.J., Harris, J.W., Rickard, R.S. and Moore, R.O., 1985. Premier Mine diamond inclusions. Trans Geol Soc S Afr, 88: 301-310.

Harris, J.W., 1987. Recent physical, chemical and isotopic research of diamond. In: P. Nixon (Editor), Mantle Xenoliths. John Wiley and Sons Ltd, pp. 477-500.

Harris, J.W., 1992. Diamond geology. In: J.E. Field (Editor), The properties of natural and synthetic diamond. Academic Press, London, pp. 345-393.

Hood, C.T.S. and McCandless, T.E., 2004. Systematic variations in xenocryst mineral composition at the province scale, Buffalo Hills kimberlites, Alberta, Canada. Lithos, 77(1-4): 733-747.

Hutchison, M.T., Cartigny, P. and Harris, J.W., 1999. Carbon and nitrogen compositions and physical characteristics of transition zone and lower mantle diamonds from Sao Luiz, Brazil. In: J.J. Gurney, J.L. Gurney, M.D. Pascoe and S.H. Richardson (Editors), The J.B. Dawson Volume, Proceedings of the VIIth International Kimberlite Conference. Red Roof Design, Cape Town, pp. 372-382.

Irifune, T., 1987. An experimental investigation of the pyroxene-garnet transformation in a pyrolite composition and its bearing on the constitution of the mantle. Physics of the Earth and Planetary Interiors, 45(4): 324-336.

Jaques, A.L. et al., 1989. Composition of crystalline inclusions and C-isotopic composition of Argyle and Ellendale diamonds. In: J. Ross et. al (Editor), Kimberlites and Related Rocks. 2. Their Mantle/Crust Setting. Geol. Soc. Aust., Spec. Publ. 14, pp. 966-989.

Kaminsky, F.V., Zakharchenko, O.D., Griffin, W.L., Channer, D.M.D. and Khachatryan-Blinova, G.K., 2000. Diamond from the Guaniamo area, Venezuela. Canadian Mineralogist, 38: 1347-1370.

Kaminsky, F.V. et al., 2001. Superdeep diamonds from the Juina area, Mato Grosso State, Brazil. Contributions to Mineralogy and Petrology, 140(6): 734-753.

Kirkley, M.B., Gurney, J.J., Otter, M.L., Hill, S.J. and Daniels, L.R., 1991. The application of C isotope measurements to the identification of the sources of C in diamonds: a review. Applied Geochemistry, 6(5): 477-494.

Köhler, T. and Brey, G.P., 1990. Calcium exchange between olivine and clinopyroxene calibrated as geothermobarometer for natural peridotites from 2 to 60 kb with applications. Geochimica et Cosmochimica Acta, 54: 2375-2388.

Kopylova, M.G., Russell, J.K., Stanley, C. and Cookenboo, H., 2000. Garnet from Cr- and Ca-saturated mantle: implications for diamond exploration. Journal of Geochemical Exploration, 68(3): 183-199.

Luth, R.W., 1993. Diamonds, eclogites, and the oxidation state of the Earth's mantle. Science, 261(5117): 66-68.

McCandless, T.E. and Gurney, J.J., 1997. Diamond eclogites: Comparison with carbonaceous chondrites, carbonaceous shales, and microbial carbon-enriched MORB. Geologiya I Geofizika, 38(2): 371-381.

Meyer, H.O.A., 1987. Inclusions in diamond. In: P.H. Nixon (Editor), Mantle xenoliths. John Wiley & Sons Ltd., Chichester, pp. 501-522.

Mossop, G. and Shetsen, I., (compilers) 1994. Geological Atlas of the western Canada sedimantary basin. Canadian Society of Petroleum Geologists and Alberta Research Council, Calgary, AB, 510 pp.

Orlov, Y., 1973. The mineralogy of diamond. John Wiley and Sons, 264 pp.

Ringwood, A.E., 1991. Phase transformations and their bearing on the constitution and dynamics of the mantle. Geochimica et Cosmochimica Acta, 55(8): 2083-2110.

Ringwood, A.E., Kesson, S.E., Hibberson, W. and Ware, N., 1992. Origin of Kimberlites and Related Magmas. Earth and Planetary Science Letters, 113(4): 521-538.

Robinson, D., Scott, J., Van Niekerk, A. and Anderson, V., 1989. The sequence of events reflected in the diamonds of some southern African kimberlites, 4th International Kimberlite Conference. Geol. Soc. Australia, Sp. Pub. 14, pp. 990-999.

Schulze, D.J., 1989. Constraints on the abundance of eclogite in the upper mantle. Journal of Geophysical Research-Solid Earth and Planets, 94(B4): 4205-4212.

Sellschop, J., Madiba, C., Annegarn, H. and Shongwe, S., 1979. Volatile light elements in diamond. Diamond Research. Industrial Diamond Information Bureau, London, United Kingdom, 24-30 pp.

Shirey, S.B. et al., 2002. Diamond genesis, seismic structure, and evolution of the Kaapvaal-Zimbabwe craton. Science, 297(5587): 1683-1686.

Sobolev, E., Lisoivan, V. and Lenskava, S., 1968. The relation between the "spike" extra reflections in the Laue patterns of natural diamonds and their optical properties. Soviet Physics-Crystallography, 12: 665-668.

Sobolev, N.V., 1984. Crystalline inclusions in diamonds from New South Wales, Australia. In: J. Glover and P. Harris (Editors), Kimberlite occurrence and origin: a basis for conceptual models in exploration. Geological Department University Extension, University of Western Australia, pp. 213-226.

Sobolev, N.V., Lavrent'ev, Y.G., Pokhilenko, N.P. and Usova, L.V., 1973. Chrome-rich garnets from the kimberlites of Yakutia and their paragenesis. Contributions to Mineralogy and Petrology, 40(1): 39-52.

Sobolev, N.V. et al., 2004. Mineral inclusions in microdiamonds and macrodiamonds from kimberlites of Yakutia: a comparative study. Lithos, 77(1-4): 225-242.

Stachel, T. and Harris, J.W., 1997. Syngenetic inclusions in diamond from Birim Field (Ghana) - a deep peridotitic profile with a history of depletion and enrichment. Contributions to Mineralogy and Petrology, 127: 336-352.

Stachel, T., Harris, J.W. and Brey, G.P., 1998. Rare and unusual mineral inclusions in diamonds from Mwadui, Tanzania. Contributions to Mineralogy and Petrology, 132(3): 307.

Stachel, T., Brey, G.P. and Harris, J.W., 2000. Kankan diamonds (Guinea) I: from the lithosphere down to the transition zone. Contributions to Mineralogy and Petrology, 140: 1-15.

Stachel, T., Harris, J.W., Aulbach, S. and Deines, P., 2002. Kankan diamonds (Guinea) III: $\delta^{13}C$ and nitrogen characteristics of deep diamonds. Contributions to Mineralogy and Petrology, 142: 465-475.

Stachel, T. et al., 2004. The trace element composition of silicate inclusions in diamonds: a review. Lithos, 77: 1-19.

Taylor, W., Jaques, A., and Ridd, M. (1990) Nitrogen-defect aggregation characteristics of some Australasian diamonds: Time-temperature constraints on the source regions of pipe and alluvial diamonds. American Mineralogist, 75, 1290-1310.

Theriault, R. and Ross, G., 1991. Nd isotopic evidence for crustal recycling in the ca. 2.0 Ga subsurface of Western Canada. Canadian Journal of Earth Sciences, 28(8): 1140-1147.

Villeneuve, M. et al., 1993. Tectonic subdivision and U-Pb geochronolgy of the crystalline basement of the Alberta basin, western Canada. Geological Survey of Canada,, Bulletin 447.

Woods, G.S., 1986. Platelets and the Infrared-Absorption of Type-Ia Diamonds. Proceedings of the Royal Society of London Series A-Mathematical Physical and Engineering Sciences, 407(1832): 219-238.

Wyllie, P.J. and Huang, W.L., 1976. Carbonation and melting reactions in the system CaO-MgO-SiO2-CO2 at mantle pressures with geophysical and petrological applications. Contributions to Mineralogy and Petrology, 54: 79-107.

Table 2.1:
Physical, carbon isotope and nitrogen characteristics and inclusions in diamonds from the Buffalo Heads Hills, Alberta.

Pipe	Sample	Weight (mg)	Shape	Col.	P.D.	$\delta^{13}C$ (‰)	N (ppm)	% B	Type	H	Para.	Assem.
K252	A100	2.7	agg thh	c	n	-6.40	116.0	0	IaA	n		serp
K252	A101	1.8	thh	ly	n	-7.71	18.0	41	IaAB	n		
K252	A102	2.9	thh	b	n	-4.71	0		II	n		serp
K252	A103	1.1	thh	b	n	-4.13	0		II	y		
K252	A104	1.6	twin thh	c	n	-6.73	1494.1	12	IaAB	y		
K252	A105	1.2	thh	b	y	-5.93	939.9	17	IaAB	y		
K252	A106	1.8	thh frag	b	y	-20.99	39.4		IaB	y		
K252	A107	1.5	thh	b	y	-18.06	140.3		IaB	y		
K252	A109	2.4	thh	c	y	-16.19	15.8	71	IaAB	y		calc
K252	A110	1.9	thh	c	n	-17.38	37.6	0	IaA	y	e	grt
K252	A111	1.7	thh	c	n	-14.80	ns					
K252	A112	3.1	thh	c	n	-15.84	0		II	y	p	ol
K252	A113	1.9	thh	b	n	-17.93	ns					
K252	A114	1.6	thh	c	n	-7.91	737.8	2	IaA	n		
K252	A115	1.7	thh	b	y	-17.60	13.5		IaAB	y	e	grt
K252	A116	2.4	twin thh	b	n	-15.36	23.1	100	IaB	y		
K252	A117	2.4	twin thh	c	n	-17.17	74.9		IaB	y		
K252	A118	2.1	thh	c	n	-5.29	0		II	y		
K252	A119	2.8	twin thh	c	n	-15.12	139.6	100	IaB	y	e	cpx
K252	A120	1.8	thh	lb	y	-6.54	2266.6	15	IaAB	y		
K252	A121	2.1	agg octa	b	n	-13.90	1358.6	100	IaB	y		
K252	A122	2.2	thh frag	c	n	-8.40	0		II	y		
K252	A123	0.7	thh frag	c	n	-3.94	0		II	n	e	grt
K252	A124	0.4	agg thh	c	n	-17.24	99.2	100	IaB	y		
K252	A125	0.8	irr	c	y	-15.30	1615.4	100	IaB	y		
K252	A126	2.0	octa frag	c	n	-13.95	0		II	y		
K252	A127	0.5	thh frag	y	n	-4.74	24.0	100	IaB	y		serp
K252	A128	2.6	thh frag	c	y	-6.84	36.6		IaB	y	e	grt
K252	A129	1.4	thh frag	c	y	-10.19	0		II	y		
K252	A130	2.6	thh frag	c	n	-8.00	130.5	100	IaB	y		serp
K252	A131	1.8	irr	b	y	-7.69	913.3	1	IaA	y	e	cpx
K252	A132	2.6	thh	c	y	-4.67	504.8	10	IaA	n		

Table 2.1 cont.

Pipe	Sample	Weight (mg)	Shape	Col.	P.D.	$\delta^{13}C$ (‰)	N (ppm)	% B	Type	H	Para.	Assem.
K252	A133	3.1	thh	b	n	-17.30	17.6	91	IaB	y		serp
K252	A134	2.3	thh frag	c	n	-8.53	1571.0		IaAB	y		
K252	A135	4.6	agg thh	b	y	-13.27	22.7		IaB	y		serp
K252	A136	2.3	agg thh	lb	y	-15.52	1241.7	98	IaB	y		
K252	A137	2.4	agg thh	c	n	-5.59	33.9	50	IaAB	y		
K252	A138	2.3	thh	c	n	-3.10	0		II	n		
K252	A139	1.5	agg thh	b	n	-15.52	0		II	y		
K252	A140	3.0	agg thh	b	y	-13.75	94.7	100	IaB	n		
K252	A141	1.5	thh frag	c	n	-22.78	88.3	53	IaAB	y	wh	gt
K252	B100	0.9	thh	c	n		1597.1	100	IaB	y		
K252	B101		thh	c	n		1434.7	28	IaAB	y		
K252	B102		octa	c	n		374.35	100	IaB	y		
K252	B103	0.8	thh frag	c	y	-5.77	0		II	n		
K252	B104		thh	c	n		177.6	10	IaA	n		
K252	B105		frag	ly	n		0		II	y		
K252	B106		thh frag	ly	y		40.5	75	IaAB	y		
K252	B107		irr	c	n		827.3	100	IaB	y		
K252	B108		frag	b	n		1816.4	100	IaB	y		
K252	B109		frag	c	n		0		II	n		
K252	B110	1.7	octa frag	c	n	-2.48	0		II	y		
K252	B111	0.9	agg octa	b	n	-6.39	91.2	24	IaAB	n		
K252	B112		irr	c	n		1243.4	6	IaA	y		
K252	B113		twin octa	c	n		141.9	100	IaB	y		
K252	B114		thh	lg	n		1299.2	25	IaAB	y		
K252	B115		frag	c	n		0		II	y		
K252	B116		frag	lb	n		0		II	y		
K252	B117		frag	lb	n		35.1	96	IaB	y		
K252	B118		frag	lb	n		320.9	0	IaA	n		
K252	B119		thh	b	n		42.7	100	IaB	y		
K252	B120		thh	c	n		1252.1	100	IaB	y		
K252	B121		frag	lb	y		99.9	100	IaB	y		
K252	B122	2.9	thh	c	n	-3.26	1842.2	0	IaA	y		
K252	B123		frag	lb	n		109.1	68	IaAB	y		

Table 2.1 cont.

Pipe	Sample	Weight (mg)	Shape	Col.	P.D.	$\delta^{13}C$ (‰)	N (ppm)	% B	Type	H	Para.	Assem.
K252	B124		irr	c	n		1140.7	17	IaAB	y		
K252	B125		twin thh frag	c	n		12.0	88	IaAB	y		
K252	B126		frag	lb	n		1525.3	100	IaB	y		
K252	B127	1.4	frag	ly	n	-10.37	606.5	72	IaAB	y		
K252	B128		thh	c	n		1952.1	13	IaAB	y		
K252	B129		thh frag	b	n		1437.2	28	IaAB	y		
K252	B130		thh	c	n		2466.4	66	IaAB	y		
K252	B131		thh frag	c	n		226.7	100	IaB	y		
K252	B132		octa frag	c	n		28.0	96	IaB	y		
K252	B133		frag	lb	n		1533.9	28	IaAB	y		
K252	B134		twin thh frag	b	n		1348.1	23	IaAB	n		
K252	B135		frag	c	y		890.1	34	IaAB	y		
K252	B136		frag	c	n		615.9	100	IaB	y		
K252	B137		octa	c	n		83.7	100	IaB	y		
K252	B138	0.4	agg octa	c	n	-6.37	374.5	14	IaAB	y		
K252	B139		thh	c	n		349.0	0	IaA	n		
K252	B140		agg octa	c	n		13.0	75	IaAB	y		
K252	B141		frag	lb	n		180.1	58	IaAB	y		
K252	B142		thh	c	n		1791.7	9	IaA	y		
K252	B143	0.5	thh	c	n	-4.67	1818.6	44	IaAB	y		
K252	B144		thh frag	c	n		0		II	n		
K252	B145		twin thh	c	n		1710.0	39	IaAB	y		
K252	B146		irr	c	n		554.1	100	IaB	y		
K252	B147		thh frag	c	n		1264.8	49	IaAB	y		
K252	B148		frag	lb	n		1864.7	86	IaAB	y		
K252	B149		thh frag	lb	n		1247.6	54	IaAB	y		
K252	B150		thh frag	ly	y		56.3	100	IaB	y		
K252	B151		thh frag	c	y		41.7	100	IaB	y		
K252	B152	1.1	octa frag	c	n	-2.77	15.3	97	IaB	y		
K252	B153	1.0	thh	c	n	-6.13	1473.8	9	IaA	y		
K252	B154		thh	lb	n		1518.8	63	IaAB	n		
K252	B155		frag	y	n		44.4	100	IaB	n		
K252	B156		octa frag	c	n		655.1	15	IaAB	n		

Table 2.1 cont.

Pipe	Sample	Weight (mg)	Shape	Col.	P.D.	$\delta^{13}C$ (‰)	N (ppm)	% B	Type	H	Para.	Assem.
K252	B157	1.3	frag	c	y	-3.85	108.4	76	IaAB	y		
K252	B158		frag	c	n		103.3	12	IaAB	y		
K252	B159		thh frag	y	n		0		II	y		
K252	B160		frag	c	y		0		II	n		
K252	B161		thh	c	n		43.1	100	IaB	n		
K252	B162		part res oct	c	n		34.7	100	IaB	y		
K252	B163		frag	b	n		490.2	100	IaB	y		
K252	B164		thh frag	b	n		30.2	94	IaB	y		
K252	B165		octa frag	c	n		170.6	100	IaB	y		
K252	B166		frag	c	n		260.7	100	IaB	y		
K252	B167		frag	c	n		388.2	100	IaB	y		
K252	B168		thh	c	n		502.8	9	IaA	n		
K252	B169		octa	c	n		40.4	100	IaB	y		
K252	B170		frag	lb	n		352.4	100	IaB	y		
K252	B171	0.3	twin octa	c	n	-3.01	132.1	89	IaAB	y		
K252	B172		frag	c	n		1056.3	100	IaB	y		
K252	B173		frag	lb	y		30.4	100	IaB	y		
K252	B174		agg octa	c	n		oversat			y		
K11	A201	2.9	octa frag	c	n	-3.65	0		II	n	e	rutile
K11	A202	0.9	agg octa	c	n	-7.81	0		II	n		
K11	A203	3.1	irr	c	n	-3.59	16.8	27	IaAB	n		serp
K11	A204	2.6	irr	c	n	-8.61	0		II	n		serp
K11	A205	1.0	thh frag	c	n	-11.03	5.9	92	IaB	y	p	ol
K11	A206	0.1	octa	y	n	-6.07	0		II	y	p	ol
K11	A207	1.8	thh	c	n	-4.33	0		II	n		
K11	A208	1.5	irr	c	n	-16.62	0		II	n		biot
K11	A209	2.2	agg octa	ly	n	-5.61	0		II	y	p	maj
K11	B200		thh	c	n		0		II	n		
K11	B201	0.2	twin octa	lb	n	-5.86	9.2	0	IaA	n		
K11	B202	1.5	twin thh frag	lb	n	-6.52	0		II	n		
K11	B203		octa	c	n		30.7	0	IaA	n		
K11	B204	0.3	frag	y	n	-16.93	44.8	51	IaAB	y		
K11	B205		thh	c	n		8.4	81	IaAB	y		

Table 2.1 cont.

Pipe	Sample	Weight (mg)	Shape	Col.	P.D.	$\delta^{13}C$ (‰)	N (ppm)	% B	Type	H	Para.	Assem.
K11	B206		octa frag	c	n		117.1	9	IaA	y		
K11	B207		agg octa	c	n		764.5	48	IaAB	y		
K11	B208	0.5	octa frag	c	n	-5.70	14.9	21	IaAB	y		
K11	B209		part res oct	c	n		22.0	54	IaAB	y		
K11	B210		octa frag	c	n		17.6	100	IaB	n		
K11	B211		frag	ch	n		0		II	n		
K91	A301	2.9	twin thh	c	n	-5.83	1004.8	23	IaAB	n		
K91	A302	1.7	thh frag	y	n	-13.57	62.4	40	IaAB	y		
K91	A303	1.2	octa	c	y	-17.98	292.1	100	IaB	y		dol
K91	A304	2.0	octa	c	n	-4.26	231.7		IaB	y		
K91	B300		irr	c	n		893.0	2	IaA	y		
K91	B301	0.5	frag	b	n	-9.61	38.2	98	IaB	y		
K91	B302	1.4	frag	c	n	-8.87	859.8	37	IaAB	y		
K91	B303	1.6	frag	c	n	-19.51	2080.0	65	IaAB	y		
K91	B304		octa frag	lb	n		32.6	100	IaB	y		
K91	B305		twin octa	b	n		952.4	100	IaB	y		
K91	B306		thh frag	lb	n		271.1	79	IaAB	y		
K91	B307		frag	c	n		419.4	100	IaB	y		
K91	B308		thh	c	n		0		II	y		
K91	B309		frag	c	n		2137.2	65	IaAB	y		
K91	B310		oct	c	n		138.8	100	IaB	y		
K91	B311	2.3	thh	c	n	-5.10	2263.4	5	IaA	y		
K91	B312		frag	b	y		0		II	n		
K91	B313		frag	c	n		957.7	100	IaB	y		
K91	B314		oct	c	n		662.6	28	IaAB	y		
K91	B315		thh frag	ly	n		1457.4	73	IaAB	y		
K91	B316		frag	c	y		31.5	100	IaB	y		
K91	B317	0.4	octa	c	n	-3.03	735.2	100	IaB	y		
K91	B318	1.8	thh	c	n	-4.01	3279.8	100	IaB	y		

thh=tetrahexahedra, frag=fragment, octa=octahedra, irr=irregular Col.=color: c=colorless, b=brown, lb=light brown, y=yellow, ly= light yellow, P.D.=plastic deformation, H= hydrogen Para.=paragenesis: p=peridotitic, e=eclogitic, wh=wehrlitic; Assem.=mineral assemblage: grt=garnet, cpx=clinopyroxene, ol=olivine, serp=serpentine, calc= calcite, biot=biotite, dol=dolomite, calc=calcite; ns=no suitable samples

Table 2.2:
Electron microprobe analyses of mineral inclusions.

Sample	**A115-1**	**A115-2**	**A128**	**A141**	**A209**	**A112**	**A205-1**	**A205-2**	**A206**	**A119-1**	**A119-2**	**A131**	**A201**
Mineral	grt	grt	grt	grt	maj	ol	ol	ol	ol	cpx	cpx	cpx	rutile
Paragenesis	E	E	E	Wh	P	P	P	P	P	E	E	E	E
SiO2	39.6	39.9	38.9	40.7	43.9	40.2	39.3	40.8	40.5	55.1	53.4	50.0	≤0.03
TiO2	0.94	0.95	0.95	0.45	0.10	≤0.03	≤0.03	≤0.03	≤0.03	0.22	0.23	0.94	99.02
Al2O3	21.5	21.6	21.8	18.8	13.0	≤0.03	≤0.03	≤0.03	≤0.03	7.35	7.71	2.03	0.39
Cr2O3	0.12	0.11	0.11	5.37	6.32	≤0.03	≤0.03	≤0.03	≤0.03	≤0.03	≤0.03	≤0.03	≤0.03
MgO	10.8	10.5	10.1	18.2	22.0	49.8	50.8	48.9	50.6	10.4	10.1	14.7	≤0.03
CaO	7.48	7.50	7.93	7.06	5.34	≤0.03	0.11	0.14	0.03	15.0	16.9	19.0	≤0.03
MnO	0.48	0.49	0.49	0.36	0.29	0.15	0.10	0.11	0.09	0.06	0.06	0.36	≤0.03
FeO	19.6	19.6	20.5	8.11	8.43	9.59	8.80	8.88	8.04	6.05	6.35	12.2	0.41
Na2O	0.33	0.34	0.35	0.05	0.24	≤0.03	0.04	≤0.03	0.07	4.29	4.16	0.28	≤0.03
K2O	≤0.03	≤0.03	≤0.03	≤0.03	≤0.03	≤0.03	≤0.03	≤0.03	≤0.03	≤0.03	0.04	≤0.03	≤0.03
Oxide Total	101	101	101	99	100	100	99	99	99	99	99	100	100
Si	5.94	5.96	5.85	5.96	6.41	0.99	0.97	1.01	0.99	2.01	1.96	1.90	
Ti	0.11	0.11	0.11	0.05	0.01	0.00	0.00	0.00	0.00	0.01	0.01	0.03	
Al	3.79	3.81	3.86	3.25	2.23	0.00	0.00	0.00	0.00	0.32	0.33	0.09	
Cr	0.01	0.01	0.01	0.62	0.73	0.00	0.00	0.00	0.00	0.00	0.00	0.00	
Mg	2.41	2.34	2.26	3.99	4.78	1.82	1.87	1.80	1.85	0.56	0.55	0.83	
Ca	1.20	1.20	1.28	1.11	0.84	0.00	0.00	0.00	0.00	0.59	0.66	0.77	
Mn	0.06	0.06	0.06	0.04	0.04	0.00	0.00	0.00	0.00	0.00	0.00	0.01	
Fe2+	2.46	2.45	2.58	1.00	1.03	0.20	0.18	0.18	0.16	0.18	0.19	0.39	
Na	0.09	0.10	0.10	0.01	0.07	0.00	0.00	0.00	0.00	0.30	0.30	0.02	
K	0.00	0.00	0.00	0.00	0.00	0.00	0.00	0.00	0.00	0.00	0.00	0.00	
Cation Total	16.09	16.06	16.14	16.05	16.13	3.01	3.03	2.99	3.01	3.98	4.02	4.04	

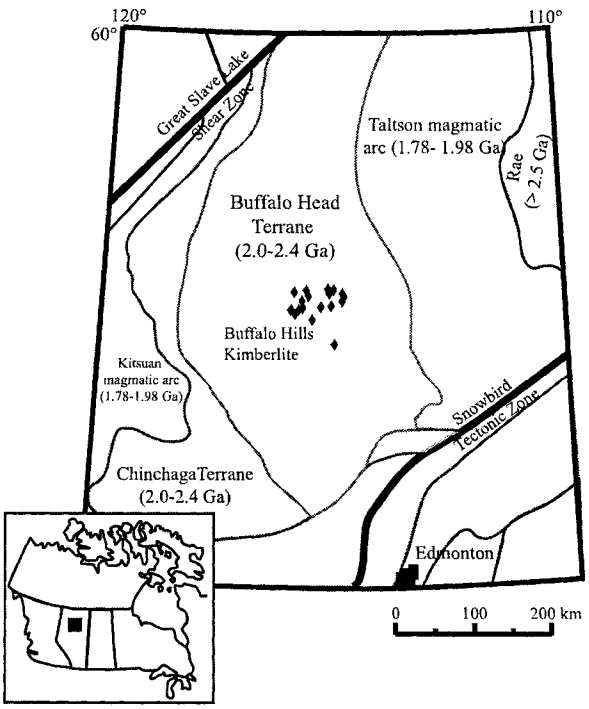

Fig 2.1 Locality map of the Buffalo Head Terrane showing the major geological boundaries and location of the Buffalo Hills kimberlite field. Modified after Eccles et al. (2003).

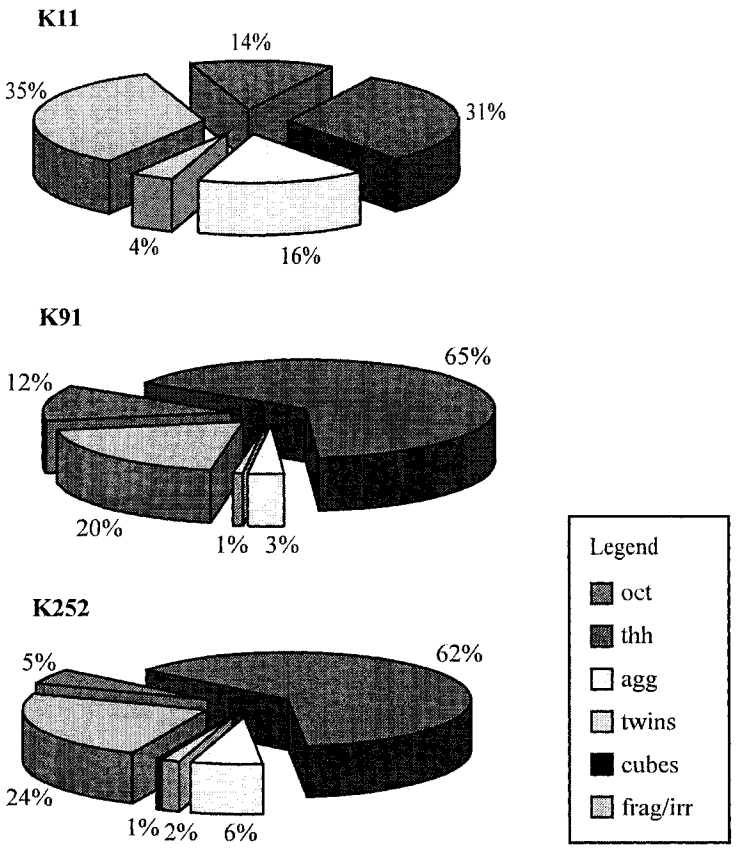

Fig. 2.2 Distribution of diamond shapes between pipes K11, K91 and K252. The tetrahexahedroidal shape dominates the distribution in all 3 pipes. Abbreviations are the same as used in Table 2.1.

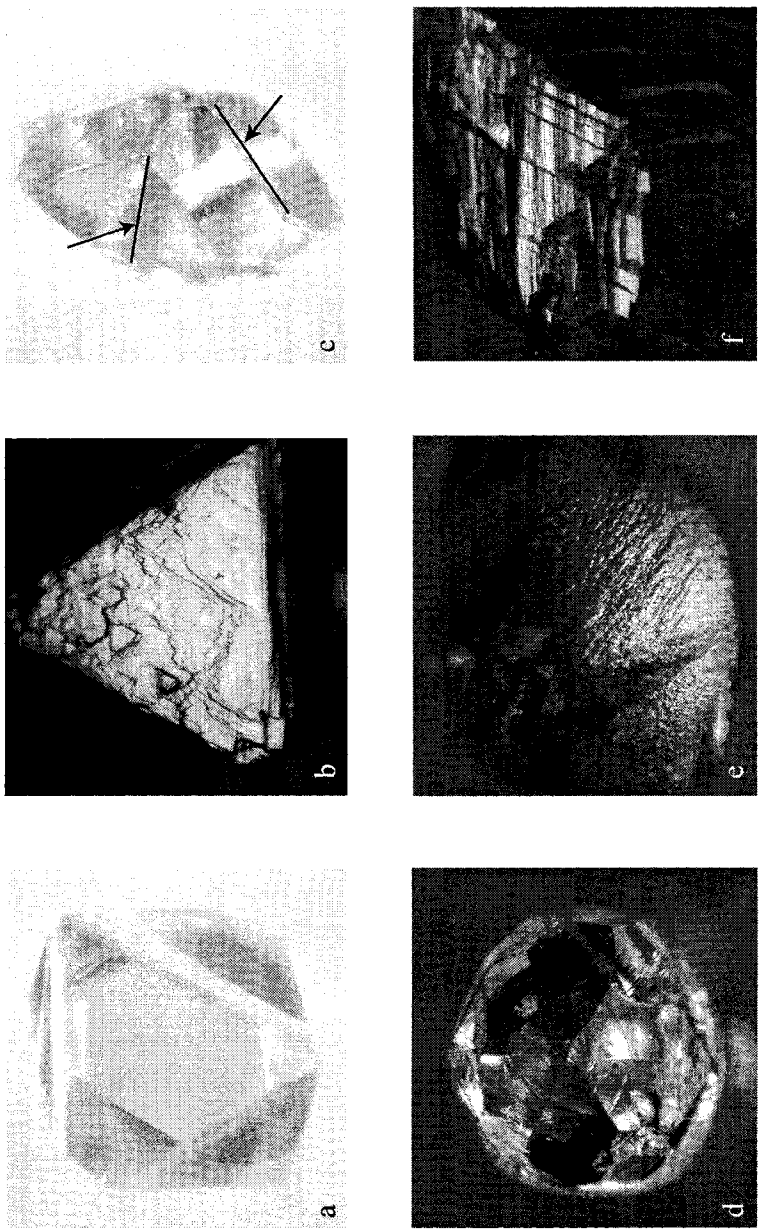

Fig. 2.3 Characteristic features of diamonds from K11, K91, K252: a) Sharp-edged octahedron, colorless and transparent. b) Octahedral face with minor negative trigons and abundant serate laminae. c) Doubly twinned octahedral crystal, twin planes are indicated by arrows. d) Fully resorbed colorless octahedron: tetrahexahedroid. Shows smooth, shiny face with broad, flat hillocks (pattern 2 and 3, see text). e) Fine, narrow elongate hillocks (pattern 1, see text) on tetrahexahedroidal face, produce rough surface texture and dull appearance. f) Brown colored tetrahexahedroidal fragment showing lamination lines (evidence of plastic deformation).

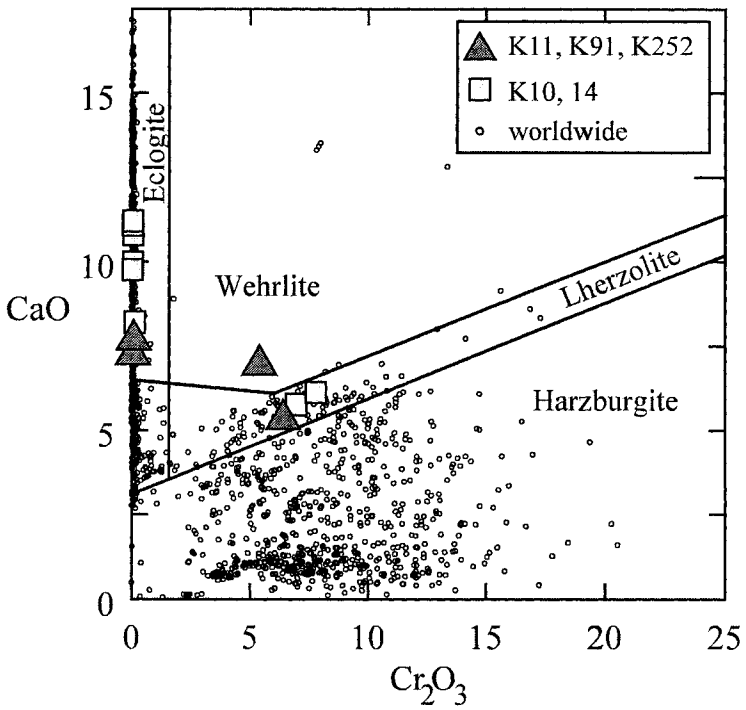

Fig. 2.4 CaO vs Cr_2O_3 (wt%) for garnet inclusions in diamond. Open symbols K11, K91, K252: this study; solid symbols K10, K14: Davies et al. (2004). Lherzolite field from Sobolev et al. (1973). Eclogite field after Gurney (1984).

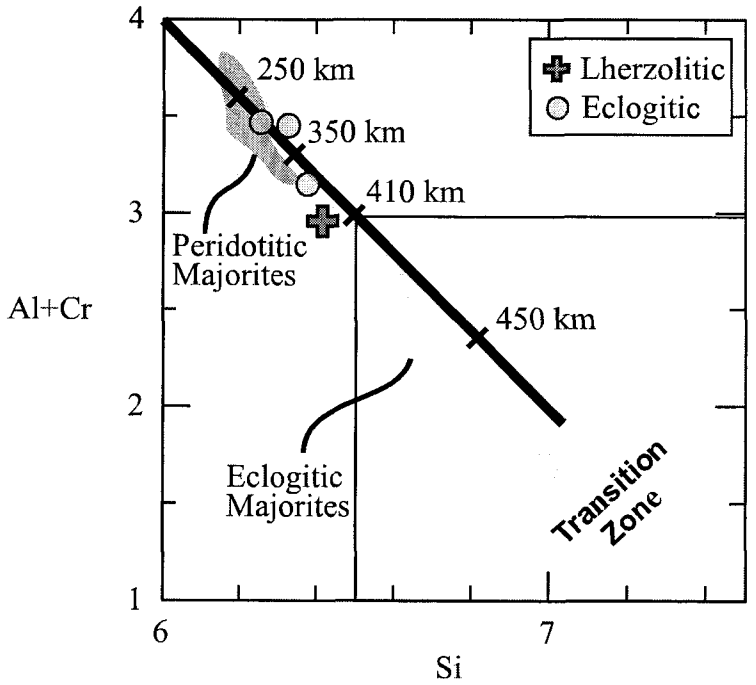

Fig 2.5 Atomic proportions of Al+Cr vs. Si (based on 24 oxygen). Majoritic garnets indicate formation beneath the lithosphere. The three eclogitic majorites are from Davies et al. (2004). Depth estimates are based on the experimental data of Irifune (1987). Compositional fields of eclogitic and peridotitic majorites from world-wide occurences are shown for reference.

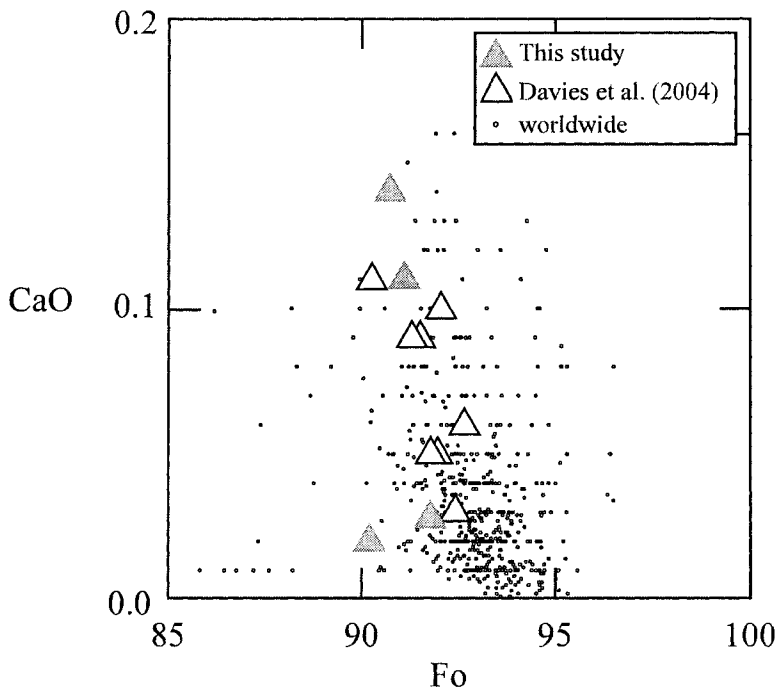

Fig 2.6 CaO wt% vs. Fo (100*Mg/Mg+Fe) content for olivine inclusions. Olivine inclusions with CaO <0.04 wt% are of certain harzburgitic affinity. Olivine inclusions with CaO 0.11 - 0.14wt% are of wehrlitic affinity.

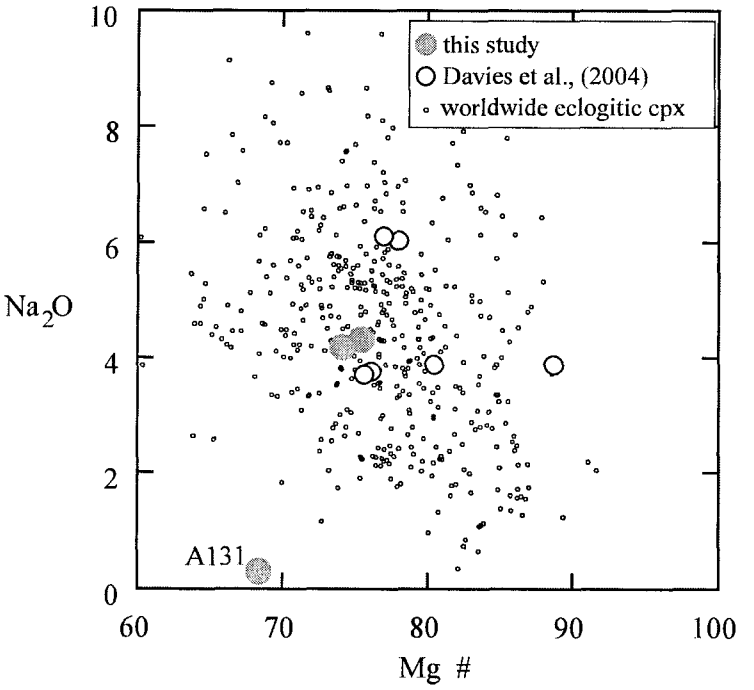

Fig. 2.7 Clinopyroxene compositions from Buffalo Hills diamonds plot within the worldwide database for eclogitic clinopyroxenes, the exception being A131 with the composition of an augite.

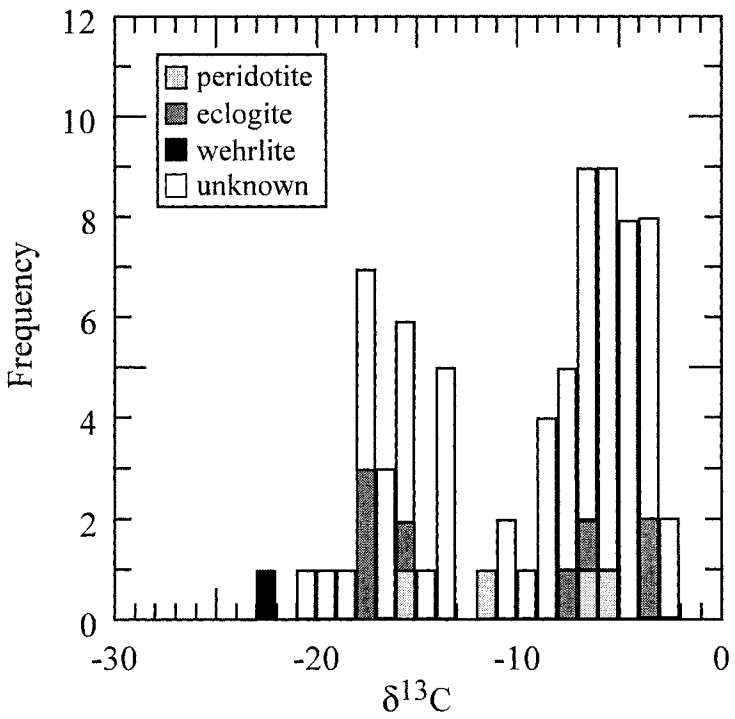

Fig. 2.8 Carbon isotope composition of 73 diamonds from pipes K11, K91 and K252. A bimodal distribution is evident with modes at ~-5 ‰ and ~ -17‰.

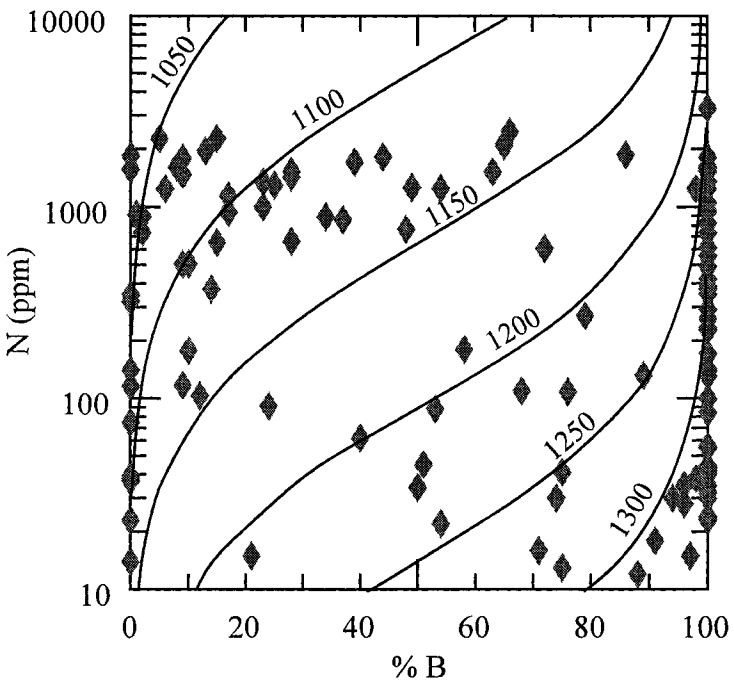

Fig. 2.9 Nitrogen contents and aggregation states for diamonds from K11, K91 and K252. Solid lines are isotherms for a mantle residence time of 1 Ga (after Taylor et al., 1990).

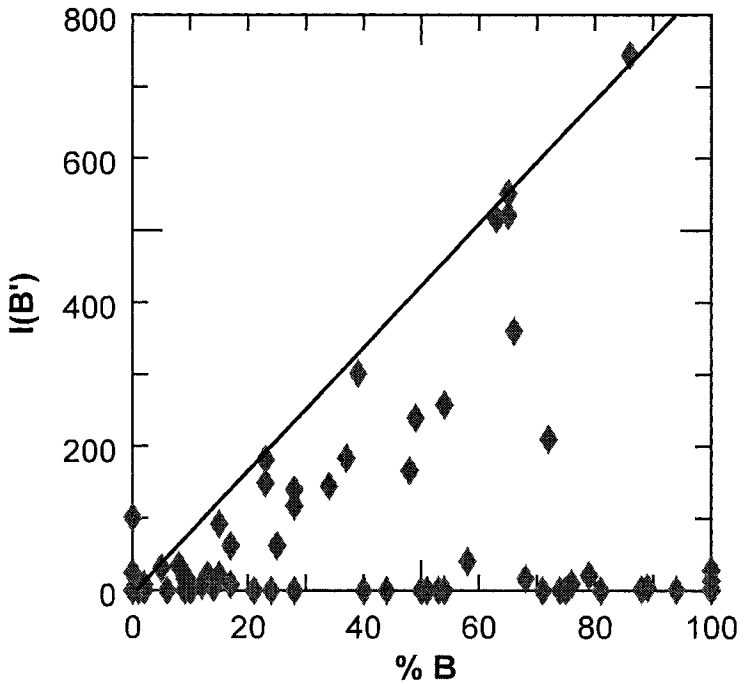

Fig. 2.10 The integrated absorption of the platelet peak (I(B')) vs. the percent of nitrogen in the B-center (%B) in Type Ia diamonds. A correlation previously established by Woods (1986; shown as solid line) where platelet intensity increases systematically with increasing aggregation is only evident for a few samples . However, most samples show catastrophic platelet degradation (i.e. plot below the trend line) indicating transient heating events affected the diamonds during mantle storage (Evans et al., 1995).

CHAPTER 3

METASOMATISM RECORDED BY GARNET INCLUSIONS FROM THE DE BEERS POOL, SOUTH AFRICA

The content of this chapter is in preparation to be submitted for publication as:
Ancient metasomatism recorded by ultra-depleted garnet inclusions in diamonds from De Beers Pool, South Africa
Banas, A., Stachel, T., Shimizu, N., Viljoen, K.S. (Fanus)

3.1 Introduction

Inclusions in diamonds and xenoliths found in kimberlites are our only direct samples of the deep subcratonic lithospheric mantle. Xenoliths, as open systems, preserve evidence of complex mantle processes. Over time, this may obscure the original composition of these samples of lithospheric mantle through a process of refertilization. Hence, inclusions in diamonds, unlike xenoliths, represent our only pristine samples of lithospheric mantle at the time of diamond crystallization as they are armored by their inert hosts since their encapsulation during the diamond crystallization event. These syngenetic inclusions therefore provide unadulterated information on chemical conditions in the mantle at the time of diamond crystallization and provide direct evidence of mantle compositions at that time.

Trace elements are sensitive tracers of metasomatic processes (Griffin et al., 1996) and record a more detailed sequence of events than is evident from major elements alone. Previous trace element studies on garnet inclusions in diamonds have already largely covered the known compositional space except for ultra-depleted compositions (Stachel et al., 2004a and references therein). These studies have shown that even for Archean inclusions in diamonds (Richardson et al., 1984) the original depletion signature invariably associated with lithospheric peridotites is overprinted by metasomatic events often representing multiple phases of re-enrichment. The ultra-depleted signature characteristic of garnet inclusions in diamonds from the De Beers Pool kimberlites (e.g. ultra-low Ca contents; Phillips et al., 2004) suggests that peridotitic diamond sources beneath Kimberley experienced little re-enrichment in major elements prior to diamond formation, remaining very similar to the harzburgite/dunite melting residues that were originally emplaced to

form the sub-cratonic lithosphere (Ringwood, 1975). Therefore, if the pre-metasomatic trace element composition of Archean lithospheric mantle was still preserved somewhere, then the ultra-depleted garnets from De Beers Pool could be one of the few places world-wide to observe it. Consequently, this study focuses on the trace element composition of the De Beers Pool garnet inclusions in order to investigate geochemical processes associated with the crystallization of diamond in highly depleted peridotitic mantle.

3.1.1 Background

De Beers Pool diamonds represent the pooled production from four kimberlites: Bultfontein, De Beers, Du Toitspan and Wesselton. Major element compositions of 228 peridotitic garnet inclusions recovered from 207 De Beers Pool diamonds are reported by Phillips et al. (2004). The garnet inclusions are predominantly subcalcic (i.e. >90% of the harzburgitic paragenesis) with the majority of these (~72%) containing less than 1.8 wt% CaO (the chemical border of ultra-depleted harzburgite or dunite garnets as defined by Grütter et al. 1999). Lherzolitic garnets form a minor component (6%) of the total garnet population at De Beers Pool. An unusually large number of garnet-orthopyroxene inclusion pairs (from 35 diamonds) in the study of Phillips et al. (2004) allowed these authors to accurately constrain the pressure-temperature conditions of diamond formation beneath the Kimberley area. Based on garnet-orthopyroxene geothermobarometry (thermometer of Harley, (1984) combined with the barometer of Brey and Köhler, (1990)) average pressure and temperature conditions of diamond formation are 6.3 GPa and 1200°C for non-touching inclusion pairs and 5.4 GPa and 1080°C for touching inclusion pairs (Phillips et al., 2004). Non-touching inclusion pairs define a model geotherm equivalent to 40 mW/m^2 surface heat flow, which is slightly hotter than the Cretaceous paleo-geotherm constrained by mantle xenoliths from Group 1 kimberlites at 38 mW/m^2 (Griffin et al., 2003). Geothermobarometry on touching inclusion pairs, however, defines a geotherm of 38 mW/m^2 coincident with the xenolith derived paleo-geotherm, suggesting that touching inclusions re-equilibrated to cooling mantle conditions during their mantle residence.

Two major kimberlite eruption events have sampled the mantle beneath the Kaapvaal Craton: kimberlites of Group 2 composition have ages >110 Ma whereas Group 1 kimberlites mainly erupted 85-90 Ma ago. The De Beers Pool pipes are the type locality for Group I kimberlites (Smith, 1983) and correspondingly show Late Cretaceous emplacement ages (Allsopp et al., 1989). Studies of mantle xenocrysts and xenoliths from both kimberlite groups indicate significant differences in metasomatic modification and thermal state of the deep lithosphere between the two kimberlite eruption events (e.g. Griffin et al., 2003). Still,

even data for the composition of the mantle lithosphere during the earlier Group 2 event already indicate a modified (i.e. metasomatised) mantle composition. Peridotitic garnet inclusions from diamonds from the De Beers Pool have been dated at 3.3 Ga (Richardson et al., 1984). The De Beers Pool inclusions, thus, represent a unique opportunity to study pristine samples of Archean lithospheric mantle.

3.1.2 Samples and Methods

3.1.2.1 Samples

From the sample set of Phillips et al. (2004) we chose 44 peridotitic garnet inclusions (40 of harzburgitic and 4 of lherzolitic paragenesis) for rare earth element analyses (Fig. 3.1; Table 3.1). The selected samples cover the entire compositional range for peridotitic garnets in diamonds from De Beers Pool but focus primarily on highly depleted (low-Ca) compositions. Preference was placed on samples with co-existing mineral inclusions (36 garnets, co-existing mainly with orthopyroxene) to explore correlations between pressure-temperature conditions and degree and style of possible metasomatic overprint. Additional trace elements (Sr, Ba Ti, Y, Zr, Nb) were analysed for a subset of 31 garnets (29 harzbugites, 2 lherzolites).

3.1.2.2 Methods

For ion probe analysis, the polished garnet inclusions were coated with a thin film (~20nm) of gold. Rare earth and other trace elements were measured on a Cameca IMS 3f Ion Microprobe at Woods Hole Oceanographic Institute. The samples were bombarded with a beam of negatively charged oxygen ions with a net energy of approximately 12.5 keV. Spot size (diameter of primary ion beam) was approximately 20μm for REE analyses and 3-5μm for other trace elements. An energy offset of 60 V and 90 V for REE and other trace elements, respectively, was applied in order to suppress molecular interferences. Element abundances were calculated using empirical relationships between intensity and concentrations established for standards (working curves). Analytical uncertainties based on counting statistics range from <1-20% (relative) for ppm concentrations but become increasingly larger at sub ppm concentrations.

3.2 Trace Element Composition of De Beers Pool Garnets

3.2.1 Sample homogeneity

Individual garnet inclusions and garnets in mineral intergrowths were found to be compositionally homogeneous. Although minor variations in major element chemistry among non-touching garnet inclusions were detected in 9 of 35 diamonds containing

multiple garnets (Phillips et al., 2004), our trace element analyses of garnet pairs from three diamonds show compositions that are identical within error limits (Fig. 3.2). This suggests that within individual diamonds multiple inclusions are not recording successive metasomatic events but represent an equilibrium assemblage. The trace element composition of garnets intergrown with orthopyroxene falls in the compositional range of isolated inclusions and, in the one case where we analyzed both types of garnets (i.e. intergrown garnet and isolated garnet) from the same sample, we obtained a perfect match. These observations imply that garnet-orthopyroxene intergrowths at De Beers Pool did not form as a consequence of exsolution (e.g. from formerly majoritic garnet).

3.2.2 Trace element patterns

The garnet inclusions are divided into six principal groups according to similarities in their REE_N (N denotes normalization to the C1-chondrite composition of McDonough and Sun, 1995). Trace element compositions of "low-Ti" ($\leq$0.02 wt% TiO_2) and "high-Ti" (0.06-0.24 wt%) garnets are distinct and therefore are shown with separate symbols (filled symbols for the former, open symbols for the latter). It should be noted that the "high-Ti" group in this study still falls into the normal range of Ti contents for peridotitic garnets occurring as inclusions in diamonds worldwide; furthermore, Ti contents are low compared to the titanium-rich garnets found as megacrysts and in hot sheared peridotites which may contain TiO_2 up to 1 wt% (e.g. Boyd, 1987).

Six principal REE_N patterns are recognized for De Beers Pool garnets (Table 2.2):

3.2.2.1 Straight REE pattern

This group contains two harzburgitic garnets which are characterized by high LREE contents, with positive slopes in the $LREE_N$ (peak at Ce), negative slopes in the $MREE_N$ up to Dy, and slightly positive slopes in the $HREE_N$ (Fig. 3.3a). Other trace elements were not measured for these two samples using SIMS but, based on low TiO_2 (0.02 wt%) concentrations determined using EPMA, they can still be classified as members of the low-Ti garnet group. Both garnets have CaO <1.8 wt% and Mg # ~90 (Fig. 3.5).

3.2.2.2 "Normal" REE pattern

This group of three garnets (one harzburgitic, two lherzolitic) is characterized by steep positive slopes in the $LREE_N$ from La to Nd; fairly flat slopes in the $MREE_N$ with slightly positive slopes in the $HREE_N$ (Fig. 3.3b). Other trace elements were measured for two samples (DP 387 and 448), both of which have high concentrations of Ti, Zr and Y (Fig.

3.4a). Garnet DP 374 is also part of the high-Ti group (0.08 wt% TiO_2 determined with EPMA). All three garnets have CaO contents > 1.8 wt% and low Mg # (Fig. 3.5).

3.2.2.3 Weakly sinusoidal pattern

This group contains the majority of the analyzed garnets (13 harzburgitic and one lherzolitic). The patterns have positive slopes in the $LREE_N$ to Nd, negative slopes in the $MREE_N$ to Dy-Er and shallow, predominantly positive slopes in the $HREE_N$ (Fig. 3.3c). Five of the garnets belong to the high-Ti group and are distinct in having relatively high Y and Zr concentrations (Fig. 3.4b) and falling in the higher range of REE concentrations especially for the MREE and HREE. The high-Ti garnets have CaO >1.8 wt% (with the exception of DP 391) and variable Mg # (89-93). All of the low-Ti harzburgitic garnets have CaO <1.8 wt% and Mg # >89 (Fig. 3.5). The single lherzolitic garnet has a low Ti content (0.01 wt%) and low Mg # (87).

3.2.2.4 Sinusoidal - low Er pattern

This group consists of six harzburgitic and one lherzolitic garnets. Generally, the garnets have positive slopes in the $LREE_N$ to Nd, negative slopes in the $MREE_N$ with a trough at Er and steep positive slopes in the $HREE_N$ (Fig. 3.3d). Two samples (DP32 and 248) have very low LREE concentrations with very steep slopes in the $LREE_N$ to Nd, flat $MREE_N$ slopes to Eu, but negative slopes to Er and positive slopes in the $HREE_N$. All samples have low Ti contents and low corresponding Zr and Y concentrations with the exception of DP 32 which has the lowest measured Ti but relatively high Zr content (Y is within the range of the low-Ti garnets; Fig. 3.4c). These garnets have variable Ca contents (0.4-4.6 wt%) and low Mg # (<90) (Fig. 3.5).

3.2.2.5 Humped pattern

This group consists of eight harzburgitic garnets that are characterized by a broad range of LREE concentrations (0.1-5 times chondritic abundance) with positive slopes in the $LREE_N$ to Nd (except DP 181 which peaks at Ce; Fig. 3.3e). The five low-Ti samples have negative slopes in the $MREE_N$ and $HREE_N$, CaO <1.8 wt% and high Mg # (≥90). The three high-Ti garnets have steep negative slopes from Nd_N (or Ce_N) to Sm_N only and shallower negative slopes through the remaining $MREE_N$ and $HREE_N$. The high-Ti garnets have enriched REE concentrations, especially in the MREE and HREE, elevated Y, Zr (Fig. 3.4d) and CaO (>1.8 wt%) contents and lower Mg # (<90) compared to their low-Ti counterparts (Fig. 3.5).

3.2.2.6 Sinusoidal - low Dy pattern

This group consists of seven harzburgitic garnets with positive slopes in the $LREE_N$ (to Nd, except DP 392 and 440 which peak at Sm), negative slopes in the $MREE_N$ with a trough at Dy and positive slopes in the $HREE_N$ (Fig. 3.3f). DP 392 and 440 have exceptionally low LREE contents and very steep positive slopes in the $LREE_N$ to Sm. Among the six groups of REE patterns for De Beers Pool garnets this group has the lowest overall REE concentrations. All the samples have low Ti, Zr and Y concentrations (Fig. 3.4e). The garnets have variable Ca contents (0.6-3.4 wt%) and Mg # (89-93) (Fig. 3.5).

3.2.2.7 High-Ti garnets

High-Ti garnets (TiO_2 = 0.06 to 0.24 wt%) occur in three of the above groups of REE patterns: *normal, weakly sinusoidal* and *humped* (Fig. 3.3 b,c,e). A common feature of the high-Ti garnets is that they have higher CaO contents (>1.8 wt%; with the exception of DP 391; Fig. 3.6). The high-Ti garnets are also associated with generally higher concentrations of LREE, and are highly enriched in MREE and HREE, Zr and Y.

3.2.3 Geothermobarometry and trace element chemistry

The examined garnets cover the whole pressure (4.0-7.5 GPa) and temperature (1000-1325°C) range recorded by the De Beers Pool inclusion data set of Phillips et al. (2004) based on garnet-orthopyroxene geothermobarometry (Table 3.2; Figs. 3.6 & 3.7). Linear correlations between REE concentrations and pressure-temperature conditions are not evident but certain broad associations are recognized.

High-Ti garnets are restricted to lower pressures (<6 GPa) and temperatures (<1100°C, see Fig. 3.6). Including some samples from the low-Ti group, all garnets with high REE, Y and Zr, with CaO >1.8 wt% and with Mg # <89 are restricted to these lower equilibration conditions as well. Among the low-Ti garnets the *sinusoidal - low Er* group shows a similar, restricted range in PT conditions (<6 GPa and <1100°C, see Fig. 3.6). This group also has the highest LREE-MREE of the low-Ti garnets. The remaining low-Ti garnet groups, with *humped, weakly sinusoidal,* and *sinusoidal-low Dy* REE_N patterns, cover almost the entire range of pressure and temperature conditions (4.5-7.5 GPa and 1050-1325°C, see Fig. 3.6) observed for De Beers Pool inclusions. The three lherzolitic samples for which geothermobarometric data are available equilibrated at the lower end of the De Beers Pool PT spectrum (<5 GPa and <1100°C).

Garnets with negative slopes in the HREE are restricted to higher PT conditions and garnets with positive slopes in the HREE are generally restricted to lower PT, although

some overlap does exist. The broadest range of La contents and LREE-MREE slopes are also restricted to lower PT conditions.

3.3 Discussion

Combining the highly depleted major element compositions of De Beers Pool garnet inclusions (Phillips et al., 2004) with our trace element data it becomes apparent that these samples derive from a source characterized by strong depletion in major elements and subsequent re-enrichment in trace elements (Frey and Green, 1974) typical of diamondiferous mantle source regions worldwide (e.g. Stachel et al., 2004a).

3.3.1 Mantle processes recorded by major elements

The ultra-depleted character of the De Beers Pool inclusion suite is reflected in the highly subcalcic compositions of the garnets (Fig. 3.1). Along with high Cr/Al and Mg/Fe ratios, this indicates that the diamond source region experienced a high degree of melt extraction. The garnets have a broad range in Cr_2O_3 contents (3-13 wt%) overlapping almost the entire compositional range defined by peridotitic garnet inclusions worldwide (Stachel et al., 2004a). Chromium content of garnet has been linked to the bulk rock compositions of lithospheric peridotites (Griffin et al., 1999a) suggesting that Cr-enrichment in garnets may be used as an indicator for sources depleted by melt extraction. However, this simplistic picture is somewhat complicated through the pressure dependent distribution of Cr/Al between garnet and spinel in Mg-chromite bearing diamond sources. Stachel et al., (1998) review experimental evidence and conclude that garnets with Cr_2O_3 contents $\geq$ 4 wt% (such as the bulk of the De Beers Pool garnets) can only be derived from protoliths that experienced melt extraction at low pressures (<20 kbar), i.e. in the spinel stability field. Based on empirical evidence, Grütter et al. (1999) report that 1.8 wt% CaO in garnet is an important divide in many data sets, separating "normal" subcalcic garnets from those derived from ultra-depleted harzburgitic or dunitic mantle sources. Based on experimental data Grütter et al. (1999) conclude that "normal' subcalcic garnets indicate melt extraction in excess of 20% in order for melting to proceed to clinopyroxene exhaustion whilst ultra-depleted garnets with CaO <1.8 wt% derive from residues that formed through the extraction of about 50% melt of komatiitic composition from a mantle source resident in the comparatively shallow stability field for spinel peridotite. It is not clear if the large variability in Ca-Cr space seen for De Beers Pool garnets is entirely a consequence of different degrees of partial melting over a depth range or if secondary metasomatic re-enrichment in major elements in part reversed the original depletion.

3.3.2 Mantle processes recorded by trace elements

3.3.2.1 High-Ti versus low-Ti compositions

A clear distinction is evident between the REE signatures for low- ($TiO_2 \leq 0.02$ wt%) and high-Ti ($\geq$0.06 wt%) garnets. Three groups of REE_N patterns contain high-Ti garnets: *normal, humped,* and *weakly sinusoidal* (Fig. 3.3). The high-Ti garnets in each group are higher in REE than low-Ti garnets (especially in the case of the 'humped' REE group). The average compositions of these three high-Ti groups fall between the average REE composition of harzburgitic and lherzolitic garnet inclusions worldwide (Stachel et al., 2004a) (Fig 3.8). Comparatively elevated Ca and Fe concentrations in high-Ti harzburgitic garnets suggest that their source may also have experienced re-enrichment in major elements such as Ca.

Five groups of REE_N patterns, *straight, humped, weakly sinusoidal, sinusoidal - low Dy* and *- low Er,* contain low-Ti garnets (Fig. 3.3). The weakly *sinusoidal* and *humped* groups have both low- and high-Ti garnets whereas the *straight* and *sinusoidal - low Dy* and *- low Er* groups are composed solely of low-Ti garnets. The average REE compositions of the low-Ti garnet groupings plot well below the worldwide harzburgitic average as demonstrated in Fig. 3.8.

3.3.2.2 Depletion events

In peridotite the principal host for HREE is garnet, hence the $HREE_N$ pattern of garnet mimics that of the host rock. Positive $HREE_N$ slopes (represented by Er and Yb in our data set), seen in many of the samples examined, indicate that the protoliths of the diamond sources experienced melt extraction which preferentially removed LREE and MREE, resulting in very low LREE/HREE (Stachel et al. 1998). Strong preferential retention of HREE in the residue may relate to partial melting in the presence of either garnet or near-liquidus clinopyroxene (Blundy et al., 1998), i.e. either in the garnet or spinel peridotite field. The observation of highly fractionated Cr/Al ratios in the diamond sources requiring melt extraction in the spinel stability field may be reconciled with garnet as the cause for fractionated LREE/HREE ratios if polybaric decompression melting, commencing in the garnet stability field, is assumed (c.f. Stachel et al., 1998).

The two groups with sinusoidal REE_N (*low Dy* and *low Er* groups) have the steepest slopes in the $HREE_N$ indicating that either the source for these samples experienced the greatest degree of LREE/HREE fractionation or that the original depletion signature is most prominently preserved within these samples. Similarly, significant variability in the $HREE_N$ slopes among garnets from these two sinusoidal groups indicates either variable depletion or subsequent re-enrichment of HREE. Extreme depletion of the protoliths for sinusoidal

garnets is additionally reflected by their overall low REE and HFSE concentrations, low Ca contents and high Mg #.

Garnets with flat/negative slopes in the $HREE_N$ (*humped* group) are compatible with a source which experienced HREE re-enrichment, thereby completely overprinting an original depletion signature. Although flat slopes may reflect a primitive (i.e. undepleted) signature, this is unlikely considering the major element compositions and depleted REE contents (with respect to a primitive garnet composition) of the garnets. Additionally, all garnets with negative slopes in $HREE_N$ are restricted in their major element composition to low CaO (<1.8 wt%) and high Cr_2O_3 (>5 wt%) contents indicating derivation from ultra-depleted harzburgitic/dunitic sources. In view of these highly depleted major and trace element compositions flat/negative slopes in the $HREE_N$ can only be a consequence of re-enrichment by a fluid/melt with LREE/HREE > 1.

Averaged REE patterns show that there is a distinct separation between the absolute HREE concentrations of the low- and high-Ti groups. Because of their moderately positive $HREE_N$ slopes, the overall higher HREE contents of the high-Ti garnets cannot exclusively result from metasomatic overprint, as this should create negative $HREE_N$ slopes. Lower modal garnet abundance causes higher $HREE_N$ concentrations in garnet; however, systematically lower garnet in sources with higher Ca and Ti and generally lower Mg # is unlikely. Thus the difference in the HREE concentrations of the low- and high-Ti groups reflect, at least in part, different degrees of primary melt depletion.

3.3.2.3 Enrichment events

Sinusoidal REE_N patterns have been reported for subcalcic garnets from peridotite xenoliths (Hoal et al., 1994; Nixon et al., 1987), in heavy mineral concentrates (Shimizu and Richardson, 1987) and as inclusions in diamonds (Stachel et al., 2004a). Nearly all De Beers Pool garnet inclusions have some degree of sinuosity in their REE_N patterns. Steep positive slopes within the $LREE_N$ with a hump at ~Nd_N are an artifact of rapidly increasing compatibility from LREE towards MREE. Normalization to a primitive garnet composition (J4 garnet of Jagoutz and Spettel, c.f. Stachel et al., 1998) eliminates these crystal chemical effects (Fig. 3.8). When normalized to J4 garnet (REE_{J4}) the De Beers Pool inclusions have LREE enriched patterns which are broadly V-shaped and similar to those observed for garnet inclusions worldwide (Stachel et al., 2004a) although with generally lower overall REE concentrations (Fig. 3.8).

Melt depletion with associated preferential removal of LREE and MREE from a protolith should be reflected in later-crystallized garnets as REE_{J4} patterns with steep positive slopes from LREE to HREE. Hence, the V-shaped patterns with negative slopes from LREE to

MREE and positive slopes within the HREE imply re-introduction of LREE and MREE to the source region. Average REE_{J4} patterns of the six groups of garnets recognized above show increasing concentrations and decreasing sinuosity of REE_N from the *sinusoidal-low Dy* group to the *normal* group (Fig. 3.8) which suggests increasing metasomatic re-enrichment.

The *sinusoidal - low Dy* group has the lowest LREE and MREE concentrations and the negative slope in $LREE_{J4}$-$MREE_{J4}$ increases significantly within the MREE. Such a complex pattern requires re-enrichment in LREE-MREE by a metasomatic agent that not only has a high LREE/HREE ratio but that also experienced some minor LREE fractionation to cause almost flat La-Nd in the fluid/melt. Similar but more extreme modification of LREE/MREE slopes is documented by convex up $MREE_{J4}$ patterns recognized among harzburgitic garnet inclusions from Mwadui (Stachel et al., 1999) and Orapa (Stachel et al. 2004b)

The *sinusoidal - low Er* and *low-Ti - weakly sinusoidal* groups have higher average concentrations of LREE and MREE and $LREE_{J4}$-$MREE_{J4}$ slopes that are fairly constant. The gentle positive slopes from Dy_{J4}-Yb_{J4} for the *weakly sinusoidal* group suggests that metasomatic re-enrichment also involved some HREE.

The low-Ti garnets of the *humped* group, share properties of both the *sinusoidal - low Dy* group (flat $LREE_{J4}$) and the *weakly sinusoidal* group (absence of a positive slope in $HREE_{J4}$). This requires a HREE bearing metasomatizing agent that fractionated a LREE phyllic phase (e.g. chrichtonite).

Normalization to J4 shows that garnets with *straight* REE_N require extreme enrichment of LREE over MREE. Similar to the *low-Ti - humped* group the metasomatizing agent must have contained some HREE to eliminate the original positive Er-Yb slope.

The high-Ti garnets present in the *normal, weakly sinusoidal* and *humped* groups have the highest REE contents. The correlation of high Ti contents with high Y, Zr, and (with one exception) high Ca contents suggests that these garnets interacted with a (second?) metasomatic agent re-enriching both trace and major elements. The trace element patterns of high-Ti garnets are approaching the more primitive composition typically seen among lherzolitic garnets from world-wide sources (Stachel et al., 2004a).

3.3.3 Metasomatic agents

3.3.3.1 Fluid dominated metasomatism

The fractionated REE_{J4} patterns of De Beers Pool garnet inclusions (Fig. 3.8) suggest interaction with a metasomatic agent with very high LREE/HREE. Pervasive infiltration of such metasomatic agents may have resulted in re-enrichment of incompatible trace elements throughout the entire deep lithosphere. Extremely high LREE/HREE and LREE/Ti are

generally interpreted to indicate fluid rather than melt involvement during metasomatic re-enrichment (e.g. Griffin and Ryan, 1995). As an alternative to CHO fluids Burgess and Harte (2002) propose progressive fractionation of REE in silicate melts in the course of garnet fractionation. They show that the composition of garnet in equilibrium with such an evolving melt will gradually progress to higher LREE/HREE ratios and LREE-MREE concentrations. As such an evolving melt percolates through the lithosphere it may impart increasingly fractionated REE patterns to the peridotitic host rocks. However, a distinction between metasomatism through CHO-dominated fluids and such highly fractionated and thereby volatile enriched "melts" appears arbitrary, in particular in view of the possible absence of a solvus between hydrous fluids and silicate melts in the deep lithosphere (Bureau and Keppler, 1999; Wyllie and Ryabchikov, 2000).

As discussed above, flat or even negative slopes in the HREE of some garnets indicate re-enrichment in these elements. High partition coefficients of HREE between garnet and melt-fluid imply that a metasomatizing agent does not require high concentrations of HREE to cause slight HREE enrichment. Additionally, as garnet is the only major host for HREE in peridotite, low modal abundance of garnet results in greater apparent HREE enrichment. The partial involvement of HREE in the metasomatic process suggests a metasomatic agent that is transitional between a pure CHO fluid and a melt.

However, evidence of purely fluid induced metasomatism is exhibited by sample DP32: this garnet has very low Ca, high Mg # and the lowest Ti content of our sample set along with a sinusoidal REE_{J4} pattern. Strong enrichment in Zr without concomitant increase in Y and Ti place DP32 along the low-temperature or fluid metasomatism trend defined by Griffin et al. (1995) (Fig. 3.9).

3.3.3.2 Melt dominated metasomatism

Based on Y-Zr relationships most of the De Beers Pool garnets plot within the "depleted" field (Fig. 3.9) defined by Griffin et al. (1995), similar to most garnet inclusions in diamonds worldwide. HFSE (high field strength element) metasomatism is characterized by simultaneous enrichment in Y and Zr caused by infiltration of high temperature melts (Griffin et al., 1999b). Generally, trace element enrichment in garnet inclusions tends to involve both Y and Zr thereby plotting along this melt metasomatic trend (e.g. Akwatia, (Stachel and Harris, 1997); Kankan, (Stachel et al., 2000); Orapa, (Stachel et al., 2004b)). For the high-Ti garnets from De Beers Pool co-variations in Y-Zr define a trend straddling the boundary between the fields of melt and fluid metasomatism indicating that these garnets were affected by a HFSE-rich metasomatic agent approaching melt-like characteristics. The major element composition of some of the high-Ti garnets suggests that this melt

phase also carried Ca and Fe. Melt metasomatism has been interpreted to be the result of the infiltration of asthenospheric melts (Ehrenberg, 1979; Harte and Hawkesworth, 1989 and references therein; Smith and Boyd, 1987).

3.3.3.3 Timing of metasomatic event(s) and diamond formation

Richardson et al. (1984) obtained a Sm-Nd model age of 3.3 ± 0.2 Ga for a composite of subcalcic garnet inclusions from De Beers Pool. Harzburgitic garnet inclusions from the Premier kimberlite (Richardson et al., 1993) also indicate Middle Archean crystallization ages (>3 Ga) whereas garnet and clinopyroxene composites for the lherzolitic inclusion paragenesis yield a younger isochron age of 1.93 ± 0.04 Ga. At De Beers Pool the trace element composition of the garnet inclusions shows no separation between the lherzolitic and harzburgitic parageneses in trace element abundance. Both parageneses have overlapping and indiscernible REE compositions described by three of the above patterns (*normal, weakly sinusoidal* and *sinusoidal – low Er*). It is difficult to constrain the timing of the metasomatic events relative to each other or to attribute the effects to a single or to multiple events. Thus the mantle lithosphere may have experienced repeated metasomatic pulses causing multiple episodes of diamond growth or the De Beers Pool diamonds may have originated during a single pervasive and compositionally evolving metasomatic event at around 3.3 Ga.

3.3.4 Correlation with PT

Geothermobaromatric results for the low-Ca (<1.8 wt%) garnets indicate crystallization over a wide depth range within the cratonic lithosphere whereas garnets with higher Ca concentrations are restricted to "shallower" depths (<6 GPa and <1100°C; Fig. 3.7). The two groups overlap in the shallower depth ranges and when combined result in a kinked trend of decreasing Ca content with increasing pressure and temperature (depth; Fig. 3.6). Additionally, Mg # below 90 are restricted to shallower portions of the diamond stability field. Assuming that higher Ca and Fe/Mg are not a primary signature of the shallower lithosphere this suggests that its inclusions population experienced more diverse, possibly multiple, metasomatic events compared to diamonds from deeper parts of the craton.

Xenolith data for the Kimberley pipes show that the mantle lithosphere at the time of kimberlite eruption (80-95 Ma) was composed mainly of variably enriched lherzolite and only minor harzburgite (Schulze, 1995) with melt metasomatised lherzolite being dominant at the base of the lithosphere (Griffin et al., 2003). Between the Group 2 and Group 1 kimberlite eruption events there is a significant increase in fertility, with variably

enriched lherzolite becoming more prevalent throughout the lithospheric section (Griffin et al., 2003). This is accompanied by an increase in heat flow (from 35mW/m^2 to 38mW/m^2 surface heat flow) and a decrease in the thickness of the stable cratonic root (Griffin et al., 2003). Our inclusion data provide evidence that the composition of the lithosphere in the Archean was even more depleted than documented by the Group 2 xenoliths. Taking the garnet inclusion data at face value they suggest that highly depleted harzburgite dominated the base of the craton with more fertile (including lherzolite) compositions increasing in abundance at shallower depths (<180 km). At the time of diamond formation the base of the depleted lithosphere extended to greater depths (~230 km; Fig. 3.4) and fell on a higher geothermal gradient (documented by the non-touching inclusion pairs, Phillips et al. 2004) than recorded by the xenoliths in Group 1 kimberlites.

3.5 Conclusions

The De Beers Pool garnet inclusions preserve some of the most depleted compositions observed worldwide, both in major and trace elements. In particular, this is documented by abundant ultra-depleted garnet compositions with CaO <1.8 wt% and Mg # >90. The garnet compositions record the initial depletion event as evidenced by the presence of positive $HREE_N$ slopes and high Cr contents (i.e. high Cr/Al ratios) suggesting that melt depletion occurred partially in the garnet stability field and proceeded into the spinel stability field. The presence of variable REE compositions suggests the Kaapvaal lithosphere beneath Kimberley was affected by multiple metasomatic processes before and during diamond formation. The variability and diversity of trace element (in particular REE) enrichment provides evidence of both fluid and melt metasomatic events. Fluid dominated metasomatism affected all sampled source regions and preferentially re-enriched LREE and MREE, whereas melt metasomatism additionally introduced major elements (Ca and Fe) and HFSE such as Ti, Y and HREE. Geothermobarometric data show that melt metasomatism was restricted to shallower depths (<180 km) whereas fluid metasomatism was pervasive throughout the lithosphere (down to 230 km). LREE enrichment in every single garnet inclusion establishes an intimate relationship between mantle metasomatism and diamond formation.

Comparison with data for xenolith from Group 1 and Group 2 kimberlites shows that the lithosphere subsequently experienced multiple additional metasomatic events from the Archean to the Cretaceous.

References

Allsopp, H.L. et al., 1989. A summary of radiometric dating methods applicable to kimberlites and related rocks. In: J. Ross et al. (Editors), Kimberlites and Related Rocks. GSA Special Publication No 14. Blackwell Scientific, Carlton, pp. 343-357.

Blundy, J.D., Robinson, J.A.C. and Wood, B.J., 1998. Heavy REE are compatible in clinopyroxene on the spinel lherzolite solidus. Earth and Planetary Science Letters, 160(3-4): 493-504.

Boyd, F.R., 1987. High- and low-temperature garnet peridotite xenoliths and their possible relation to the lithosphere-asthenosphere boundary beneath southern Africa. In: P.H. Nixon (Editor), Mantle Xenoliths. John Wiley & Sons Ltd., Chichester, pp. 403-412.

Brey, G.P. and Köhler, T., 1990. Geothermobarometry in four-phase lherzolites II. New thermobarometers, and practical assessment of existing thermobarometers. Journal of Petrology, 31: 1353-1378.

Bureau, H. and Keppler, H., 1999. Complete miscibility between silicate melts and hydrous fluids in the upper mantle: experimental evidence and geochemical implications. Earth and Planetary Science Letters, 165: 187-196.

Burgess, S.R. and Harte, B., 2002. Tracing lithosphere evolution through the analysis of heterogenous G9/G10 garnets in peridotite xenoliths, II: REE chemistry. Journal of Petrology, 45(3): 609-634.

Ehrenberg, S.N., 1979. Garnetiferous ultramafic inclusions in minette from the Navajo volcanic field. In: F.R. Boyd and H.O.A. Meyer (Editors), The mantle sample: inclusions in kimberlites and other volcanics. AGU, Washington, pp. 213-226.

Frey, F.A. and Green, D.H., 1974. The mineralogy, geochemistry and origin of lherzolite inclusions in Victorian basanites. Geochimica et Cosmochimica Acta, 38: 1023-1059.

Griffin, W.L. and Ryan, C.G., 1995. Trace-Elements in Indicator Minerals - Area Selection and Target Evaluation in Diamond Exploration. Journal of Geochemical Exploration, 53(1-3): 311-337.

Griffin, W.L., Smith, D., Ryan, C.G., O'Reilly, S.Y. and Win, T.T., 1996. Trace-element zoning in mantle minerals: Metasomatism and thermal events in the upper mantle. Canadian Mineralogist, 34(6): 1179-1193.

Griffin, W.L., O'Reilly, S.Y. and Ryan, C.G., 1999a. The composition and origin of subcontinental lithospheric mantle. In: Y. Fei, C.M. Bertka and B.O. Mysen (Editors), Mantle Petrology: Field Observations and High Pressure Experimentation: A tribute to Francis R. (Joe) Boyd. Special Publication. The Geochemical Society, Houston, pp. 13-45.

Griffin, W.L., Shee, S.R., Ryan, C.G., Win, T.T. and Wyatt, B.A., 1999b. Harzburgite to lherzolite and back again: metasomatic processes in ultramafic xenoliths from the Wesselton kimberlite, Kimberley, South Africa. Contributions to Mineralogy and Petrology, 134(2-3): 232-250.

Griffin, W.L., O'Reilly, S.Y., Natapov, L.M. and Ryan, C.G., 2003. The evolution of lithospheric mantle beneath the Kalahari Craton and its margins. Lithos, 71(2-4): 215-241.

Grütter, H.S., Apter, D.B. and Kong, J., 1999. Crust-mantle coupling: evidence from mantle-derived xenocrystic garnets. In: J.J. Gurney, J.L. Gurney, M.D. Pascoe and S.H. Richardson (Editors), The J.B. Dawson Volume, Proceedings of the VIIth International Kimberlite Conference. Red Roof Design, Cape Town, pp. 307-313.

Harley, S.L., 1984. An experimental study of the partitioning of iron and magnesium between garnet and orthopyroxene. Contributions to Mineralogy and Petrology, 86: 359-373.

Harte, B. and Hawkesworth, C.J., 1989. Mantle domains and mantle xenoliths. In: J. Ross et al. (Editors), Kimberlites and related rocks. GSA Spec Publ 14. Blackwell, Carlton, pp. 649-686.

Hoal, K.E.O., Hoal, B.G., Erlank, A.J. and Shimizu, N., 1994. Metasomatism of the mantle lithosphere recorded by rare earth elements in garnets. Earth and Planetary Science Letters, 126(4): 303-313.

McDonough, W.F. and Sun, S.-S., 1995. The composition of the Earth. Chemical Geology, 120: 223-253.

Nixon, P.H., van Calsteren, P.W.C., Boyd, F.R. and Hawkesworth, C.J., 1987. Harzburgites with garnets of diamond facies from Southern African kimberlites. In: P.H. Nixon (Editor), Mantle Xenoliths. John Wiley & Sons Ltd., Chichester, pp. 523-533.

Phillips, D., Harris, J.W. and Viljoen, K.S., 2004. Mineral chemistry and thermobarometry of inclusions from De Beers Pool diamonds, Kimberley, South Africa. Lithos, 77: 155-179.

Pollack, H.N. and Chapman, D.S., 1977. On the regional variation of heat flow, geotherms, and lithospheric thickness. Tectonophysics, 38: 279-296.

Richardson, S.H., Gurney, J.J., Erlank, A.J. and Harris, J.W., 1984. Origin of Diamonds in Old Enriched Mantle. Nature, 310(5974): 198-202.

Richardson, S.H., Harris, J.W. and Gurney, J.J., 1993. Three generations of diamonds from old continental mantle. Nature, 366(6452): 256-258.

Ringwood, A.E., 1975. Composition and petrology of the Earth's upper mantle. McGraw-Hill, London, 618 pp.

Schulze, D.J., 1995. Low-Ca garnet harzburgites from Kimberley, South Africa: Abundance and bearing on the structure and evolution of the lithosphere. Journal of Geophysical Research-Solid Earth, 100(B7): 12513-12526.

Shimizu, N. and Richardson, S.H., 1987. Trace element abundance patterns of garnet inclusions in peridotite-suite diamonds. Geochimica et Cosmochimica Acta, 51(3): 755-758.

Smith, C.B., 1983. Pb, Sr and Nd isotopic evidence for sources of southern African Cretaceous kimberlites. Nature, 304: 51-54.

Smith, D. and Boyd, F.R., 1987. Compositional heterogeneities in a high-temperature lherzolite nodule and implications for mantle processes. In: P.H. Nixon (Editor), Mantle Xenoliths. John Wiley & Sons Ltd., Chichester, pp. 551-561.

Sobolev, N.V., Lavrent'ev, Y.G., Pokhilenko, N.P. and Usova, L.V., 1973. Chrome-rich garnets from the kimberlites of Yakutia and their paragenesis. Contributions to Mineralogy and Petrology, 40(1): 39-52.

Stachel, T. and Harris, J.W., 1997. Diamond precipitation and mantle metasomatism - evidence from the trace element chemistry of silicate inclusions in diamonds from Akwatia, Ghana. Contributions to Mineralogy and Petrology, 129(2-3): 143-154.

Stachel, T., Viljoen, K.S., Brey, G.P. and Harris, J.W., 1998. Metasomatic processes in lherzolitic and harzburgitic domains of diamondiferous lithospheric mantle: REE in garnets from xenoliths and inclusions in diamonds. Earth and Planetary Science Letters, 159(1-2): 1-12.

Stachel, T., Harris, J.W. and Brey, G.P., 1999. REE patterns of peridotitic and eclogitic inclusions in diamonds from Mwadui (Tanzania). In: J.J. Gurney, J.L. Gurney, M.D. Pascoe and S.H. Richardson (Editors), The P.H. Nixon Volume, Proceedings of the VIIth International Kimberlite Conference. Red Roof Design, Cape Town, pp. 829-835.

Stachel, T., Brey, G.P. and Harris, J.W., 2000. Kankan diamonds (Guinea) I: from the lithosphere down to the transition zone. Contributions to Mineralogy and Petrology, 140: 1-15.

Stachel, T. et al., 2004a. The trace element composition of silicate inclusions in diamonds: a review. Lithos, 77: 1-19.

Stachel, T., Viljoen, K.S., McDade, P. and Harris, J.W., 2004b. Diamondiferous lithospheric roots along the western margin of the Kalahari Craton - the peridotitic inclusion suite in diamonds from Orapa and Jwaneng. Contributions to Mineralogy and Petrology, 147(1): 32-47.

Wyllie, P.J. and Ryabchikov, I.D., 2000. Volatile components, magmas, and critical fluids in upwelling mantle. Journal of Petrology, 41(7): 1195-1206.

Table 3.1: REE and other trace element analyses for De Beers Pool garnet inclusions.

sample	14	23	32	42	49	68	70	180	181
La	0.05	0.09	0.02	0.15	0.09	0.04	0.21	0.13	1.13
Ce	0.47	1.05	0.14	1.95	1.24	0.41	3.42	1.74	11.01
Nd	0.91	1.70	2.59	9.46	2.59	0.91	3.53	2.34	5.02
Sm	0.39	0.23	0.71	1.41	0.79	0.31	0.36	0.35	0.62
Eu	0.12	0.06	0.34	0.38	0.23	0.08	0.10	0.06	0.23
Dy	0.27	0.11	0.49	0.99	0.49	0.19	0.22	0.09	0.69
Er	0.13	0.06	0.13	0.46	0.18	0.10	0.13	0.08	0.41
Yb	0.10	0.07	0.21	0.63	0.21	0.08	0.17	0.08	0.36
Ti	144.4	93.2	9.1	1205.4	386.2	48.1	141.9	55.2	786.9
Sr	0.88	2.94	2.64	4.13	0.93	0.77	3.34	1.49	8.85
Y	1.04	0.48	1.09	8.90	2.77	1.98	1.95	0.74	5.63
Zr	8.23	2.72	31.75	45.22	11.55	7.40	7.32	1.48	47.12
Nb	0.61	0.64	0.82	2.04	0.91	0.55	2.19	1.90	2.21
Ba	0.49	0.58	0.37	0.74	0.66	0.60	4.28	0.65	0.56

sample	182	209	217	218	248	321	325	332	364
La	0.07	0.09	0.04	0.29	0.02	0.19	0.25	0.50	0.25
Ce	1.39	1.88	0.58	2.51	0.40	2.18	3.25	5.55	2.73
Nd	1.44	2.37	1.85	1.82	1.14	4.46	5.40	6.87	1.83
Sm	0.29	0.57	0.38	0.29	0.39	0.97	1.11	0.77	0.22
Eu	0.04	0.12	0.12	0.06	0.12	0.22	0.25	0.29	0.04
Dy	0.05	0.16	0.09	0.09	0.12	0.42	0.25	0.87	0.09
Er	0.13	0.14	0.07	0.06	0.04	0.26	0.07	0.52	0.04
Yb	0.29	0.17	0.07	0.19	0.08	0.30	0.11	0.52	0.09
Ti	75.5	92.1		90.2	23.1		72.6	1621.5	34.9
Sr	1.52	2.57		2.34	0.56		2.07	4.80	3.14
Y	0.52	0.90		0.83	0.27		0.65	6.34	0.90
Zr	3.80	4.94		1.95	2.82		4.52	67.47	1.69
Nb	0.99	0.66		0.72	0.25		1.23	2.13	1.21
Ba	0.29	0.68		1.23	0.83		0.66	0.93	0.47

sample	368	374	387	391	392avg	398	400	405	406
La	1.46	0.21	0.12	0.56	0.01	0.08	0.11	0.04	0.20
Ce	5.23	1.73	1.58	4.82	0.07	0.98	1.14	1.69	2.37
Nd	2.38	1.77	2.08	4.43	0.26	1.54	2.23	3.13	2.82
Sm	0.40	0.46	0.57	1.06	0.23	0.31	0.22	0.26	0.41
Eu	0.09	0.11	0.22	0.36	0.06	0.07	0.06	0.05	0.12
Dy	0.24	0.32	0.71	0.35	0.12	0.14	0.05	0.06	0.10
Er	0.18	0.31	0.47	0.24	0.12	0.05	0.10	0.06	0.02
Yb	0.19	0.44	0.57	0.28	0.18	0.05	0.11	0.08	0.11
Ti			1369.7	570.8	68.5	61.6	25.1	45.5	79.1
Sr			1.97	5.46	0.47	1.05	1.15	2.20	5.73
Y			5.87	3.11	0.95	0.39	0.30	0.62	0.41
Zr			26.15	13.01	1.85	2.13	1.05	1.82	3.40
Nb			1.14	0.42	0.28	1.08	0.58	0.74	0.49
Ba			0.28	0.32	0.15	0.52	0.36	0.65	0.28

Table 3.1 cont.

sample	418avg	421	422avg	440	448	449	457	460	470
La	0.12	0.09	0.29	0.02	0.14	0.11	0.14	0.12	0.06
Ce	2.12	1.61	3.53	0.14	1.06	2.16	2.12	1.51	0.36
Nd	3.59	2.46	2.06	0.39	1.34	4.09	3.25	2.45	1.35
Sm	0.68	0.41	0.49	0.20	0.51	1.02	0.51	0.52	0.33
Eu	0.18	0.06	0.10	0.05	0.15	0.38	0.20	0.20	0.07
Dy	0.22	0.13	0.14	0.07	0.52	0.82	0.44	0.27	0.05
Er	0.16	0.13	0.08	0.06	0.54	0.26	0.28	0.24	0.07
Yb	0.15	0.07	0.11	0.06	1.04	0.36	0.34	0.29	0.07
Ti	71.5		89.3	37.9	512.2	394.3	450.6		33.5
Sr	2.12		2.83	0.78	1.53	1.71	2.57		0.82
Y	1.15		0.66	0.32	5.66	4.60	3.92		0.44
Zr	3.30		2.36	2.43	5.25	30.28	13.21		1.16
Nb	1.23		0.98	0.25	1.96	1.47	0.74		0.41
Ba	0.37		0.74	0.46	0.93	0.28	0.37		0.37

sample	481	486	492	493	503
La	0.03	0.14	0.13	0.31	0.04
Ce	0.39	1.64	1.40	1.62	0.48
Nd	1.18	3.37	1.85	0.76	1.26
Sm	0.34	0.60	0.28	0.17	0.27
Eu	0.09	0.09	0.05	0.08	0.09
Dy	0.28	0.18	0.05	0.07	0.07
Er	0.13	0.11	<0.01	0.10	0.09
Yb	0.11	0.10	0.05	0.09	0.09
Ti	50.2	109.4	82.6		40.8
Sr	1.08	1.30	1.04		0.78
Y	2.36	1.15	1.62		0.29
Zr	7.18	3.82	3.01		2.51

Table 3.2: REE groups and pressure temperature conditions for De Beers Pool garnets.

sample	group	para.	assem.	touching	Mg # (Ca)	*T-Harley (°C)*	*P-BKN (GPa)*
14	humped-low Ti	H	2gt,opx	n	91	1173	5.3
23	weakly sinusoidal-low Ti	H	gt,gt-opx	y	89	1112	6.1
32	sinusoidal-low Er	H	gt		90		
42	high Ti- humped	H	gt,ol	n	89		
49	weakly sinusoidal-high Ti	H	gt-opx,gt	y	89	1021	4.7
68	humped-low Ti	H	gt-opx	y	91	1112	5.9
70	weakly sinusoidal-low Ti	H	gt-gt-opx	y	93	1133	5.5
180	weakly sinusoidal-low Ti	H	gt-opx	y	91	1107	5.9
181	high Ti- humped	H	gt		88		
182	sinusoidal-low Dy	H	gt-opx	y	89	1055	4.6
209	weakly sinusoidal-low Ti	H	gt-opx-chr	y	89	1166	7.1
217	weakly sinusoidal-low Ti	H	gt	n	92		
218	sinusoidal-low Er	L	gt-opx	y	86	1036	4.6
248	sinusoidal-low Er	H	gt	n	92		
321	weakly sinusoidal-low Ti	L	gt		87		
325	sinusoidal-low Er	H	gt-opx	y	89	997	4.2
332	high Ti- humped	H	gt	n	87		
364	sinusoidal-low Er	H	gt-opx	y	90	1092	5.2
368	straight	H	gt	n	90		
374	normal	L	gt,cpx		87		
387	normal	H	fper,gt	n	89		
391	weakly sinusoidal-high Ti	H	2gt,opx	n	91	1099	5.7
392avg	sinusoidal-low Dy	H	2gt,opx		89	1084	5.6
398	humped-low Ti	H	gt-opx	y	91	1105	5.4
400	sinusoidal-low Dy	H	gt-opx	y	90	1086	5.5
405	sinusoidal-low Dy	H	gt-opx	y	91	1142	6.2
406	sinusoidal-low Er	H	gt-opx	y	89	1097	5.9
418avg	weakly sinusoidal-low Ti	H	2gt,opx	n	90	1259	6.4
421	weakly sinusoidal-low Ti	H	gt		90		
422avg	weakly sinusoidal-low Ti	H	gt,gt-opx	y	90	1046	5.3
440	sinusoidal-low Dy	H	2gt,opx	n	93	1293	6.4
448	normal	L	gt,opx	n	88	1066	4.3
449	weakly sinusoidal-high Ti	H	gt-opx	y	91	1098	5.6
457	weakly sinusoidal-high Ti	H	gt-opx-chr	y	93	1046	5.8
460	weakly sinusoidal-high Ti	H	gt,ol	n	92		
470	sinusoidal-low Dy	H	gt	n	89		
481	humped-low Ti	H	gt,opx	n	90	1321	7.2
486	humped-low Ti	H	gt,opx	n	90	1071	4.7
492	sinusoidal-low Er	H	gt		90		
493	straight	H	gt		91		
503	sinusoidal-low Dy	H	gt-opx,opx	y	93	1121	4.7

Abbreviations: para: paragenesis, H: harzburgite, L: lherzolite; Assem.: assemblage, gt: garnet, opx: orthopyroxene, ol: olivine, chr: chromite, fper: ferropericlase, cpx: clinopyroxene; Mg # (Ca): Ca-corrected Mg #

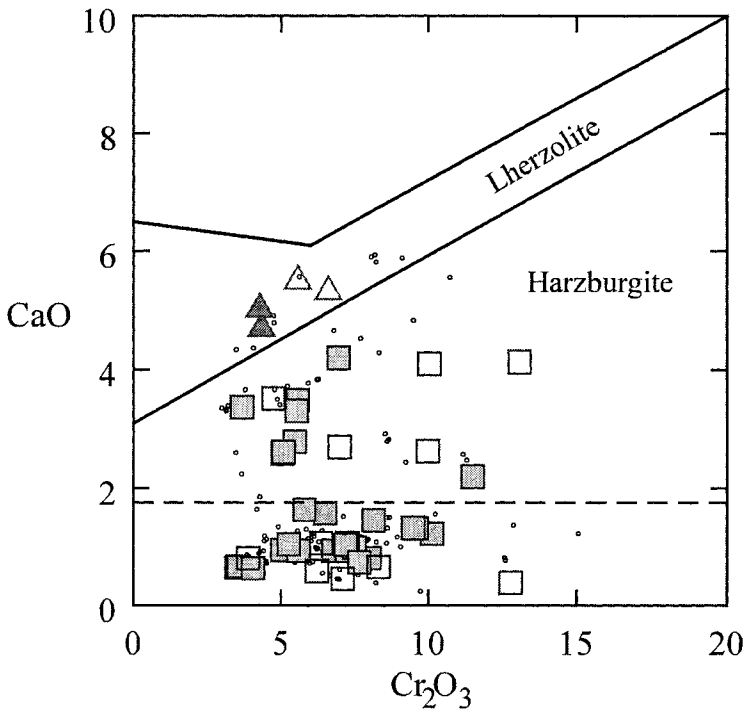

Fig. 3.1 CaO vs. Cr_2O_3 (wt%) of De Beers Pool peridotitic garnet inclusions. Lherzolite field from Sobolev et al. (1973). Filled symbols refer to garnets co-existing with orthopyroxene, allowing determination of equilibration conditions. Dashed line (1.8 wt% CaO) limit of ultra-depleted harzburgitic/dunitic garnet compositions as defined by Grütter et al. (1999).

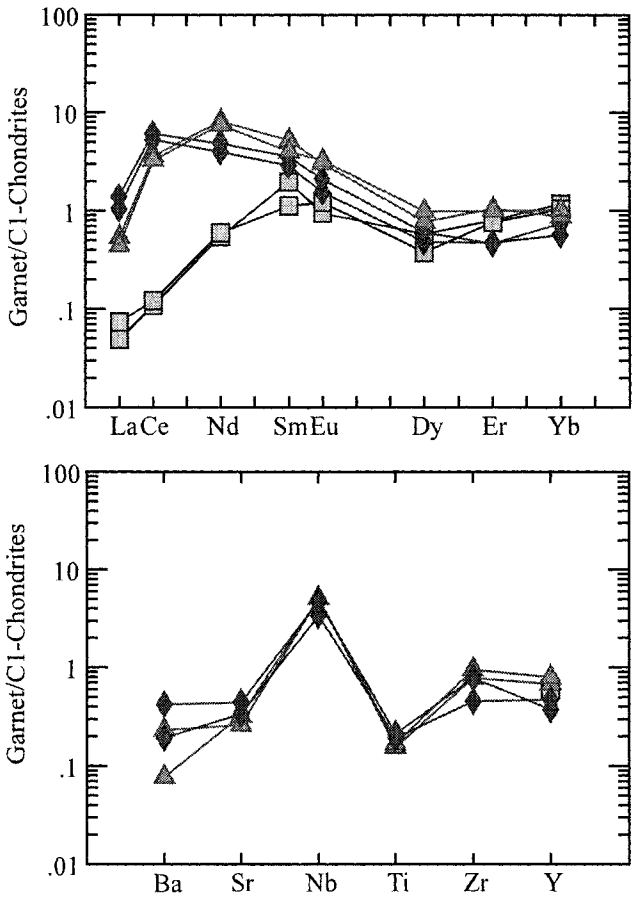

Fig. 3.2 REE and trace element compositions of garnet pairs recovered from diamonds DP 392, 418, 422. The individual pairs show REE and trace element concentrations that are identical, within error, indicating the garnets grew under equilibrium conditions.

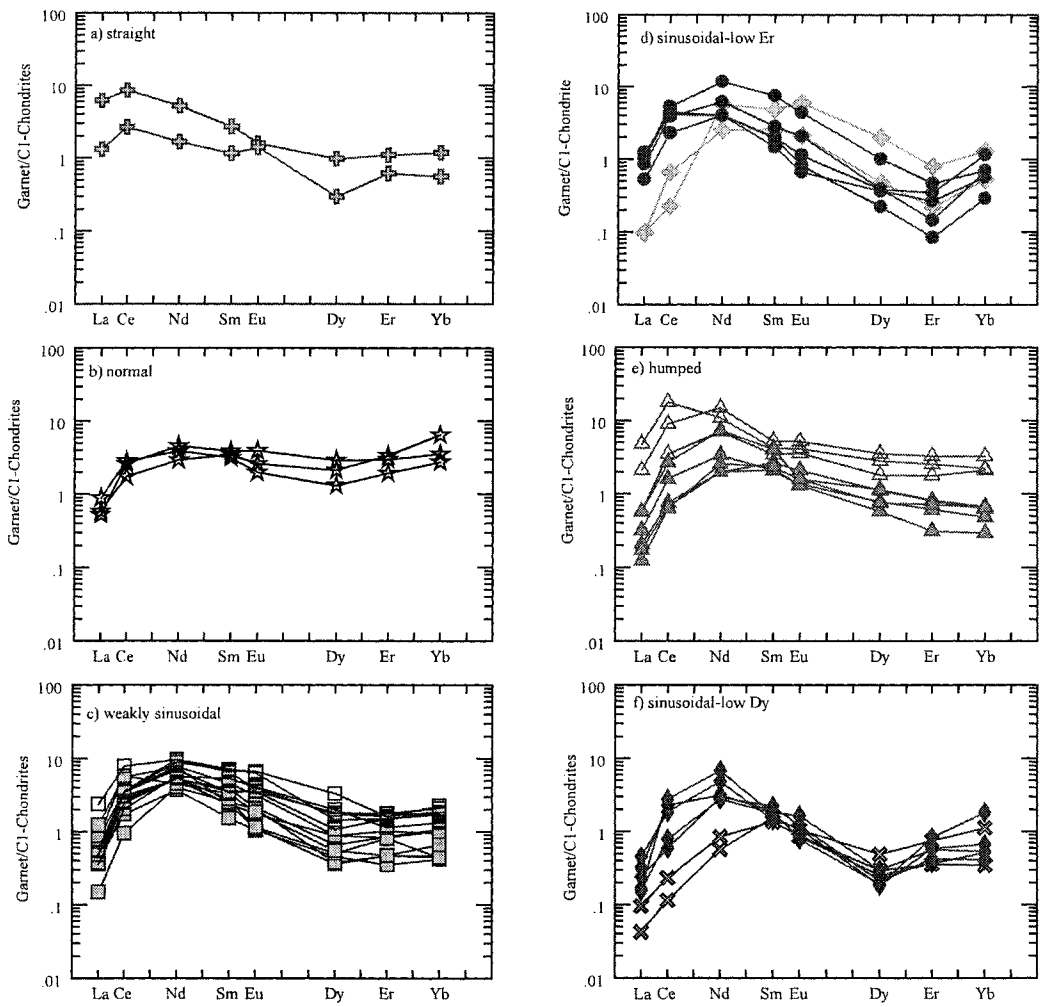

Fig. 3.3 REE (normalized to C1 chondrite of McDonough and Sun, 1995) patterns for De Beers Pool garnet inclusions. a) Straight group. b) Normal group. c) Weakly sinusoidal group d) Sinusoidal-low Er group, cross-symbols emphasize garnets with extremely depleted LREE contents. e) Humped group. f) Sinusoidal-low Dy group, X-symbols emphasize garnets with extremely depleted LREE contents . Filled symbols are low-Ti garnet with <0.02wt% TiO_2, open symbols are high-Ti garnet with >0.06 wt % TiO_2.

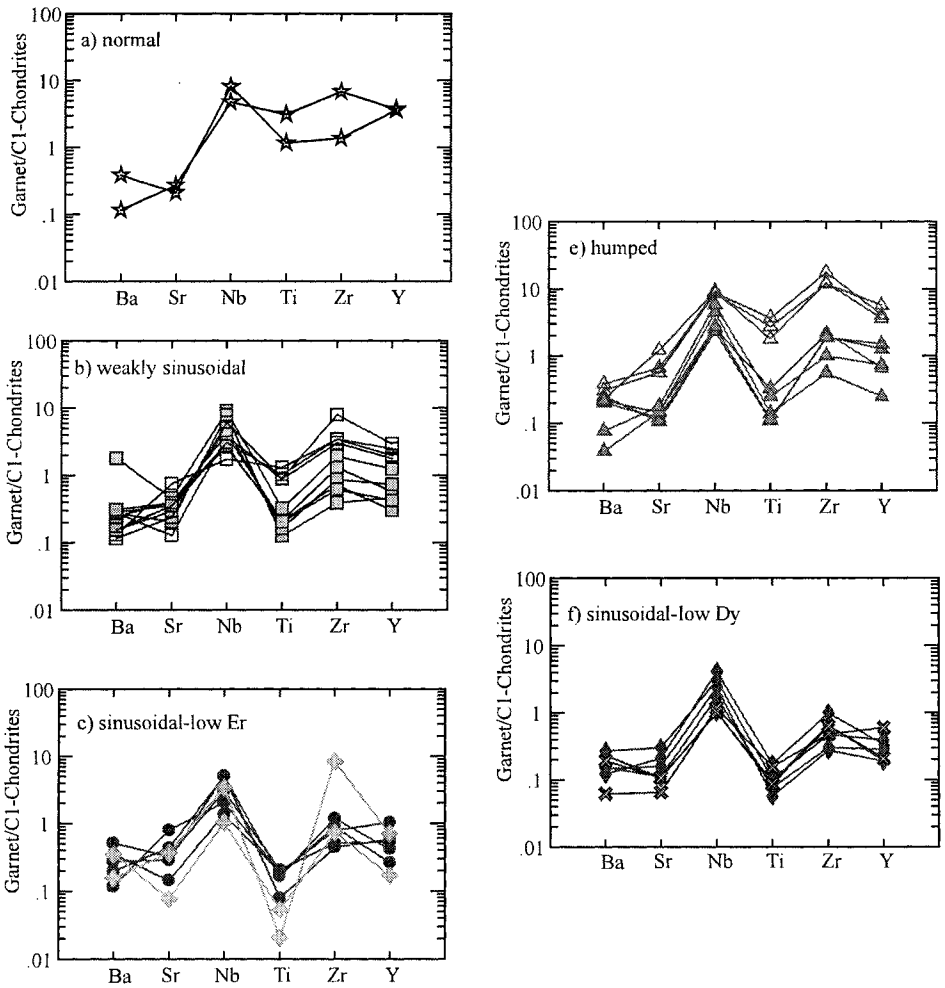

Fig. 3.4 Non-REE trace element compositions for De Beers Pool garnet inclusions. a) Normal group. b) Weakly sinusoidal group. c) Sinusoidal-low Er group, cross-symbols emphasize garnets with extremely depleted LREE contents. d) Humped group. e) Sinusoidal-low Dy group, X-symbols emphasize garnets with extremely depleted LREE contents. Filled symbols are low-Ti garnet with <0.02 wt% TiO_2, open symbols are high-Ti garnet with >0.06 wt % TiO_2.

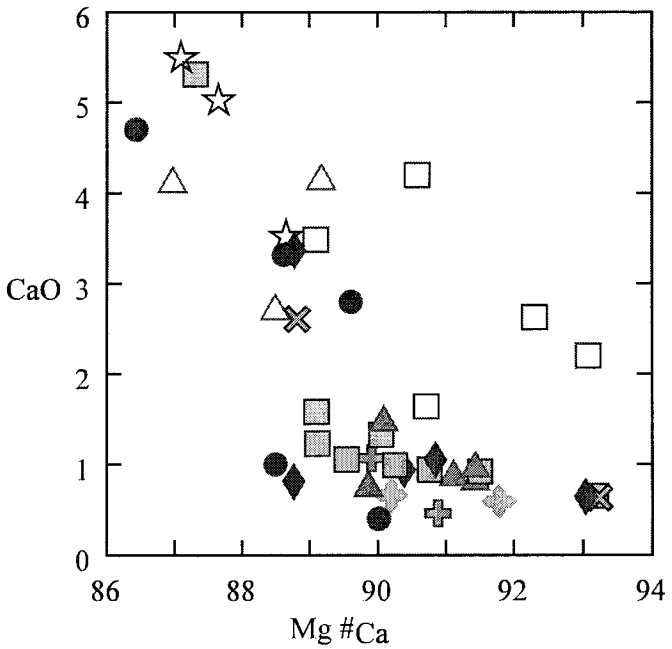

Fig. 3.5 $Mg\#_{Ca}$ vs. CaO (wt%) for De Beers Pool garnets. The high-Ti garnets (open symbols) are almost exclusively restricted to higher Ca contents (>1.8 wt%), but span the whole range of Mg #. Symbols are defined in Fig. 3.3.

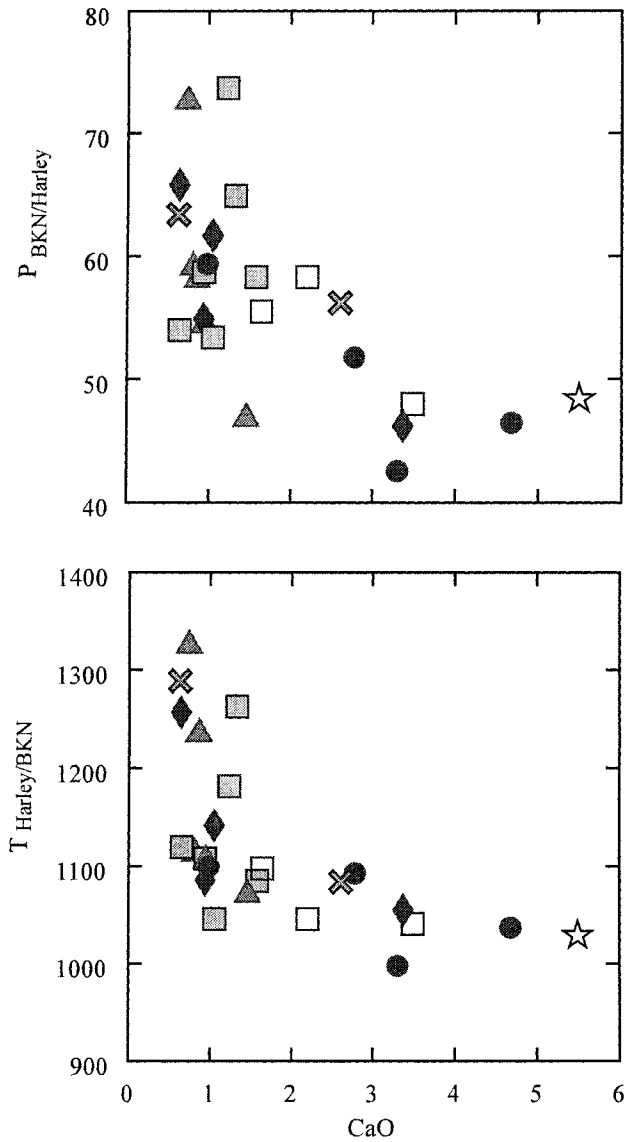

Fig. 3.6 CaO (wt%) vs PT (iterative calculations using T_{Harley} 1984 and P_{BKN} 1990). High-Ti garnets are restricted to lower PT conditions whereas as low-Ti garnets span the whole PT range. Symbols as defined in Fig. 3.3.

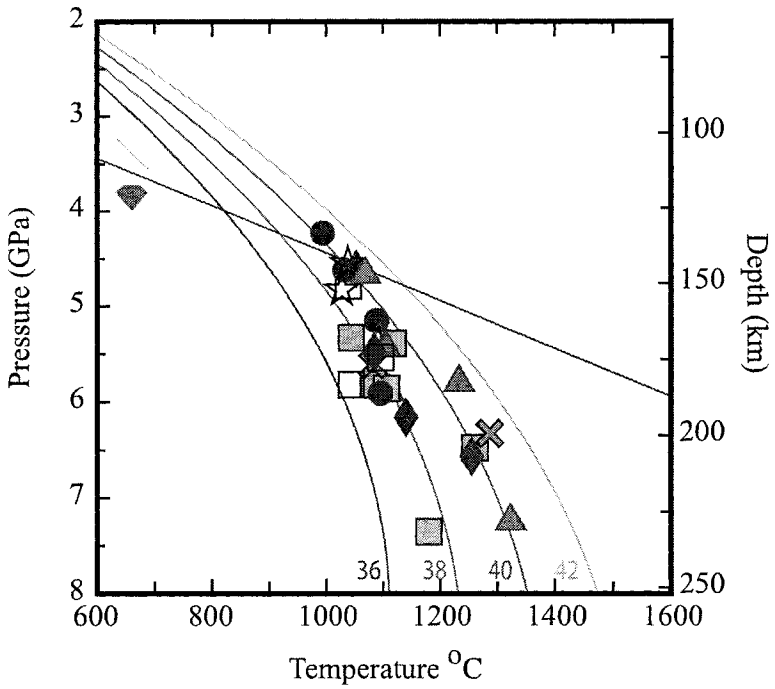

Fig. 3.7 Equilibration conditions for De Beers Pool garnets based on garnet-orthopyroxene inclusion pairs (T_{Harley}, P_{BKN}). Non-touching inclusion pairs define a 40 mW/m^2 geotherm, whereas touching inclusion pairs re-equilibrated to a cooler geotherm of 38mW/m^2. (Geotherms after Pollack and Chapman, 1977). All high-Ti garnets (open symbols) are restricted to shallower depths of formation. Symbols as defined in Fig. 3.3.

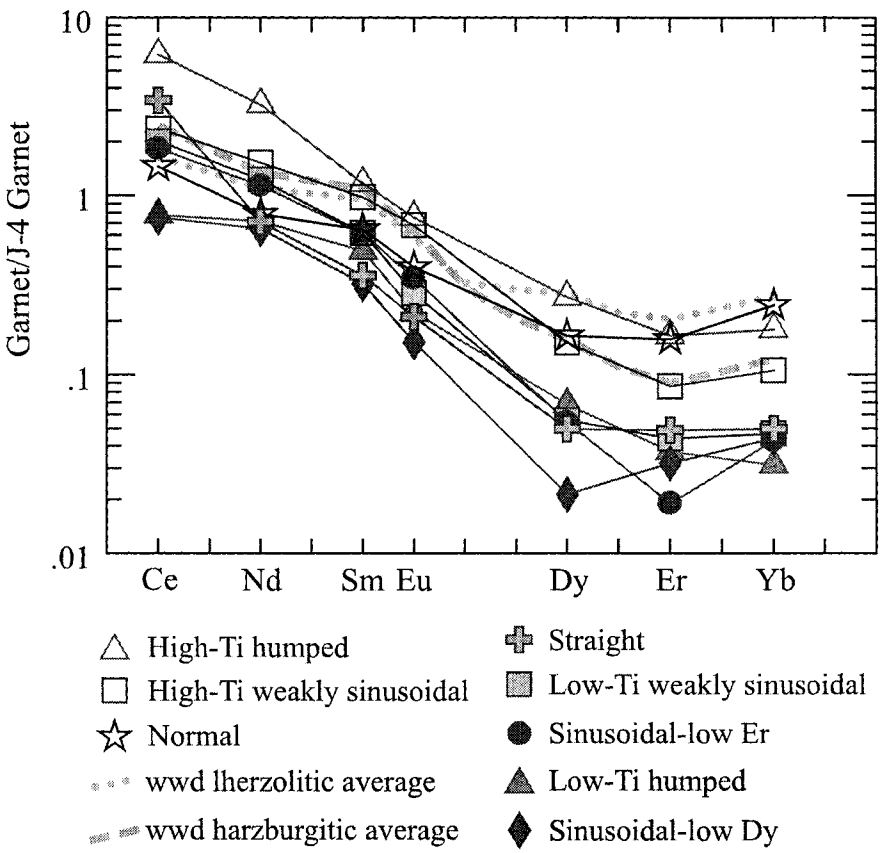

Fig. 3.8 Average REE$_{J4}$ compositions (J4 indicates normalisation to primitive garnet composition of Jagoutz and Spettzle from Stachel et al., 1998). Worlwide average compositions for harzburgite (dashed line) and lherzolite (dotted line) from Stachel et al. (2004a). High-Ti garnets straddle worldwide averages, whereas the low-Ti garnets plot well below the harzburgitic average.

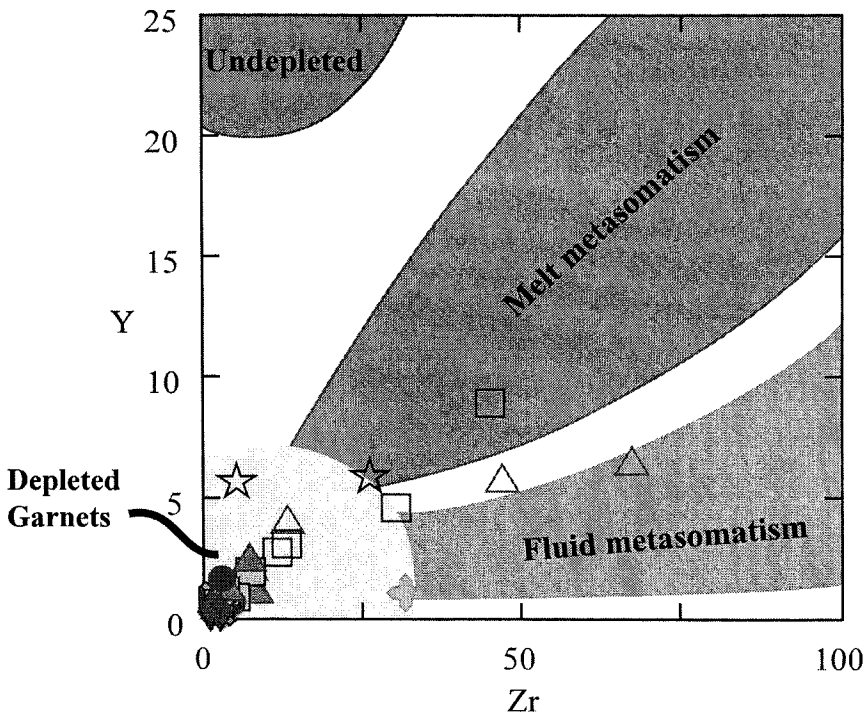

Fig. 3.9 The Y-Zr co-variations recorded by the high-Ti De Beers Pool garnet inclusions indicate metasomatism from a mixed fluid-melt source (fields from Griffin et al., 1995). The majority of garnets plot in the depleted field and are affected by LREE-rich fluid metasomatism. Symbols as defined in Fig. 3.3.

CHAPTER 4

CONCLUSIONS

Worldwide, the diamond bearing lithospheric mantle has been characterized through studies of mantle derived xenoliths and xenocrysts (e.g. Boyd, 1989; Griffin et al., 2003; Schulze, 1989) and inclusions in diamonds (e.g. Gurney, 1989; Harris, 1992; Meyer, 1987; Stachel et al., 2004). These studies have shown that within the diamond source regions the lithospheric mantle is dominated by peridotite, with only a minor eclogite component. Diamond exploration has traditionally been focused on ancient cratons with characteristically depleted lithospheric signatures where historically lucrative economic deposits have been discovered. The scope of this thesis encompasses the study of two very different diamond source regions from geologically distinct areas. The De Beers Pool mines in the Kimberley area are the type locality of a classical primary diamond deposit, located within the confines of the Archean Kaapvaal craton, whereas the Buffalo Head Hills represent an unconventional diamond deposit located within the Proterozoic Buffalo Head Terrane.

4.1 Diamond sources beneath the Buffalo Head Hills, Alberta

Diamonds recovered from kimberlite pipes K11, K91 and K252 in the Buffalo Head Hills, northern Alberta have provided an ideal opportunity to study the composition and structure of the Proterozoic subcontinental lithospheric mantle in this region. Studies of the xenocryst and xenolith suites show a scarcity of typical mantle indicator minerals and a relatively fertile mantle composition dominated by lherzolite with minor components of wehrlite, Ca-rich harzburgite, websterite, pyroxenite and eclogite (Aulbach et al., 2004; Hood and McCandless, 2004). These characteristics indicate that the mantle sources beneath the Buffalo Hills are distinctly different from the majority of diamond occurrences worldwide.

The diamonds themselves also show a distinctive set of characteristics providing additional support for derivation from an atypical source. The Type I diamonds range in nitrogen contents from 6 ppm to 3300 ppm and in aggregation states from low (IaA) to complete

(IaB). However, the Type IaB diamonds extend to the lowest nitrogen concentrations yet observed at such high aggregation states, implying that mantle residence occurred at temperatures well above normal lithospheric conditions. Additionally the unusually large abundance of Type II (no detectable nitrogen) diamonds (20%) may suggest that a portion of the diamonds grew at high temperatures (great depth).

Syngenetic mineral inclusions indicate derivation from a combination of lherzolitic, harzburgitic, wehrlitic and eclogitic sources. The peridotitic paragenesis is characterized by pyropic garnet and forsteritic olivine, including one lherzolitic garnet inclusion which has a moderately majoritic composition indicating a formation depth of ~400 km. A wehrlitic paragenesis is documented by a Ca-rich, high-chromium garnet and very CaO-rich (0.11-0.14 wt%) olivine. Omphacitic pyroxene and almandine-rich garnet are characteristic of the eclogitic paragenesis.

A bimodal $\delta^{13}C$ distribution with peaks at ~ -5‰ and -17‰ is observed for diamonds from all three kimberlite pipes. A large proportion (~40%) of isotopically light diamonds ($\delta^{13}C < -10$ ‰) indicates a predominantly eclogitic paragenesis. An association between isotopically light compositions and the eclogitic paragenesis is widely recognized; however, the mechanism by which this signature is imparted to the diamonds (i.e. isotopic fractionation vs. subduction of organic matter) is still highly debated.

Diamond formation beneath Buffalo Head Terrane occurred during multiple events in an atypical mantle setting. The presence of majorite and abundance of Type II and Type IaB diamonds suggests formation under sublithospheric conditions, possibly in a subducting slab and resulting megalith (an accumulation of subducted oceanic lithosphere at the transition zone/lower mantle boundary). Additionally, diamond formation at lower temperatures (i.e. under "normal" lithospheric conditions) is suggested by the presence of Type IaA to IaAB diamonds. Combined, all these characteristics define a diamond deposit which is distinctive in character from typical primary diamond deposits worldwide. This study emphasizes that unconventional tectonic settings may host economically viable diamond deposits albeit with unique characteristics requiring a fresh approach to diamond exploration.

4.2 Diamond formation beneath the Kimberley area, South Africa

Extensive studies of the subcontinental lithospheric mantle of the Kaapvaal craton have been conducted due to the abundant availability of xenoliths and diamonds (and their inclusions) from its many productive diamond mines and other kimberlites. Griffin et al. (2003) have suggested that "more data are available on the composition of the upper mantle beneath this area than on the rest of the world's cratons combined". However these data

are mainly based on xenolith (and xenocryst) analyses which preserve information about the subcontinental lithospheric mantle at the time of kimberlite eruption. In the case of the Kaapvaal Craton, xenoliths and xenocrysts provide samples from two time slices, the older Group 2 kimberlite event (>110 Ma) and the younger Group 1 kimberlite event (<90 Ma). Comprehensive analyses of samples from these two groups reveal that the subcontinental lithospheric mantle in this region has experienced extensive metasomatism between the two eruption events. Constraints on the composition of the subcontinental lithospheric mantle in the Archean are only available from inclusions in diamonds.

The peridotitic garnet inclusions in diamonds from the De Beers Pool mines represent samples from an extremely depleted mantle source. A large number of the garnet inclusions have CaO contents of less than 1.8 wt% suggesting that initial melt depletion in the cratonic root beneath the Kaapvaal Craton proceeded to a further degree than typically observed from cratonic peridotites worldwide. However, rare earth and trace element analyses show that the De Beers Pool garnet inclusions were affected by metasomatic enrichment processes similar to those recorded by diamond inclusions from around the world. The garnets have a wide range of REE concentrations with variably sinusoidal chondrite normalized abundance patterns. The sinuosity of REE_N patterns generally decreases with increasing fertility (higher Ca Ti, Fe, Y, and Zr). However, no distinction is evident between the REE_N signatures of garnets of harzburgitic and lherzolitic paragenesis.

The REE signatures indicate that the source region of De Beers Pool garnets was affected by at least two phases of metasomatism. LREE-MREE enrichment is preserved by all garnets and indicates interaction with a fluid of highly fractionated character. The variable LREE-MREE concentrations of the garnet inclusions result from progressive evolution of the fluid to higher LREE/HREE ratios during continued equilibration with or precipitation of garnet. This metasomatic fluid was pervasive and affected the entire depth section of the lithosphere documented by inclusions in diamonds. A second phase of re-enrichment encompasses HREE, other HFSE and major elements (Ca and Fe) and thus likely relates to a melt. Melt metasomatism affected only a portion of the diamond source regions and was restricted to "shallower" depths of the lithosphere (<180 km). Diamond precipitation was likely associated with both styles of metasomatic re-enrichment. REE patterns and concentrations for the lherzolitic from harzburgitic garnets overlap completely suggesting diamonds of both parageneses were formed concurrently.

The major element composition of the garnet inclusions indicates that the deep lithosphere at the time of diamond formation was even more depleted than evident from xenoliths in the Group 2 kimberlites. Taking Meso-Archean inclusion ages as diamond crystallization ages

the De Beers Pool garnet inclusions document complex metasomatic processes operating during the Archean and illustrate the intimate association of mantle metasomatism and diamond formation.

References

Aulbach, S., Griffin, W.L., O'Reilly, S.Y. and McCandless, T.E., 2004. Genesis and evolution of the lithospheric mantle beneath the Buffalo Head Terrane, Alberta (Canada). Lithos, 77(1-4): 413-451.

Boyd, F.R., 1989. Compositional distinction between oceanic and cratonic lithosphere. Earth and Planetary Science Letters, 96(1-2): 15-26.

Griffin, W.L., O'Reilly, S.Y., Natapov, L.M. and Ryan, C.G., 2003. The evolution of lithospheric mantle beneath the Kalahari Craton and its margins. Lithos, 71(2-4): 215-241.

Gurney, J.J., 1989. Diamonds. In: J. Ross and e. al. (Editors), Kimberlites and related rocks. GSA Spec Publ 14. Blackwell, Carlton, pp. 935-965.

Harris, J.W., 1992. Diamond geology. In: J.E. Field (Editor), The properties of natural and synthetic diamond. Academic Press, London, pp. 345-393.

Hood, C.T.S. and McCandless, T.E., 2004. Systematic variations in xenocryst mineral composition at the province scale, Buffalo Hills kimberlites, Alberta, Canada. Lithos, 77(1-4): 733-747.

Meyer, H.O.A., 1987. Inclusions in diamond. In: P.H. Nixon (Editor), Mantle xenoliths. John Wiley & Sons Ltd., Chichester, pp. 501-522.

Schulze, D.J., 1989. Constraints on the abundance of eclogite in the upper mantle. Journal of Geophysical Research-Solid Earth and Planets, 94(B4): 4205-4212.

Stachel, T. et al., 2004. The trace element composition of silicate inclusions in diamonds: a review. Lithos, 77: 1-19.

APPENDIX A

ANALYTICAL METHODS

Appendix A

A.1 Procedure for Carbon isotope analysis of diamonds

1. Measure 0.3-2 mg of sample: preferably one large fragment, or a few large fragments. Smaller fragments (ie dust) also work but are more difficult to work with. Make sure fragments are clean and contain pure diamond. Insert into silica tube ~ 30 cm long. Label sample tube with masking tape or sharpie near sealed end.
2. Measure 1-2 g of copper oxide and add to silica glass tube containing diamond fragments.
3. Evacuate samples overnight.
4. Close valves to seal samples from vacuum. Seal tubes with blowtorch.
   To light blowtorch: Wear welding glasses. 1st open oxygen flow, 2nd open gas flow, 3rd turn on gas and light, 4th turn on oxygen and regulate both oxygen and gas until get bright blue flame (v. hot). Cut each tube and torch ends to create rounded tips.
5. Label sample tubes with heat resistant (white) marker at newly sealed end. Shake tube to mix up diamond fragments with copper oxide and try to center everything in middle of horizontal tube. Insert up to 10 tubes into oven, making sure thermocouple touches oven side. Turn on oven, set to 980°C. Leave in oven overnight.
6. Let oven cool to ~100°C before removing samples (careful, they will be hot). Let samples cool to room temperature before proceeding to extraction (couple hours min.).
7. To extract samples:
   7.1. Thoroughly clean cracking device.
   7.2. With sharpie, mark sample tubes to indicate where cuts must be made, indicate at bottom which side the cut is made on. Sample label should stick out the bottom of the cracking device.
   7.3. Put liquid nitrogen under vacuum trap.
   7.4. Evacuate vacuum line (open valves 1, 4, 5, 6 & 9) and new sample holder (open valves 2 & 3 in order, see Fig. A1).
   7.5. Using Dremel on high speed incise tube at indicated mark, deep enough so that tube will break easily.
   7.6. Insert incised sample tube into cracking device. Evacuate cracking device with unbroken sample tube (open valves 7 & 8 from top down). While evacuation proceeds the next sample tube may be incised.
   7.7. Seal (from bottom up 8 & 7) and remove from vacuum. Break sample tube and return to vacuum line, evacuate top of tube (open valve 7). Freeze sample with liquid nitrogen. Label new sample holder with sample number.
   7.8. When the vacuum is re-equilibrated open sample to vacuum (open valve 8), vacuum should not change.
   7.9. Close vacuum! (close valves 4 & 9)

7.10. Freeze gathering tube with liquid nitrogen. Make sure vacuum is closed and line is isolated (close valve 2). Make sure all valves from sample to collection trap are open (1, 5, 6, 7 & 8). Remove liquid nitrogen from sample and heat with blow-dryer. Watch until vacuum gauge jumps and falls.
7.11. When gauge drops back to background level, open vacuum (4 & 9) to clear line.
7.12. Close vacuum (4 & 9), seal off collection trap (close valve 1) and remove liquid nitrogen. Heat with blow dryer. Note pressure and record in blue book (Organic/ Inorganic Carbon).
7.13. Seal off empty sample holder from remaining line (close valve 5) and make sure the vacuum is closed (4 & 9).
7.14. Cool empty sample holder with liquid nitrogen and open valve from collection trap (2 & 1), all other valves and vacuum should be closed. Gauge should drop to background level when CO_2 transfer is complete.
7.15. When transfer is complete, open vacuum (4 & 9) to clear the system. Close valves (3 & 2) and remove tube.
7.16. Stack at the top of line for mass spectrometer analysis.
7.17. When top rack is full you can evacuate the air beneath the samples by opening valve 10, DO NOT open if there are empty spots.

8. Sample will be analyzed on mass spectrometer by Dr. Karlis Muehlenbachs or technician. Results will be left on side table. Please copy and return originals for filing.

Note: To set up vacuum line for analyses you need liquid nitrogen, ethanol and dry ice. In large cylinder mix dry ice and ethanol to form a slurpee-like consistency, put under center trap. A large cylinder filled with liquid nitrogen should be placed under the vacuum trap. Two small cylinders of liquid nitrogen are required for the sample extraction process.

To make sample tubes:
Silica glass tubes come in ~1.5 m lengths. Using a sharpie, mark the silica tube in five, 28 cm, sections. Using Dremel cut tube at the two center markings creating three sections: two two tube pieces and one one tube piece. Break tube into sections.
Set up blowtorch on bench and burn two section pieces in half (at the mark). For one section pieces use tweezers to pull off burning end to create seal.
Put tubes in oven overnight (~800°C). Let cool before removing from oven. Store clean, empty tubes wrapped in aluminum foil.

Appendix A

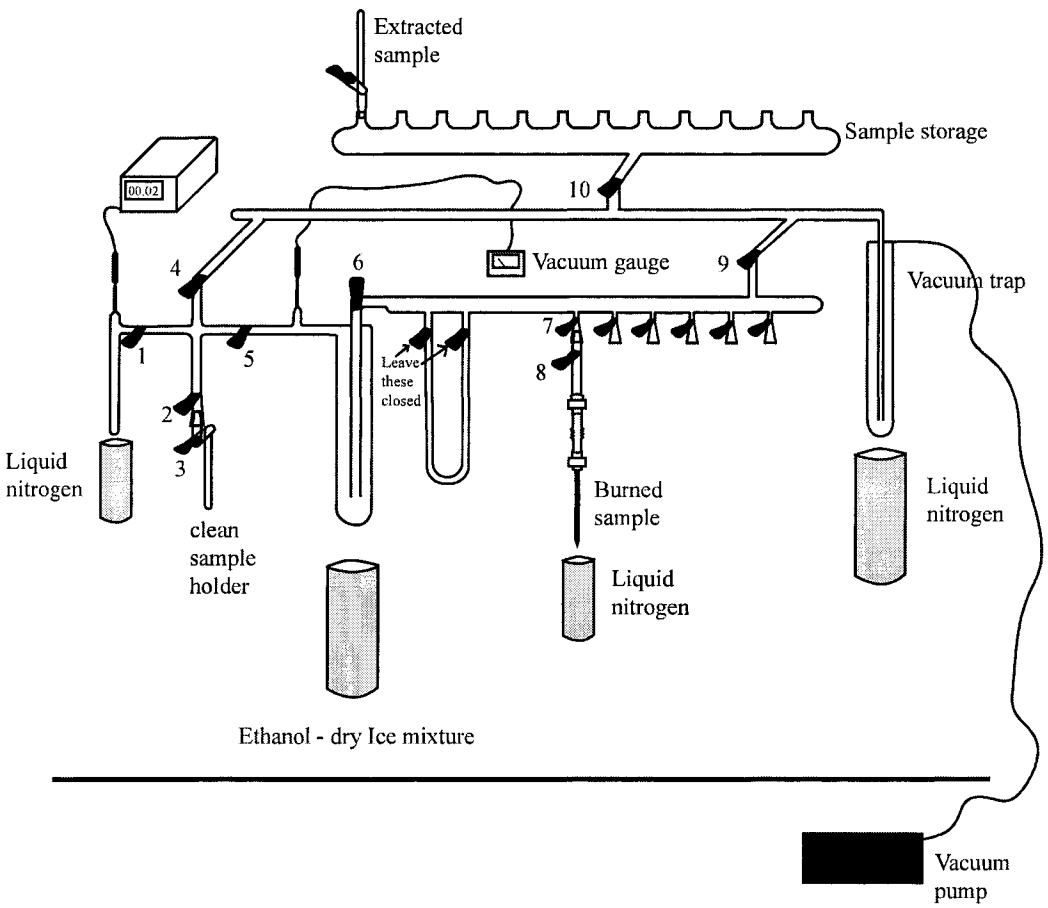

Fig. A.1 Extraction line for carbon isotope analysis.

A.2 FTIR procedure for measuring nitrogen contents in diamond

1. Turn on monitor.
2. Turn up both gas flow valves.
3. Fill detector with liquid nitrogen.
4. Open OMNIC.
4.1 Open Atlus (Atlus—Show Atlus window)
4.2 Open Configuration "diamond" (File --- Open Configuration --- "diamond.con")
4.3 Change experiment to "diamond"

5. To Collect Background:
5.1 Exp Set (1st button on toolbar)
- Collect Tab (1st folder)
  - Under Background Handling select " collect background before every sample"

OK

5.2 Align microscope through open hole (turn on reflected and transmitted lights, 1st and 2nd knob on left, turn off when centered). Turn on aperture light (3rd on left side) and align apertures using aperture focus and alignment knobs (on top of base of microscope).
5.3 Turn off aperture light.
5.4 Col Bkg (button on toolbar)
OK
(Window will show collection in progress, ~3 min)
5.5 Add to window *1* ? "Yes"
OK
5.6 Save Background: File ---- Save As ---- "01bkgrd"
5.7 Prompt " Do you want to replace "01bkgrd"?
YES
5.8 "Ctrl x" to delete background from view
Collect new background every morning and afternoon or every few hours.

6. Sample Measurement:
6.1 Under microscope choose a diamond piece with relatively smooth, flat and parallel sides. Place diamond piece over appropriate sample hole (make sure holder hole is smaller than sample to prevent sample from falling through). BlueTack can be used to set and orientate sample more securely.
6.2 Place sample on FTIR stage.
6.3 Turn on reflected light, using 10x lens find sample on Atlus screen (using joystick).
6.4 Turn on transmitted light, switch to FTIR lens and center hole in aperture on screen (using joystick) and focus to sharp image (using stage focus, large knob on right).

6.5 Turn off both lights and turn on aperture light. Focus aperture using aperture focus (on base on microscope).

6.6 Exp Set (button on toolbar)

- Collect tab
  - Under Background Handling select " use specified background file" (last option)
- Bench tab (2nd folder)
  - Using aperture alignments and focus minimize gain and maximize peak-to-peak values to increase signal intensity.
  - When finished: OK

6.7 Collect Sample (button on toolbar)

OK

- Sample collection begins in collection window.
- When collection is complete (~3 min),
  prompt "Sample name/number::
  - Enter sample name.
    OK
  Prompt "Add to Window *1*?"
  YES
- Print spectrum for your records: File ---- Print

7. Sample Manipulation

7.1 Make sure only one spectrum is open in window.

7.2 Diamond Process (button on toolbar): runs macro for spectrum manipulation, follow prompts

7.3 Saves original spectrum.

7.4 Baseline Correction

- Use top frame to correct baseline to make bottom of spectrum horizontal, when finished select "Replace" (top right corner)
- Saves corrected spectrum.

7.5 Macro performs subtraction from Type II spectrum (on file).

- Adjust factor on side bar to achieve smooth, flat line; minimize sharp positive and negative peaks.
- * **Remember factor value** * (ie 0.0304)
- Select "Add", top right corner
- Saves subtracted spectrum as .csv file

8. Deconvolution:

8.1 Open Caxbd97: tree icon, bottom left toolbar on desktop

8.2 Select "Data" sheet

- Select "Read in data" button, top left corner
- open desired file, all data will be stored in folder "Diamond"
- prompt "keep original solver solution?"
  YES

8.3 Deconvolution will show graph of nitrogen aggregation and residual.
8.4 Print graphs (File --- Print)

8.5 Repeat from "To Measure Sample" for every new sample.

Supplementary: Type II Analysis (standard)
Every few months it is beneficial to re-analyze Type II diamond to account for instrument drift.

1. Follow steps "6. Sample measurement"
2. Baseline collected spectrum
3. After baseline correction read absorbance at 1995 cm^{-1} (=xvalue)
4. Calculate: 11.94/xvalue = conversion factor (cvf)
5. Select menu: Process, multiply
   5.1. Multiply with cvf
6. Save spectrum as "Type II"
   This is the spectrum used in the sample manipulation process during subtraction.

Appendix A

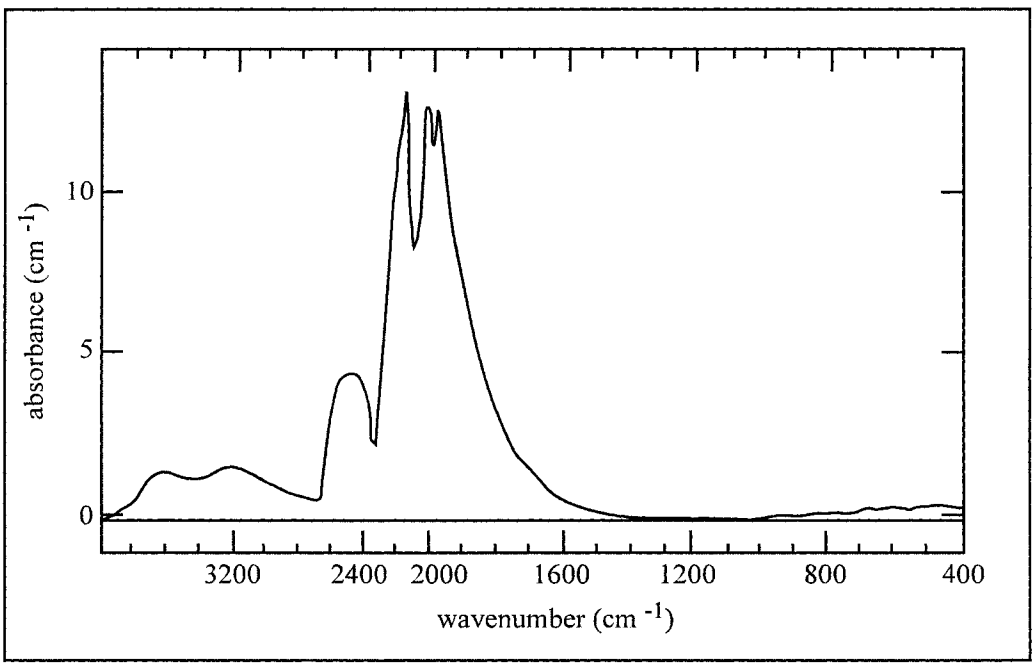

Fig. A.2 FTIR spectrum of Type II (nitrogen free) standard diamond. Type II diamonds show no significant absorbtion below 1400 cm^{-1} (region of nitrogen absorption).

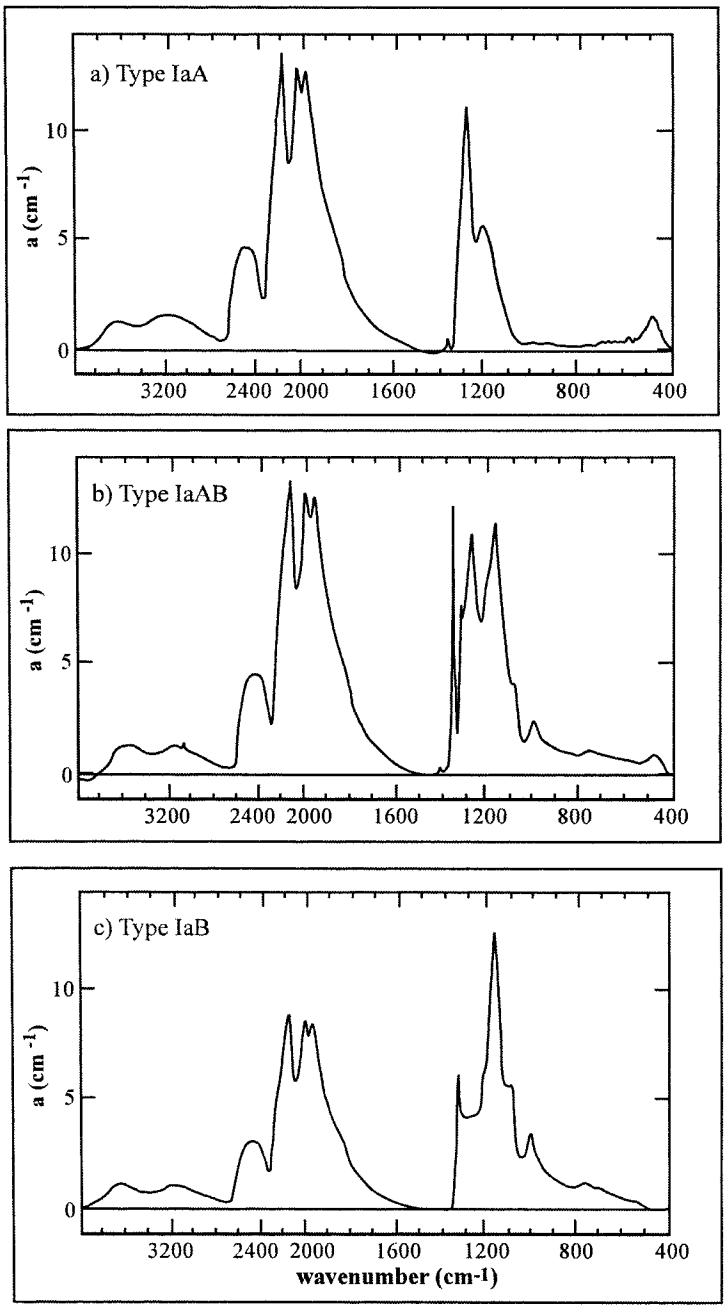

Fig. A.3 Absorbance (a) vs. wavenumber for representatvie FTIR spectra: a) Type IaA diamond: nitrogen aggregated in pairs results in a characteristic absorbance at 1282 cm^{-1} (A-center) b) Type IaAB diamond: contains both nitrogen in pairs and in rings of four plus a vacancy. An additional narrow absorbance peak at 1370 cm^{-1} is caused by the presence of platelets. c) Type IaB diamond: nitrogen aggregated in rings of four plus a vacancy results in a characteristic absorbance at 1185 cm^{-1} (B-center).

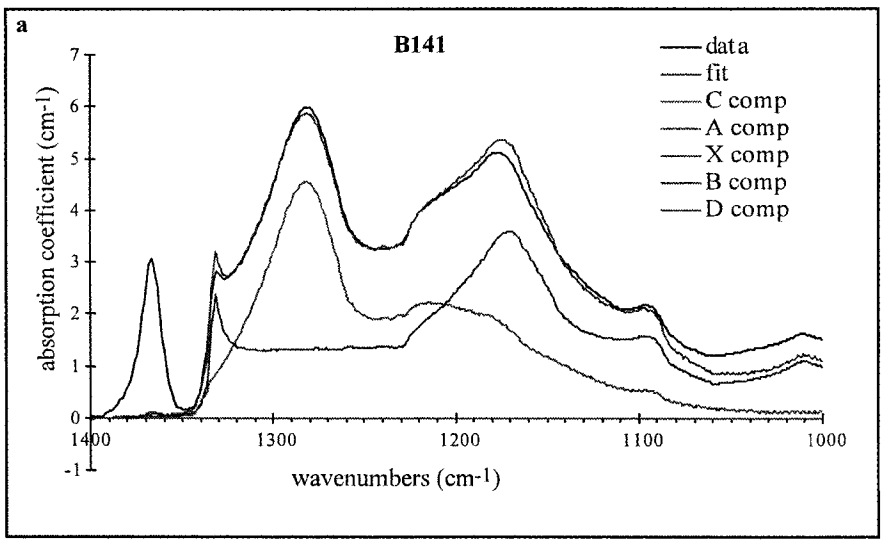

type Ib	μ(1130cm $^{-1}$)	0.00 cm^{-1}	[N_C]	0.0 ppm	
type IaA	μ(1282cm $^{-1}$)	4.54 cm^{-1}	[N_A]	74.9 ppm	
N^+	μ(1332cm $^{-1}$)	0.00 cm^{-1}	[N^+]	0.0 ppm	
type IaB	μ(1282cm $^{-1}$)	1.33 cm^{-1}	[N_B]	105.3 ppm	fit range
D	μ(1282cm $^{-1}$)	0.00 cm^{-1}	[N_T]	180.1 ppm	1001 to 1399

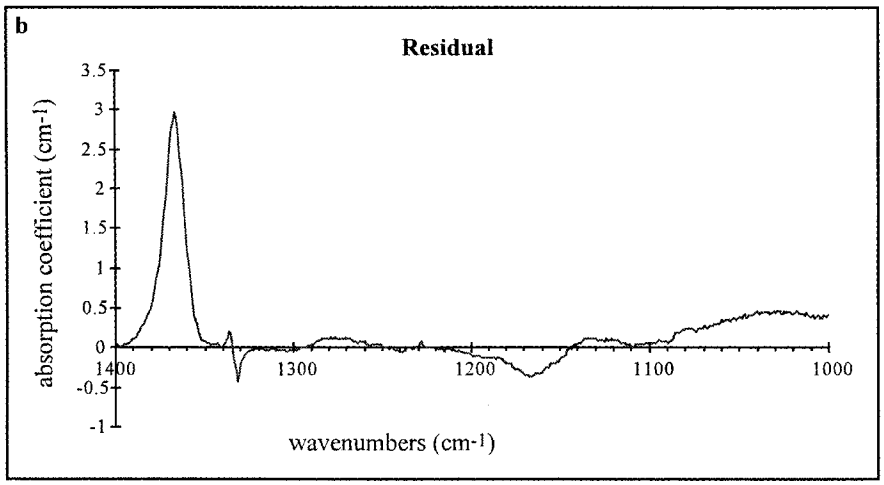

Fig. A.4 Deconvoluted spectrum of a Type IaAB diamond. a) A: nitrogen pairs, B: rings of four nitrogen plus a vacancy. b) Residual spectrum between fit and measured analysis. Peak at 1370 cm^{-1} is inidcative of the presence of platelets.

APPENDIX B

Supplementary Photographs for Buffalo Head Hills Diamonds

Appendix B

Octahedra

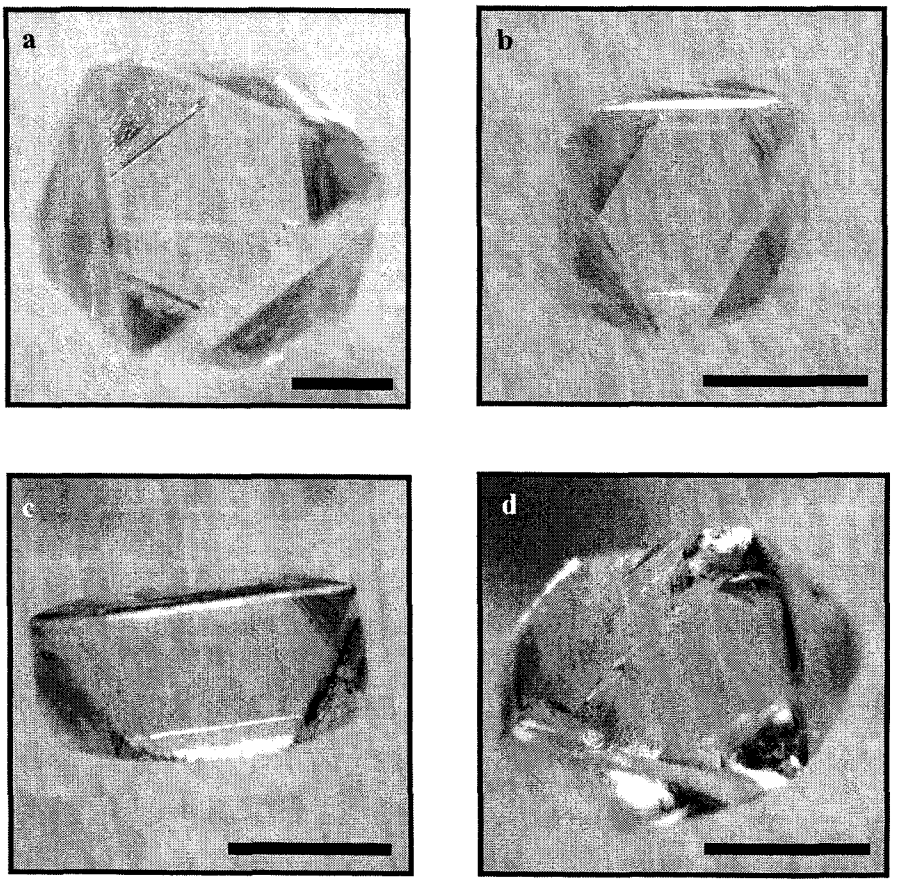

Fig. B.1 Representative octahedral crystals with smooth crystal faces. a) B169 b) B157 c) B110 - elongate octahedral shape. d) B162 - slightly resorbed octahedron, resorbtion is evident along crystal edges. Scale bar is 0.5 mm.

Appendix B

Tetrahexahedroida

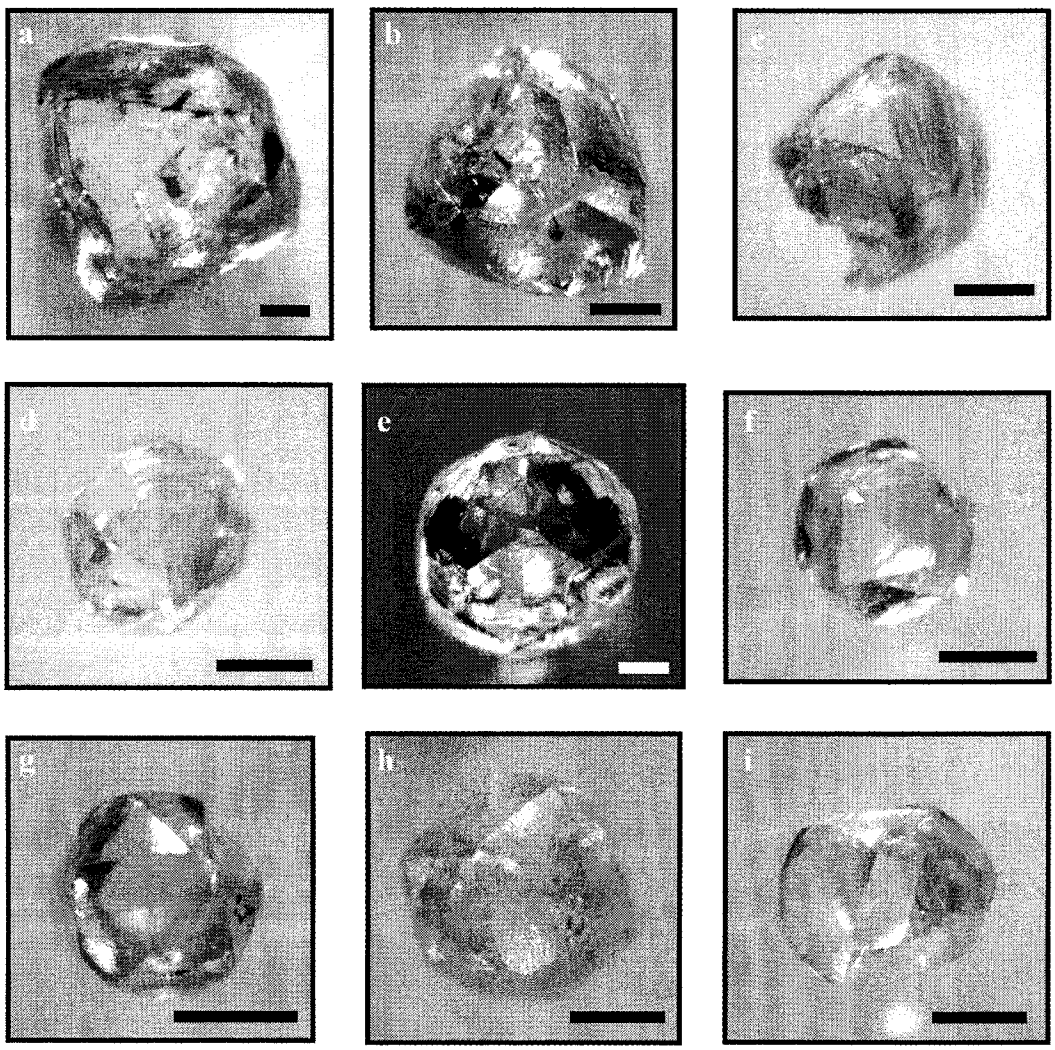

Fig. B.2 Representative tetrahexahedroid shapes. a-d) increasing degree of resorption, from 50% to 90%.. Diamonds show both thh and octahedral crystal faces. e-h) fully resorbed thh crystals i) elongate thh shape.
Scale bars are 0.5 mm.

Appendix B

Twins

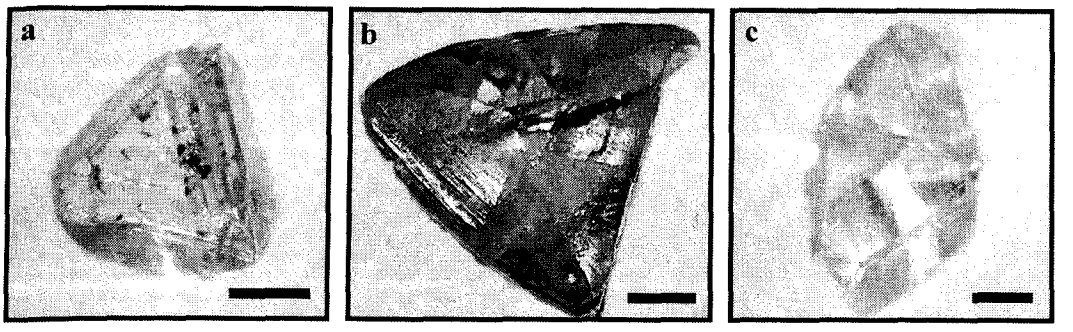

Fig. B.3 a) Octahedral macle b) Tetrahexahedroidal macle c) Complex octahedral twin. Scale bar is 1 mm.

Appendix B

Aggregates

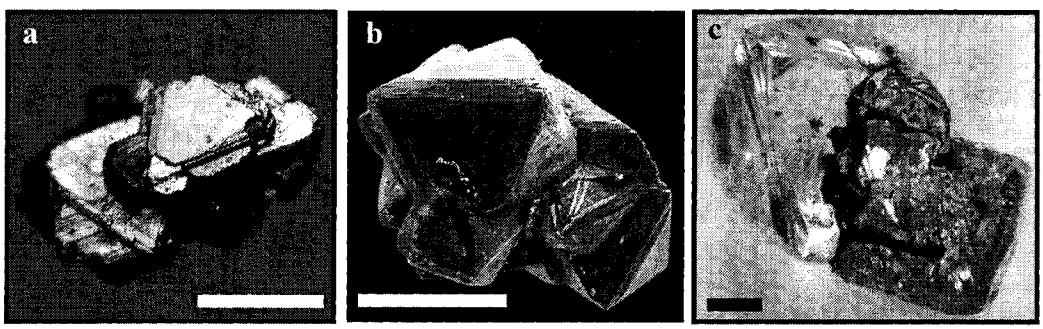

Fig. B.4 a) Octahedral aggregate of 6 crystals. b) Secondary electron image of an octahedral aggregate composed of 6 crystals c) Aggregate of partially resorbed octahedra composed of 3 crystals. Scale bar is 0.5 mm.

Appendix B

Fragments

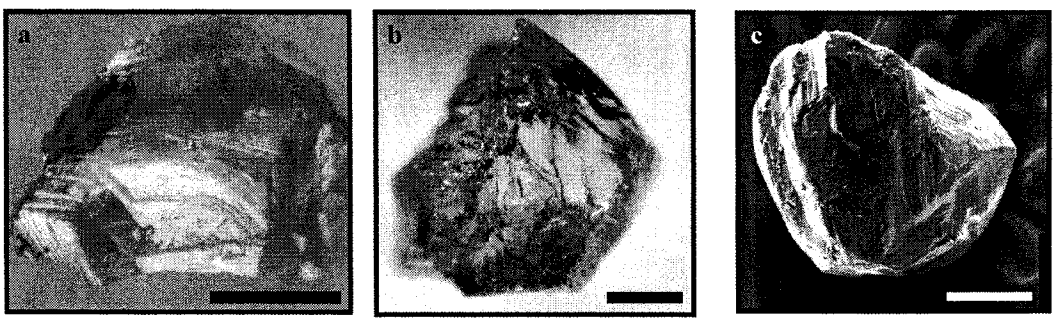

Fig. B.5 a-b) Fragments of diamond crystals showing both old and new breaks. c) Secondary electron image of a partially fractured face. Scale bar is 0.5 mm.

Appendix B

Irregular

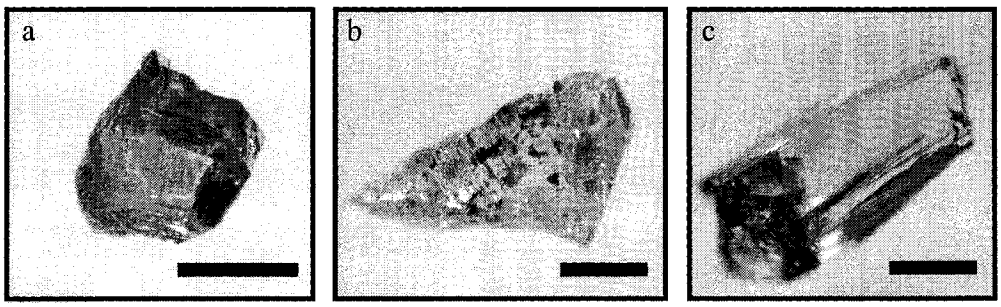

Fig. B.6 Diamonds with irregular shapes show no distinguishing characteritics that would allow them to be classified into one of the other groups. a) B301 b) B317 c) B170 Scale bar is 0.5 mm.

Terraces

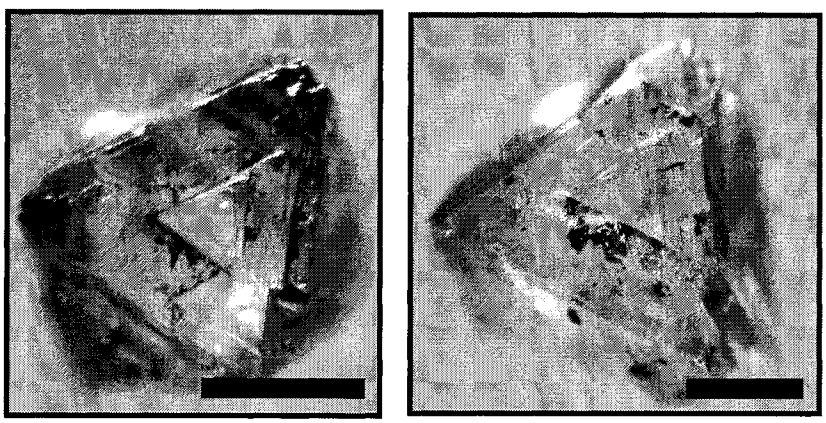

Fig. B.7 Terraces are recognised by raised octahedral gowth palnes often found on octahedral faces. Scale bar is 0.5 mm.

Appendix B

Shield and Serrate Laminae

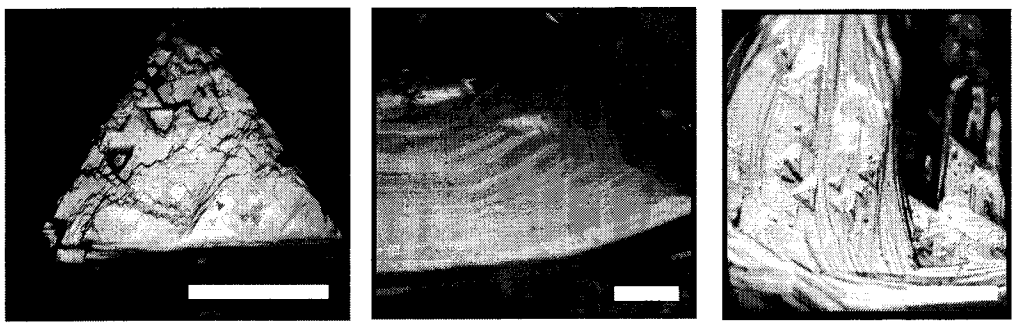

Fig. B.8 Shield and serrate laminae are expressed as thin elevated lines parallel to the octahedral/cubic growth.They are result from resorption of the diamond surface. planes. Scale bar is 0.5mm.

Appendix B

Trigons

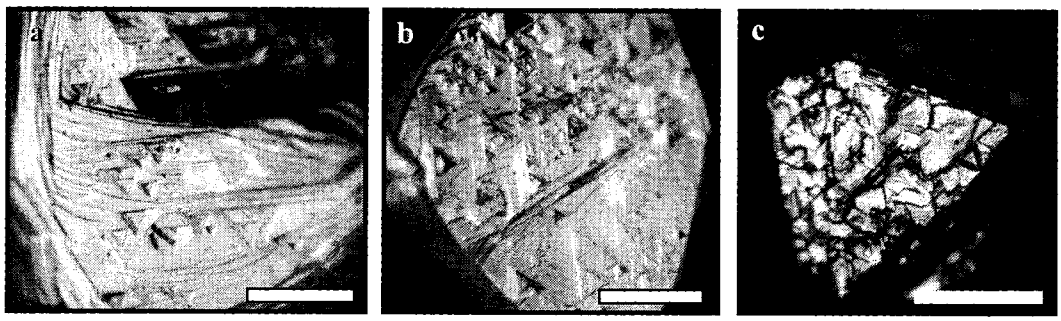

Fig. B.9 a-b) Negative trigons, trigonal shaped etch pits with negative relief, were observed on 30% of th octahedral crystal faces. c) Hexagonal etch pits (hexagons) were observed on a minor proportion of the crystals (2%). Scale bar is 0.5 mm.

Appendix B

Hillocks

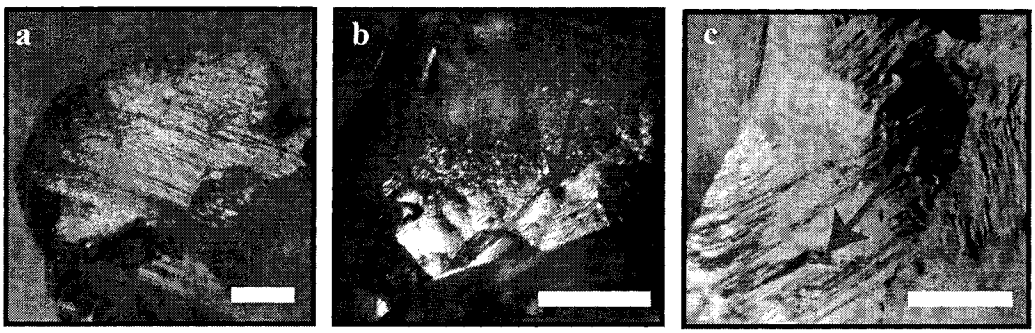

Fig. B.10 Representative examples of the three recognized hillocks patterns: a) Pervasive fine, narrow, elongate hillocks, often make the crystal surface dull and opaque b) Flat, broad hillocks. b) Pyramidal, high relief hillocks are the least common of the three types. Scale bar is 0.25 mm.

Appendix B

Lamination Lines

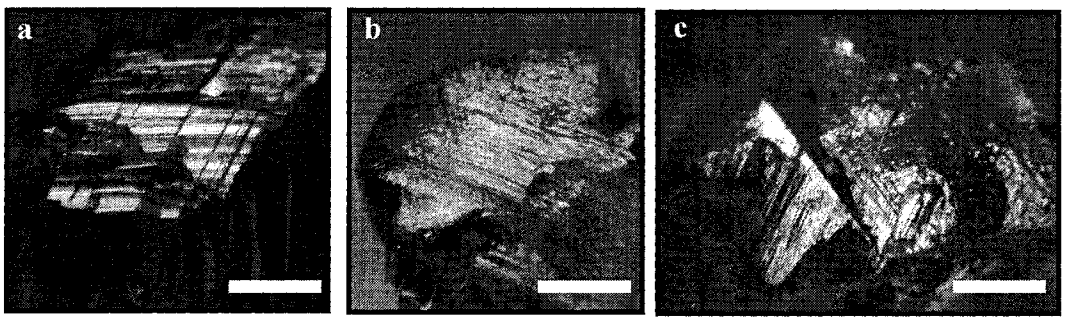

Fig. B.11 Lamination lines are the surface expression of plastic deformation evident as fine parallel lines on a crystal surface. a-b) Show plastic deformation in one direction. c) Shows plastic deformation in two directions. Scale bar is 0.5 mm.

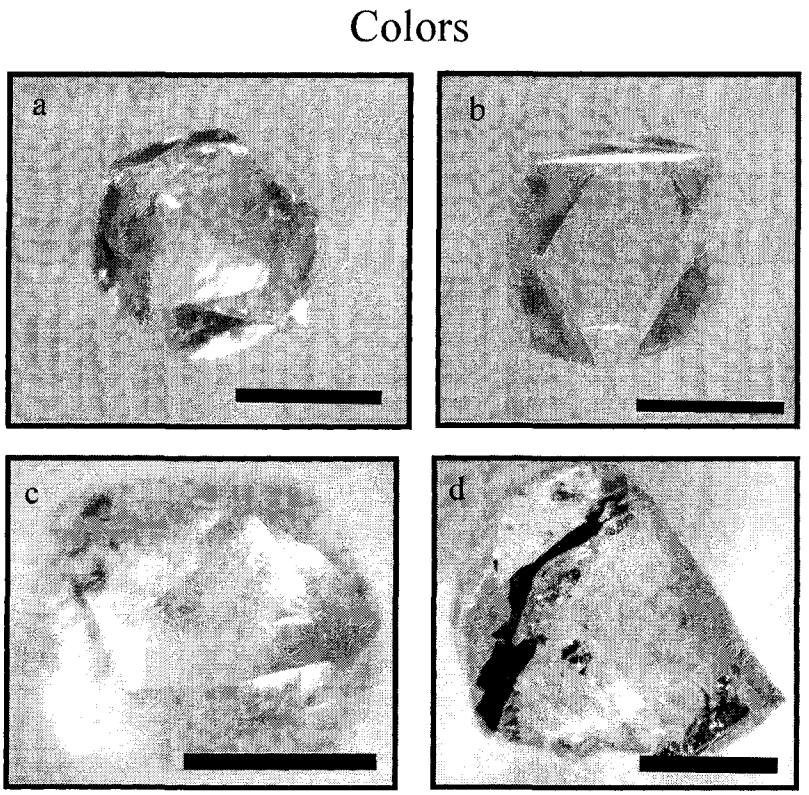

Fig. B.12 a-b) Colorless diamonds. c-d) Diamonds with yellow body colors. Scale bar is 0.5 mm.

Colors (cont.)

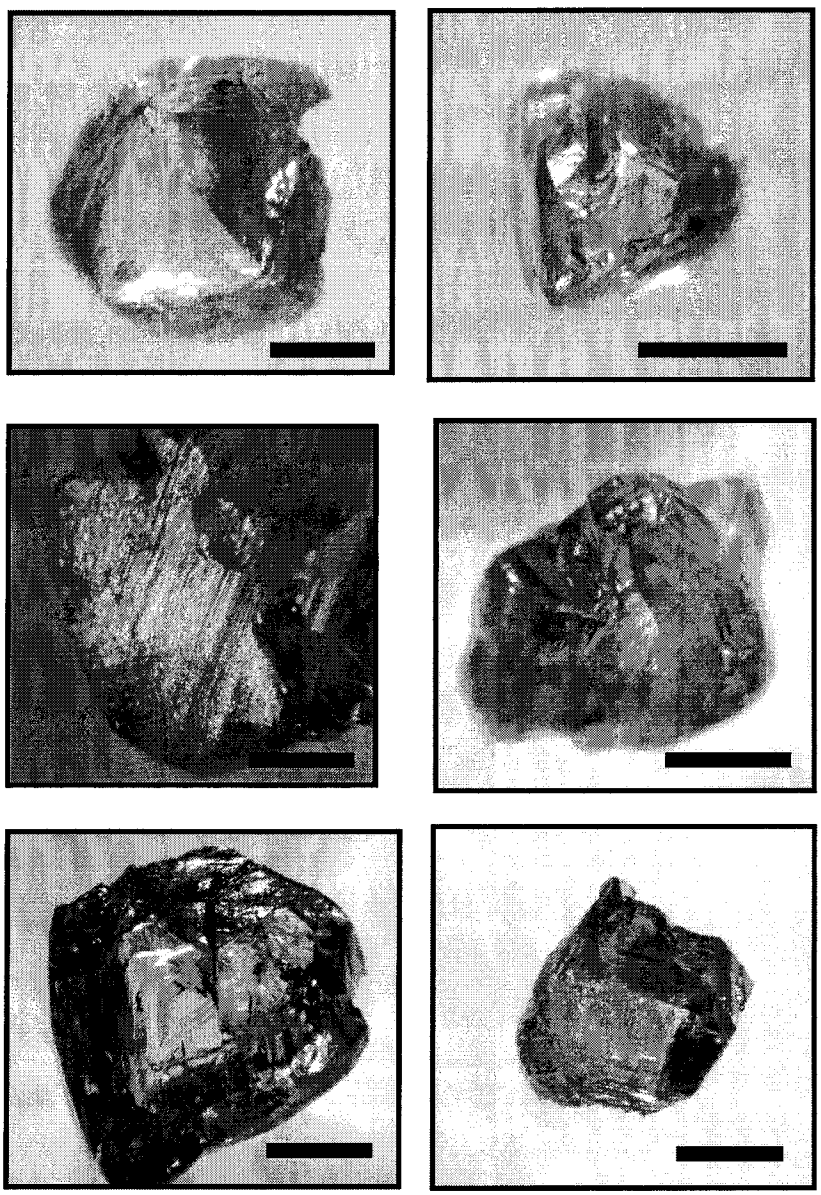

Fig. B.13 Diamonds showing a range of brown body colors. Scale bar is 0.5 mm.

APPENDIX C

SUPPLEMENTARY DATA FOR DE BEERS POOL GARNET INCLUSIONS

Table C.1: Major element data for garnet inclusions (from Phillips et al., 2004) used in SIMS analyses.

Sample	14	23	32	42	49	68	70	180	181	182	209	217	218	248	321
SiO_2	41.63	42.36	41.85	41.51	42.68	42.60	43.65	42.33	41.88	42.24	42.33	43.33	41.77	42.89	41.96
TiO_2	0.02	0.02	0.00	0.15	0.06	0.00	0.01	0.01	0.12	0.01	0.02	0.00	0.02	0.00	0.01
Al_2O_3	19.11	19.04	18.17	14.18	19.48	18.34	21.40	18.90	18.39	21.35	16.86	20.69	20.83	19.11	18.92
Cr_2O_3	7.42	6.50	8.33	13.07	5.56	8.02	3.50	7.24	6.99	3.67	10.13	4.42	4.32	6.22	6.60
V_2O_3			0.03						0.07			0.02		0.02	0.07
FeO	4.67	5.64	5.07	5.29	5.55	4.41	3.63	4.81	5.94	5.80	5.40	4.46	6.71	4.36	6.18
MnO	0.20	0.15	0.26	0.05	0.19	0.11	0.09	0.09	0.17	0.16	0.07	0.10	0.20	0.07	0.14
NiO	0.00	0.00	0.01	0.01	0.02	0.01	0.02	0.01	0.00	0.02	0.01	0.02	0.01	0.02	0.04
MgO	26.03	24.64	25.60	21.52	22.90	25.63	27.02	25.63	23.69	23.33	23.87	26.03	21.35	26.68	20.74
CaO	0.86	1.58	0.66	4.13	3.49	0.81	0.65	0.94	2.70	3.37	1.23	0.92	4.69	0.59	5.31
Na_2O	0.01	0.02	0.02	0.01	0.02	0.01	0.01	0.00	0.02	0.02	0.00	0.00	0.02	0.00	0.01
K_2O	0.00	0.00	0.00	0.00	0.00	0.00	0.00	0.00	0.00	0.00	0.00	0.00	0.00	0.00	0.01
Oxide Total	99.99	100.00	99.97	99.99	100.00	99.97	100.01	99.99	99.90	100.01	99.98	99.97	100.00	99.94	99.92
Si	5.89	6.00	5.94	6.04	6.05	6.01	6.04	5.98	5.98	5.96	6.05	6.04	5.96	6.02	6.02
Ti	0.00	0.00	0.00	0.02	0.01	0.00	0.00	0.00	0.01	0.00	0.00	0.00	0.00	0.00	0.00
Al	3.19	3.18	3.04	2.43	3.26	3.05	3.49	3.14	3.09	3.55	2.84	3.40	3.50	3.16	3.20
Cr	0.83	0.73	0.93	1.50	0.62	0.90	0.38	0.81	0.79	0.41	1.14	0.49	0.49	0.69	0.75
V	0.00	0.00	0.00	0.00	0.00	0.00	0.00	0.00	0.01	0.00	0.00	0.00	0.00	0.00	0.01
Fe^{2+}	0.55	0.67	0.60	0.64	0.66	0.52	0.42	0.57	0.71	0.68	0.65	0.52	0.80	0.51	0.74
Mn	0.02	0.02	0.03	0.01	0.02	0.01	0.01	0.01	0.02	0.02	0.01	0.01	0.02	0.01	0.02
Ni	0.00	0.00	0.00	0.00	0.00	0.00	0.00	0.00	0.00	0.00	0.00	0.00	0.00	0.00	0.00
Mg	5.49	5.20	5.42	4.67	4.84	5.39	5.57	5.39	5.04	4.91	5.08	5.41	4.54	5.58	4.44
Ca	0.13	0.24	0.10	0.64	0.53	0.12	0.10	0.14	0.41	0.51	0.19	0.14	0.72	0.09	0.82
Na	0.00	0.01	0.01	0.00	0.01	0.00	0.00	0.00	0.01	0.01	0.00	0.00	0.01	0.00	0.00
K	0.00	0.00	0.00	0.00	0.00	0.00	0.00	0.00	0.00	0.00	0.00	0.00	0.00	0.00	0.00
Cation Total	16.10	16.05	16.07	15.97	16.00	16.01	16.02	16.05	16.07	16.06	15.96	16.01	16.04	16.06	16.00

Table C.1 Cont.

Sample	325	332	364	368	374	387	391	392avg	398	400	405	406	418avg	421
SiO_2	42.12	40.91	42.77	42.99	41.58	41.89	42.77	41.99	42.58	42.49	42.73	42.14	42.39	42.88
TiO_2	0.01	0.24	0.00	0.02	0.08	0.21	0.08	0.00	0.00	0.00	0.00	0.02	0.02	0.02
Al_2O_3	20.38	16.26	19.61	19.35	19.94	20.57	18.53	20.60	20.36	19.83	20.40	18.42	17.12	17.11
Cr_2O_3	5.53	10.03	5.46	6.37	5.57	4.73	6.95	5.06	5.03	5.60	5.26	7.50	9.55	9.10
V_2O_3		0.12		0.03	0.06	0.07	0.03							0.02
FeO	5.71	6.46	5.36	5.15	6.32	5.81	4.80	5.76	4.56	5.07	4.78	5.91	5.04	4.92
MnO	0.17	0.14	0.15	0.15	0.15	0.16	0.10	0.15	0.11	0.10	0.11	0.14	0.05	0.21
NiO	0.00	0.00	0.01	0.01	0.02	0.01	0.02	0.02	0.02	0.01	0.01	0.01	0.01	0.01
MgO	22.69	21.71	23.78	24.85	20.76	22.99	22.47	23.78	26.36	25.90	25.63	24.81	24.46	24.71
CaO	3.31	4.10	2.79	1.07	5.49	3.52	4.20	2.61	0.95	0.94	1.05	0.99	1.33	0.99
Na_2O	0.01	0.01	0.01	0.01	0.02	0.03	0.02	0.01	0.00	0.01	0.01	0.02	0.00	0.01
K_2O	0.00	0.00	0.00	0.00	0.01	0.01	0.01	0.00	0.00	0.00	0.00	0.01	0.01	0.00
Oxide Total	99.98	99.86	99.98	99.97	99.94	99.93	99.95	100.00	100.00	99.98	100.01	100.02	100.01	99.96
Si	5.98	5.94	6.05	6.05	5.96	5.94	6.08	5.94	5.96	5.98	5.99	5.99	6.04	6.09
Ti	0.00	0.03	0.00	0.00	0.01	0.02	0.01	0.00	0.00	0.00	0.00	0.00	0.00	0.00
Al	3.41	2.78	3.27	3.21	3.37	3.44	3.10	3.44	3.36	3.29	3.37	3.08	2.87	2.86
Cr	0.62	1.15	0.61	0.71	0.63	0.53	0.78	0.57	0.56	0.62	0.58	0.84	1.07	1.02
V	0.00	0.01	0.00	0.00	0.01	0.01	0.00	0.00	0.00	0.00	0.00	0.00	0.00	0.00
Fe^{2+}	0.68	0.78	0.63	0.61	0.76	0.69	0.57	0.68	0.53	0.60	0.56	0.70	0.60	0.58
Mn	0.02	0.02	0.02	0.02	0.02	0.02	0.01	0.02	0.01	0.01	0.01	0.02	0.01	0.03
Ni	0.00	0.00	0.00	0.00	0.00	0.00	0.00	0.00	0.00	0.00	0.00	0.00	0.00	0.00
Mg	4.80	4.70	5.01	5.22	4.43	4.86	4.76	5.02	5.50	5.43	5.36	5.26	5.19	5.23
Ca	0.50	0.64	0.42	0.16	0.84	0.53	0.64	0.40	0.14	0.14	0.16	0.15	0.20	0.15
Na	0.00	0.00	0.00	0.00	0.01	0.01	0.01	0.00	0.00	0.00	0.00	0.01	0.00	0.00
K	0.00	0.00	0.00	0.00	0.00	0.00	0.00	0.00	0.00	0.00	0.00	0.00	0.00	0.00
Cation Total	16.01	16.06	16.02	15.98	16.03	16.05	15.97	16.06	16.08	16.07	16.03	16.05	15.99	15.97

Table C.1 Cont.

Sample	422avg	440	448	449	457	460	470	481	486	492	493	503
SiO_2	42.69	44.26	42.00	42.40	41.46	41.96	42.60	42.97	42.89	42.29	42.90	42.82
TiO_2	0.01	0.00	0.08	0.06	0.06	0.06	0.01	0.01	0.01	0.00	0.02	0.00
Al_2O_3	18.72	21.09	20.35	19.90	15.58	16.39	21.67	18.00	17.90	14.10	18.70	21.33
Cr_2O_3	7.24	3.63	4.26	5.79	11.48	9.98	3.88	7.67	8.15	12.77	7.10	4.04
V_2O_3			0.04			0.04	0.02			0.03	0.06	
FeO	5.33	3.56	6.25	4.75	4.95	4.65	3.94	4.32	5.02	4.98	4.69	3.74
MnO	0.10	0.07	0.19	0.12	0.03	0.19	0.17	0.15	0.10	0.21	0.22	0.16
NiO	0.01	0.02	0.02	0.02	0.01	0.01	0.03	0.01	0.01	0.01	0.02	0.00
MgO	24.77	26.73	21.75	25.26	24.18	24.05	26.86	26.06	24.37	24.89	25.79	27.23
CaO	1.06	0.63	5.02	1.64	2.20	2.63	0.81	0.74	1.46	0.39	0.46	0.64
Na_2O	0.01	0.01	0.03	0.02	0.00	0.02	0.01	0.02	0.01	0.02	0.02	0.01
K_2O	0.00	0.01	0.00	0.00	0.00	0.00	0.01	0.01	0.01	0.01	0.02	0.00
Oxide Total	99.99	100.02	99.95	100.00	99.99	99.99	99.99	99.99	100.00	99.67	99.94	99.99
Si	6.04	6.12	5.98	5.97	5.97	6.01	5.93	6.06	6.08	6.09	6.04	5.95
Ti	0.00	0.00	0.01	0.01	0.01	0.01	0.00	0.00	0.00	0.00	0.00	0.00
Al	3.12	3.43	3.42	3.30	2.64	2.77	3.55	2.99	2.99	2.39	3.10	3.49
Cr	0.81	0.40	0.48	0.64	1.31	1.13	0.43	0.85	0.91	1.45	0.79	0.44
V	0.00	0.00	0.00	0.00	0.00	0.00	0.00	0.00	0.00	0.00	0.01	0.00
Fe^{2+}	0.63	0.41	0.74	0.56	0.60	0.56	0.46	0.51	0.60	0.60	0.55	0.43
Mn	0.01	0.01	0.02	0.01	0.00	0.02	0.02	0.02	0.01	0.03	0.03	0.02
Ni	0.00	0.00	0.00	0.00	0.00	0.00	0.00	0.00	0.00	0.00	0.00	0.00
Mg	5.22	5.51	4.62	5.30	5.19	5.13	5.57	5.48	5.15	5.35	5.41	5.64
Ca	0.16	0.09	0.77	0.25	0.34	0.40	0.12	0.11	0.22	0.06	0.07	0.10
Na	0.00	0.00	0.01	0.01	0.00	0.01	0.00	0.01	0.00	0.01	0.01	0.00
K	0.00	0.00	0.00	0.00	0.00	0.00	0.00	0.00	0.00	0.00	0.00	0.00
Cation Total	16.00	15.97	16.06	16.04	16.08	16.02	16.03	15.97	15.97	15.98	16.01	16.08